BOUNDARY CONDITIONS OF PANEL RC SLABS FOR REALISTIC FATIGUE BEHAVIOR ANALYSIS OF BRIDGE RC SLABS

RC 床版疲労解析における輪荷重走行試験体と実橋との等価境界条件の研究

By
Arslan Qayyum KHAN

Division of Engineering and Policy for Sustainable Environment
Graduate School of Engineering
Hokkaido University
Sapporo, Japan

September 2020

BOUNDARY CONDITIONS OF PANEL RC SLABS FOR REALISTIC FATIGUE BEHAVIOR ANALYSIS OF BRIDGE RC SLABS

By
Arslan Qayyum KHAN

A dissertation submitted to Hokkaido University
in partial fulfillment of the requirements for the Degree of
Doctor of Philosophy in Engineering

Examination Committee
Prof. Takashi MATSUMOTO
Prof. Hiroshi YOKOTA
Prof. Shunji KANIE

Division of Engineering and Policy for Sustainable Environment
Graduate School of Engineering
Hokkaido University
Sapporo, Japan

September 2020

ACKNOWLEDGMENTS

First and foremost, I would like to express my sincere gratitude to my supervisor Prof. Takashi MATSUMOTO for his comprehensive guidance, invaluable suggestions, caring attitude, and endless support throughout this research work. I consider myself lucky to work with him and feel honored to conduct this research work under his supervision. In addition to his supervision of this research work, he has taught me professional independence, stress management, and how to conduct extensive research work in a short time. From him, I have also learned how to think out of the box, which I had rarely practiced in my life before coming to Hokkaido University.

I would also like to express my gratitude to the examination committee members Prof. Hiroshi YOKOTA and Prof. Shunji KANIE, for their insightful and constructive comments during the evaluation. I am grateful to them for sparing time out of their busy schedule in reading this dissertation, which led to improving the quality of this research work.

My gratitude is also extended to Asst. Prof. Pengru DENG for his valuable input and guidance throughout this research work. It has been privileged for me to have him in my research group. I am thankful to him for keeping me on track whenever I was struggling in my research, and being always there to help me whenever I needed his guidance.

Taking this opportunity, I also would wish to acknowledge the Ministry of Education, Science and Culture, Government of Japan, for awarding me a generous MEXT Scholarship to make me study and stay possible in Japan during the Doctoral program. I am also thankful to the English Engineering Education (e3) program administration for their kind cooperation throughout the whole period.

I would like to take the opportunity to thank technical staff Mr. Kenta KONDO and secretory Ms. Masako TAKIMOTO, for providing me a great environment to work in. My gratefulness and thanks are also extended to all other members of the Laboratory of Bridge and Structural Design Engineering for their kind assistance and support throughout my stay here.

Last but not least, I would like to offer my sincere and heartiest gratitude to my mother and siblings for their unconditional support, endless love, and prayers during all times.

ABSTRACT

Reinforced concrete (RC) slabs are one of the most critical members in a bridge and are susceptible to fatigue failure, as they directly experience repetitive moving wheel loads. Owing to insufficient slab thickness in previous designs, a brittle punching shear failure mode appeared as a key failure phenomenon for bridge RC slabs in service, especially with the increase in vehicle weight and traffic volume. Consequently, the fatigue strength of bridge RC slabs is significantly reduced, posing a great threat to the structure and human life. Therefore, various experimental and numerical studies have been carried out to investigate the fatigue behavior of bridge RC slabs. In these studies, a panel of the bridge RC slab has been considered in lieu of the whole bridge RC slab due to cost, time, and space restraints. The boundary conditions (BCs) comprised of simple supports along the longitudinal edges and steel I-beams along the transverse edges of the panel RC slab have been typically used to represent the bridge RC slab with continuity between adjacent spans. These studies have employed cyclic moving wheel loads, and the punching shear failure mode of bridge RC slab has been successfully reproduced. However, the panel RC slabs with typically used BCs failed to reproduce the deformation and fatigue behaviors of bridge RC slabs. Therefore, it is essential to elucidate the effects of BCs and determine appropriate BCs of the panel RC slabs, which can simulate the realistic deformation and fatigue behaviors of the bridge RC slabs.

In this study, at first, the applicability of a fatigue analysis method based on the bridging stress degradation concept for panel RC slabs subjected to a stepwise loading sequence is investigated. In recent studies, the fatigue analysis method considering the bridging stress degradation has been developed, with which the fatigue behavior of the panel RC slabs has been simulated successfully. However, in these studies, the panel RC slabs have been subjected to a constant loading sequence rather than a stepwise loading sequence, which has been newly introduced in the improved specifications of the road bridge. Therefore, in this study, fatigue analysis of a panel RC slab subjected to a stepwise loading sequence is conducted, and the fatigue analysis results are compared with the experimental ones. The comparison confirms that the developed fatigue analysis method based on the bridging stress degradation concept successfully simulates the fatigue behavior of the panel RC slab subjected to a stepwise loading sequence.

Thereafter, a method for the determination of approximate BCs for already available panel RC slabs is developed and proposed to capture the realistic behaviors of the bridge slabs. The finite element analysis (FEA) of the panel RC slab with approximate BCs shows that the approximate BCs reproduce the same bending moment distribution and displacements around the loading locations as the wheel load moves along the slab axis in the panel RC slab, which are similar to those of the bridge RC slabs. For simulation of fatigue behavior, fatigue analysis of the panel RC

slab with approximate BCs is conducted in addition to the panel RC slab with the BCs typically used in the past studies. The fatigue analysis results show that the approximate BCs do not result in a negative bending at the corners of the panel RC slab, and the cracked elements do not propagate on the top surface from the corners to the loading point, which is similar to a bridge RC slab. However, in the panel RC slab with typically used BCs, the negative bending at the corners and the propagation of the cracked elements on the top surface from the corners to the loading point produce an additional deterioration in the panel RC slab, which leads to a shorter fatigue life estimation of a bridge RC slab. Furthermore, the approximate BCs permit the propagation of the cracked elements in the panel RC slab along the longitudinal direction to a greater extent compared to the typically used BCs, which is similar to that generally observed in a bridge RC slab.

Lastly, for more accurate and realistic fatigue behavior analysis of a bridge slab, an equivalent BCs determination method is developed numerically for a panel slab. For this purpose, a static analysis of a bridge RC slab is conducted, and equivalent BCs for its corresponding panel RC slab are determined based on the calculated stiffness of the bridge RC slab. The results of the panel RC slab with equivalent BCs are found to have more similar bending moment distributions and displacement behaviors to the corresponding results of the bridge RC slab. To simulate the fatigue behavior, fatigue analysis is conducted for the panel RC slab with equivalent BCs as well for the panel RC slab with typically used BCs. The fatigue analysis results reveal that the equivalent BCs allow the propagation of cracked elements in the longitudinal and transverse directions of the panel RC slab, in a similar manner as a bridge RC slab. Moreover, in contrast to the typically used BCs, the equivalent BCs do not lead the cracked elements to propagate on the top surface from the corners to the loading point, which is similar to a bridge RC slab. Furthermore, contrary to the typically used BCs, the equivalent BCs reproduce the extensive grid crack pattern in the panel RC slab, well in accordance with that generally witnessed in a bridge RC slab.

Conclusively, this study mainly aims to elucidate the effects of BCs and develop the determination method of BCs for panel RC slabs to realistically analyze the deformation and fatigue behaviors of bridge RC slabs. The numerical results conclude that the panel RC slabs with proposed BCs behave in the same manner as bridge RC slabs, which results in a more realistic fatigue behavior analysis of the bridge RC slabs.

TABLE OF CONTENTS

ACKNOWLEDGMENTS ii
ABSTRACT iii
LIST OF TABLES viii
LIST OF FIGURES ix
Chapter 1 **INTRODUCTION** 1
1.1 BACKGROUND AND MOTIVATION 1
1.2 OBJECTIVES OF THE STUDY 3
1.3 OUTLINE OF THE DISSERTATION 4
Chapter 2 **FATIGUE ANALYSIS METHOD BASED ON BRIDGING STRESS DEGRADATION CONCEPT** 6
2.1 GENERAL 6
2.2 FATIGUE ANALYSIS METHOD 7
2.2.1 Concrete model 7
2.2.2 Reinforcement bar model 11
2.2.3 Analytical procedure 13
2.3 APPLICABILITY OF FATIGUE ANALYSIS METHOD 13
2.3.1 Details of the panel slab 14
2.3.2 Boundary conditions 14
2.3.3 Stepwise loading sequence 15
2.4 FATIGUE ANALYSIS RESULTS 16
2.4.1 Center displacement evolution 16
2.4.2 Propagation of cracked elements 17
2.4.3 Crack pattern 19
2.5 SUMMARY AND CONCLUSIONS 19
Chapter 3 **METHOD FOR DETERMINATION OF APPROXIMATE BCS FOR A PANEL SLAB**……..... 21
3.1 GENERAL 21
3.2 PROBLEM FORMULATION 21
3.3 DETERMINATION OF APPROXIMATE BCS FOR A PANEL SLAB 23
3.4 STATIC ANALYSIS OF THE PANEL SLAB 25
3.4.1 Description of the panel slab 25
3.4.2 Boundary conditions 25
3.4.3 Loading conditions 26
3.5 STATIC ANALYSIS RESULTS 27
3.5.1 Bending moment cracking zones 27

3.5.2 Displacement distribution 28
3.6 SUMMARY AND CONCLUSIONS 32
Chapter 4 **FATIGUE ANALYSIS OF A PANEL SLAB WITH APPROXIMATE BCS** 33
4.1 GENERAL 33
4.2 DETAILS OF THE PANEL SLAB 33
4.3 BOUNDARY CONDITIONS 34
4.3.1 Typically used BCs 34
4.3.2 Approximate BCs 34
4.4 LOADING SEQUENCE 35
4.5 FATIGUE ANALYSIS RESULTS 35
4.5.1 Propagation of cracked elements 35
4.5.2 Maximum principal strain distribution 38
4.5.3 Center displacement evolution 40
4.5.4 Crack patterns 41
4.6 SUMMARY AND CONCLUSIONS 43
Chapter 5 **METHOD FOR DETERMINING THE EQUIVALENT BCS FOR A PANEL SLAB** 45
5.1 GENERAL 45
5.2 PROBLEM FORMULATION 45
5.3 FINITE ELEMENT ANALYSIS OF A BRIDGE SLAB 47
5.4 DETERMINATION OF EQUIVALENT BCS FOR A PANEL SLAB 52
5.5 STATIC ANALYSIS OF THE PANEL SLAB 54
5.5.1 Description of the panel slab 54
5.5.2 Boundary conditions 54
5.5.3 Loading conditions 55
5.6 STATIC ANALYSIS RESULTS 55
5.6.1 Bending moment cracking zones 56
5.6.2 Displacement distribution 57
5.7 SUMMARY AND CONCLUSIONS 59
Chapter 6 **FATIGUE ANALYSIS OF A PANEL SLAB WITH EQUIVALENT BCS** 61
6.1 GENERAL 61
6.2 DETAILS OF THE PANEL SLAB 61
6.3 BOUNDARY CONDITIONS 62
6.4 LOADING SEQUENCE 62
6.5 FATIGUE ANALYSIS RESULTS 63
6.5.1 Evolution of cracked elements 63
6.5.2 Maximum principal strain distribution 66

6.5.3 Evolution of mid-span displacement 66
6.5.4 Crack patterns 68
6.6 SUMMARY AND CONCLUSIONS 71
Chapter 7 **CONCLUSIONS AND RECOMMENDATIONS** 72
7.1 CONCLUSIONS 72
7.2 RECOMMENDATIONS FOR FUTURE STUDIES 73
REFERENCES 76
APPENDIX 79

LIST OF TABLES

Table 2.1 Material properties [16] 14
Table 3.1 Material properties 25
Table 3.2 Comparison of maximum displacement 32
Table 5.1 Material properties [32] 48
Table 5.2 Comparison of relative displacements 59

LIST OF FIGURES

Figure 1.1 Punching shear failure of bridge RC slabs 1
Figure 1.2 Punching shear failure of the panel RC slab subjected to cyclic moving wheel loads ..2
Figure 2.1 Loading sequences 7
Figure 2.2 Stress-strain relationships of concrete 8
Figure 2.3 Crack propagation due to bridging stress degradation 10
Figure 2.4 Tensile behavior of concrete under cyclic loading 10
Figure 2.5 Crack formation [18] 11
Figure 2.6 Smeared modeling approach 12
Figure 2.7 Tensile behavior of reinforcement bar under cyclic loading 12
Figure 2.8 Analytical procedure 13
Figure 2.9 Dimensions and reinforcement details of the panel slab (mm) 14
Figure 2.10 Illustrations of the BCs (mm) 15
Figure 2.11 Stepwise loading sequence 15
Figure 2.12 Centre displacement evolution 16
Figure 2.13 Propagation of cracked elements 18
Figure 2.14 Maximum principal strain distribution on the bottom surface 18
Figure 2.15 Crack pattern 19
Figure 3.1 Illustration of a bridge slab and the corresponding panel slab, and a comparison of their deformations 22
Figure 3.2 Method for the determination of approximate BCs for the panel slab 24
Figure 3.3 Plan view of the panel slab showing the loading locations 25
Figure 3.4 Illustration of the BCs (mm) 26
Figure 3.5 Loading locations in the panel slab 27
Figure 3.6 Bending moment cracking zones 30
Figure 3.7 Displacement distributions in the longitudinal and transverse sections 31
Figure 4.1 Illustration of BCs (mm) 34
Figure 4.2 Stepwise loading sequence 35
Figure 4.3 Propagation of the cracked elements 37
Figure 4.4 Percentage of the volume of cracked elements 38
Figure 4.5 Maximum principal strain distribution on the bottom surface 39
Figure 4.6 Center displacement evolution 40
Figure 4.7 Displacement jump 40
Figure 4.8 Crack pattern 42
Figure 4.9 Crack angle along the transverse direction 43

Figure 4.10 Grid crack pattern zone (mm) 43
Figure 5.1 Illustration of the bridge slab and its corresponding panel slab (mm) 48
Figure 5.2 Bending stiffness *EI* along the transverse edge of the panel slab (load at location A) 49
Figure 5.3 Bending stiffness *EI* along the transverse edge of the panel slab (load at location D) 50
Figure 5.4 Rotational stiffness *k* along the transverse edge of the panel slab (load at location A) 51
Figure 5.5 Rotational stiffness *k* along the transverse edge of the panel slab (load at location D) 52
Figure 5.6 Cross-section and rotation of the steel I-beam 53
Figure 5.7 Illustration of the boundary conditions (mm) 53
Figure 5.8 Panel slab showing loading locations (mm) 55
Figure 5.9 Bending moment cracking zones 57
Figure 5.10 Displacement distribution 58
Figure 6.1 Details of the panel slab (mm) 62
Figure 6.2 Illustration of the boundary conditions (mm) 62
Figure 6.3 Stepwise loading sequence 63
Figure 6.4 Evolution of the cracked elements 65
Figure 6.5 Percentage of cracked elements volume 65
Figure 6.6 Maximum principal strain distribution 67
Figure 6.7 Evolution of mid-span displacement 67
Figure 6.8 Displacement jump 68
Figure 6.9 Crack patterns 69
Figure 6.10 Crack angles along the transverse direction 70
Figure 6.11 Grid crack pattern zone (mm) 70

Chapter 1

INTRODUCTION

1.1 BACKGROUND AND MOTIVATION

RC slabs are amongst the structural members of bridges that are most susceptible to fatigue failure since they directly sustain heavy traffic loads. Unfortunately, previous design codes mainly focused on the flexural capacity of the bridge RC slabs and neglected their shear capacity. As a result, a brittle and devastating punching shear failure mode appeared as a key failure phenomenon for bridge RC slabs in service, especially with the increase in vehicle weight and traffic volume [1-3]. Consequently, the fatigue strength of bridge RC slabs is significantly reduced, posing a great threat to the structure and human life [4]. **Figure 1.1** shows the punching shear failure mode of bridge RC slabs [5].

To uncover such a brittle and devastating punching shear failure of bridge RC slabs, several experimental studies have been carried out [6-10]. In these experimental studies, a panel of the bridge RC slab has been considered in place of the whole bridge RC slab due to cost, time, and space restraints. The panel RC slab has been typically supported with simple supports along its longitudinal edges and steel I-beams along its transverse edges so as to achieve the bending moments and cracking behavior comparable to those of the bridge RC slab. In these studies, cyclic moving wheel loads have been used, and the punching shear failure mode of bridge RC slab has been successfully captured under these boundary and loading conditions. **Figure 1.2** shows a typical experimental set-up for a panel RC slab and its failure in punching shear due to cyclic moving wheel loads [11].

Figure 1.1 Punching shear failure of bridge RC slabs

(a) Experimental set-up for cyclic moving wheel loads

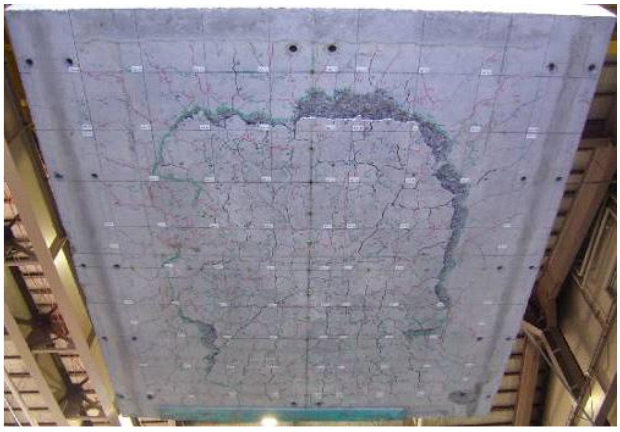

(b) Punching shear failure at the bottom surface of the panel RC slab

Figure 1.2 Punching shear failure of the panel RC slab subjected to cyclic moving wheel loads

Based on the achievements of the experimental studies, various numerical studies have also been conducted for the panel RC slabs with typically used BCs subjected to cyclic moving wheel loads [12-15]. In a numerical method, reported by the National Institute for Land and Infrastructure Management (NILIM), Japan, the stiffness of the damaged concrete elements was simply reduced by applying the damage accumulation theory [16]. However, this numerical method failed to capture the dominant degradation mechanism in the panel RC slabs under fatigue loading, because only the two extreme states (entirely damaged and undamaged) were considered, rather than reducing the stiffness of the concrete element gradually.

Li and Matsumoto (1998) introduced the bridging stress degradation concept in the crack growth analysis of fiber reinforced concrete [17]. Based on this concept, a fatigue analysis method for analyzing the fatigue behavior of the panel RC slabs was developed, with which the fatigue behavior was reproduced successfully [18]. The bridging stress degradation concept was further extended to analyze the fatigue behavior of the panel RC slabs reinforced with plain bars [19]. These studies confirm the applicability of the fatigue analysis method based on the bridging stress degradation concept for the panel RC slabs subjected to cyclic moving wheel loads. However, in these studies, the panel slabs were subjected to a constant loading sequence. In a constant loading sequence, a moving wheel load of constant amplitude is applied for a higher number of cycles. On the other hand, a stepwise loading sequence is introduced in the improved specification of the road bridge for the fatigue durability of the slab. In a stepwise loading sequence, the magnitude of moving wheel load is increased in intervals after a certain number of cycles to promote the deterioration at the early stages to save time. Thus, the applicability of the fatigue analysis method based on the bridging stress degradation concept for panel RC slabs subjected to stepwise loading sequence is to be investigated.

Although the panel slabs equipped with typically used BCs successfully capture the punching

shear failure mode of bridge slabs, they fail to reproduce the deformations and fatigue behaviors, especially crack patterns, of bridge slabs. For example, the bridge slabs experience similar bending moment distributions and deformations around the load upon movement of the load along the slab axis [20, 21]. In contrast, the panel slabs exhibit remarkable dissimilarities in bending moment distributions and deformations around the load upon movement of the load[22, 23]. Furthermore, the panel slabs experience the diagonal cracks that initiate from the loading location and extends towards the corners of the slab [5, 8-10]. This diagonal crack pattern is very different from the grid crack pattern that is commonly witnessed in bridge slabs [6, 24]. These deformations and cracking behaviors of panel slabs, which contradict those of bridge slabs, are attributed to steel I-beams employed along the transverse edges of the panel slabs. These typically used steel I-beams of panel slabs have failed to truly represent the longitudinal continuity of bridge slabs. The steel I-beams restrain the displacement and cracking of the panel slabs, especially near the steel I-beams, and these behaviors are dissimilar from those of bridge slabs. Consequently, these steel I-beams lead to forming the diagonal crack pattern that is initiated from the loading location and extends towards the corners of panel slabs [23].

Therefore, it is essential to elucidate the effects of BCs and determine appropriate BCs of the panel slabs, which can simulate the realistic deformation and fatigue behaviors the bridge slabs. In this study, at first, the applicability of the fatigue analysis method based on the bridging stress degradation concept for panel slabs subjected to stepwise loading sequence is investigated. Thereafter, a method for the determination of approximate BCs for already available panel slabs is developed and proposed to capture the realistic behaviors of the bridge slabs. By following the flowchart presented in this study, one can easily determine the approximate BCs for different dimensions of panel slabs capable of reproducing the behaviors of bridge slabs. Lastly, an equivalent BCs determination method is developed numerically for a panel slab to realistically analyze the deformation and fatigue behaviors of a bridge slab. For this purpose, a static analysis of a bridge slab is conducted, and equivalent BCs for its corresponding panel slab are determined based on the calculated stiffness of the bridge slab. In order to validate the method, fatigue analysis of a panel slab with the determined equivalent BCs is carried out along with the panel slab with the BCs typically used in previous studies. The numerical results confirm that, in contrast to the panel slab with typically used BCs, the panel slab with equivalent BCs behaves in the same manner as the bridge slab, and consequently, results in more realistic fatigue behavior analysis of the bridge slab.

1.2 OBJECTIVES OF THE STUDY

This study mainly aims to elucidate the effects of BCs and propose BCs for panel slabs to realistically analyze the deformation and fatigue behaviors of bridge slabs. The main objectives of

this study are:

- To investigate and confirm the applicability of the fatigue analysis method based on the bridging stress degradation for panel slabs subjected to a stepwise loading sequence.
- To clarify the effects of BCs and propose a method for the determination of approximate BCs for already available panel slabs in order to reproduce the deformation and fatigue behaviors of bridge slabs.
- To develop an equivalent BCs determination method for a panel of bridge slab to realistically analyze the deformation and fatigue behaviors of the bridge slab.

1.3 OUTLINE OF THE DISSERTATION

The dissertation is comprised of seven chapters, which are further divided into several sections and subsections. The organization of this dissertation is as follows:

Chapter 1 summarizes the background and motivation of this research work, objectives, and outlines of the dissertation.

In **Chapter 2**, the applicability of the fatigue analysis method based on the bridging stress degradation for a panel slab subjected to a stepwise loading sequence is investigated. For this purpose, at first, the fatigue analysis method considering the bridging stress degradation is explained in detail. Then, using this fatigue analysis method based on the bridging stress degradation concept, fatigue analysis of a panel slab subjected to a stepwise loading sequence is conducted. The fatigue analysis results of this numerical method are compared with those of the experimental and numerical studies conducted by NILIM [16].

Chapter 3 presents the method for the determination of approximate BCs for a panel slab to capture the realistic behaviors of the bridge slab. By following the flowchart shown in this chapter, one can easily determine the approximate BCs for different dimensions of panel slabs capable of reproducing the behaviors of bridge slabs.

In **Chapter 4**, using the fatigue analysis method based on the bridging stress degradation concept, fatigue analysis is conducted for a panel slab with approximate BCs determined in **Chapter 3**. Moreover, fatigue analysis of the panel slab with the BCs typically used in the past studies is also conducted for the comparison purpose.

Chapter 5 presents the method for determining the equivalent BCs for a panel slab. In this chapter, a static analysis of a bridge slab is conducted, and equivalent BCs for its corresponding panel slab are determined based on the calculated stiffness of the bridge slab. In order to validate the determined equivalent BCs, a static analysis of the panel slab with equivalent BCs is conducted.

Furthermore, a static analysis of the panel slab with typically used BCs is also conducted for the sake of comparison.

In **Chapter 6**, for realistic fatigue behavior analysis of a bridge slab, fatigue analysis of a panel slab is conducted for the equivalent BCs determined in **Chapter 5**. In addition to this analysis, a fatigue analysis is also carried out for the panel slab equipped with BCs typically used in past studies.

In the end, **Chapter 7** presents a summary and overall conclusions of this research work. Furthermore, the recommendations are also made for the future works.

Chapter 2

FATIGUE ANALYSIS METHOD BASED ON BRIDGING STRESS DEGRADATION CONCEPT

2.1 GENERAL

This study mainly aims to elucidate the effects of BCs and propose BCs for the panel slabs to realistically simulate the deformation and fatigue behaviors of bridge slabs. To simulate the fatigue behavior of bridge slabs, fatigue analyses of the panel slabs with the proposed BCs are conducted. In the fatigue analyses of the panel slabs subjected to stepwise loading sequence, a fatigue analysis method based on the bridging stress degradation concept, developed in the past studies, has been employed in this study.

The bridging stress degradation concept was first introduced by Li and Matsumoto (1998) in fatigue crack growth analysis of fiber reinforced concrete [17]. Later, this concept was used in numerical modeling to predict the fatigue behavior of panel slabs, and it efficiently predicted fatigue life of panel slabs under moving and fixed pulsating loads [18]. The applicability of the bridging stress degradation concept was further extended to predict the fatigue behavior of the panel slabs reinforced with plain reinforcement bars [19]. These studies confirm the validity of the fatigue analysis method based on the bridging stress degradation concept for panel slabs.

However, in these studies, the panel slabs were subjected to a constant loading sequence. In a constant loading sequence, a moving wheel load of constant amplitude is applied for a higher number of cycles, as shown in **Figure 2.1**. On the other hand, a stepwise loading sequence is introduced in the improved specification of the road bridge for the fatigue durability of the slab. In a stepwise loading sequence, after a specific number of loading cycles, the intensity of the wheel load is amplified in increments to stimulate deterioration during early phases to save time, as shown in **Figure 2.1**. Thus, the applicability of this fatigue analysis method for a panel slab subjected to stepwise loading sequence has to be investigated.

Therefore, in this chapter, the applicability of the fatigue analysis method based on the bridging stress degradation concept is investigated for a panel slab subjected to a stepwise loading sequence. For this purpose, fatigue analysis of a panel slab subjected to a stepwise loading sequence is conducted, and the fatigue analysis results are compared with the experimental ones. The comparison confirms that the fatigue analysis method considering the bridging stress degradation successfully simulates the fatigue behavior of the panel slab subjected to stepwise loading sequence.

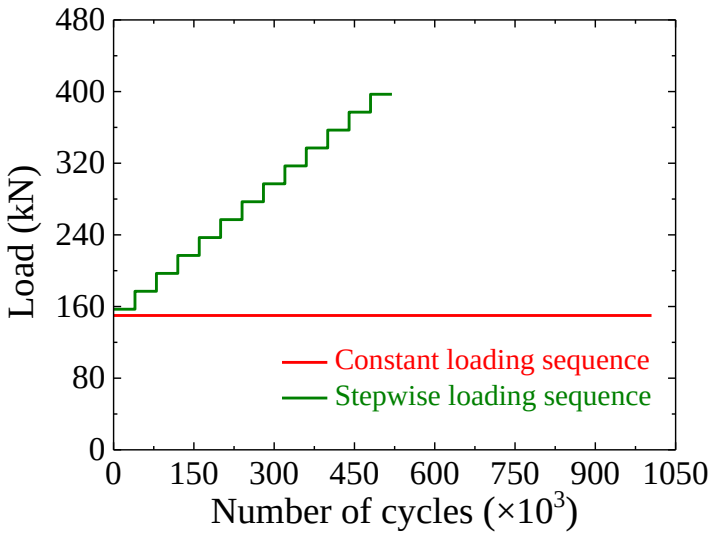

Figure 2.1 Loading sequences

This chapter is divided into two major parts: introduction of the fatigue analysis method; and applicability of the fatigue analysis method to the panel slab subjected to a stepwise loading sequence.

2.2 FATIGUE ANALYSIS METHOD

The fatigue analysis method is a finite element method (FEM) based numerical model considering the bridging stress degradation. The method consists of three major components: concrete model, reinforcement bar model, and analytical procedure.

2.2.1 Concrete model

Concrete is a compound material that is composed of different aggregates bonded together with fluid cement. Due to the composition of different materials, concrete is heterogynous, and it exhibits nonlinear inelastic behavior under various loading conditions. To represent the nonlinear behavior of concrete, a concrete model composed of nonlinear constitutive laws of concrete, bridging stress degradation due to fatigue loading, and crack formation of concrete are employed in the fatigue analysis method.

2.2.1.1. Nonlinear constitutive laws of concrete

In order to represent the stress-strain relationship of concrete, numerous empirical equations have been proposed in the past studies. However, the nonlinear model of concrete proposed by Maekawa et al. (2003) is a widely employed model to represent the stress-strain relationship of concrete [25]. Therefore, in this fatigue analysis method, the nonlinear model of concrete proposed by Maekawa et al. (2003) is employed. According to this nonlinear model, the stress-strain relationships of concrete under compression and tension can be categorized into four distinct parts, as shown in **Figure 2.2**.

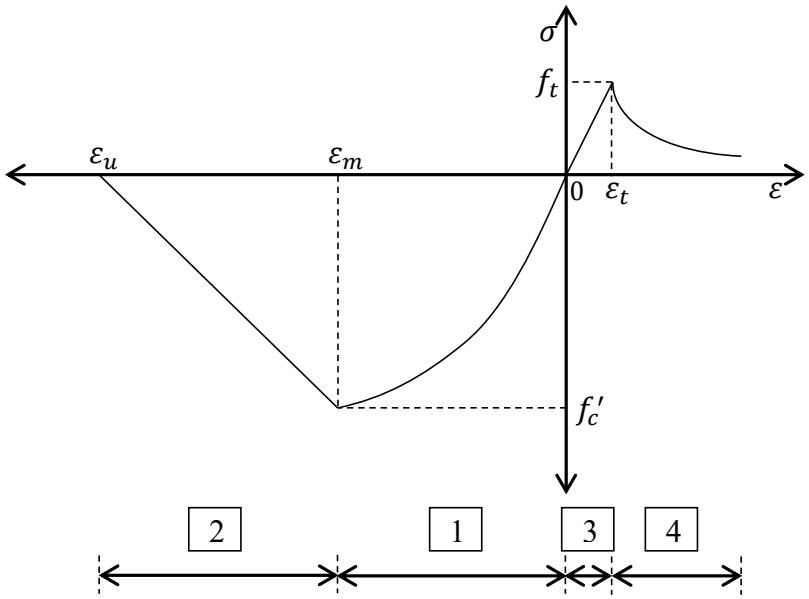

Figure 2.2 Stress-strain relationships of concrete

The first two parts represent the behavior of concrete in compression. The first part illustrates the stress-strain relationship under compression before peak stress. This peak stress is denoted by f_c', which is also called a compressive strength of concrete. This compressive relationship between stress (σ) and strain (ε) before peak stress can be expressed as:

$$\sigma = f_c' \frac{\varepsilon}{\varepsilon_m}\left(2 - \frac{\varepsilon}{\varepsilon_m}\right) \qquad \text{for } 0 \geq \varepsilon \geq \varepsilon_m \tag{2.1}$$

where ε_m is the strain value corresponding to f_c', which can be determined as follows:

$$\varepsilon_m = 2\frac{f_c'}{E_c} \tag{2.2}$$

where E_c is the elastic modulus of concrete.

The second part represents the compressive stress-strain behavior after peak stress. After peak stress, the stress-strain behavior is considered linear, as shown in **Figure 2.2**. The stress-strain relationship in this softening part can be expressed with the following equation:

$$\sigma = f_c' \frac{\varepsilon_u - \varepsilon}{\varepsilon_u - \varepsilon_m} \qquad \text{for } \varepsilon_m \geq \varepsilon \geq \varepsilon_u \tag{2.3}$$

where ε_u is the strain value corresponding to zero stress, which can be determined as follows:

$$\varepsilon_u = 3\varepsilon_m \tag{2.4}$$

The third and fourth parts represent the behavior of concrete in tension. The third part shows the stress-strain relationship under tension before cracking. Before cracking, the stress-strain relationship is considered linear until the tensile strength of concrete (f_t), which is shown by the following equation:

$$\sigma = E_c \varepsilon \qquad \text{for } \varepsilon_t \geq \varepsilon \geq 0 \tag{2.5}$$

where ε_t is the cracking strain of concrete, which can be calculated as follows:

$$\varepsilon_t = \frac{f_t}{E_c} \tag{2.6}$$

The fourth part represents the tensile stress-strain behavior after cracking. In this part, after cracking, the stress-strain behavior is considered nonlinear, as shown in **Figure 2.2**. The nonlinear stress-strain relationship in this part can be represented with the following equation:

$$\sigma = f_t \left(\frac{\varepsilon_t}{\varepsilon}\right)^{0.4} \qquad \text{for } \varepsilon > \varepsilon_t \tag{2.7}$$

2.2.1.2. Bridging stress degradation and concrete behavior under cyclic loading

The bridging stress degradation concept is employed as a fatigue-induced degradation phenomenon in this fatigue analysis. According to this degradation concept, after the application of the first loading cycle, a crack begins with length (a) and width (w), as displayed in **Figure 2.3**. However, with increases in the loading cycles, the opening and closing process of the crack occurs and results in a decrease of bridging stress between the surfaces of the crack, which is referred to as bridging stress degradation [17]. Consequently, the length and width of the existing crack increase by da and dw, respectively, leading to crack propagation. The bridging stress degradation equation is expressed as follows:

$$\frac{\sigma_N}{\sigma_1} = 1 - d\,\log(N) \tag{2.8}$$

where σ_1 and σ_N are the bridging stresses at the first and Nth cycles, respectively; and d represents the stress degradation factor, which is associated to the maximum width (W_{max}) of crack as:

$$d = d_0 + \gamma W_{max} \tag{2.9}$$

where d_0 is the stress degradation factor at $W = 0$; and γ is the slope of the linear relationship between d and W_{max} [26]. This model has been validated for plain concrete under repetitive uniaxial tensile loading by Zhang (1998) and found to have satisfactory results for d_0=0.08 and γ=4 mm^{-1} [27]. The tensile stress-strain relationship of concrete under cyclic loads is displayed in **Figure 2.4**.

2.2.1.3. Crack formation of concrete

The process of crack formation in the concrete matrix is demonstrated in **Figure 2.5** [18]. The cracks are permitted to be initiated in three perpendicular directions for each crack element. As the concrete strain in tension exceeds the cracking strain of concrete, the first crack is supposed to originate in the direction that is perpendicular to the maximum principal strain, which is shown in **Figure 2.5(a)**. Subsequently, the second crack can propagate when the tensile strain perpendicular to the first crack exceeds the cracking strain, and this is followed by the initiation of the third crack that is perpendicular to the first and second cracks when the tensile strain surpasses the cracking strain in that direction, as illustrated in **Figure 2.5(b)**.

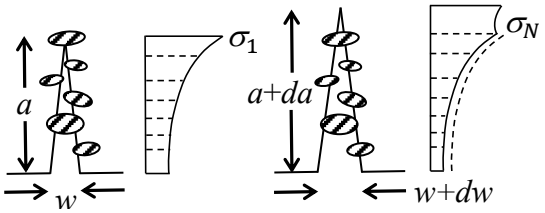

(a) First cycle **(b)** Nth cycle

Figure 2.3 Crack propagation due to bridging stress degradation

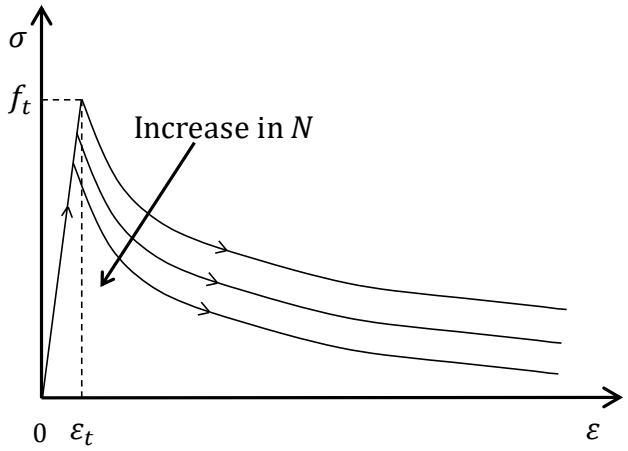

Figure 2.4 Tensile behavior of concrete under cyclic loading

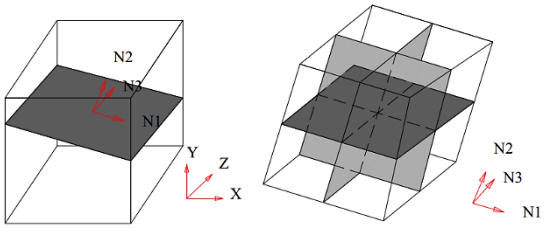

(a) Initiation of first crack **(b)** Three perpendicular crack formation

Figure 2.5 Crack formation [18]

2.2.2 Reinforcement bar model

To model the reinforcement bar embedded in the concrete, two distinct approaches are normally used; discrete and smeared approaches. In a discrete approach, the reinforcement bar is simulated as truss elements with geometric properties similar to the original reinforcement bar. These truss elements are directly generated from the nodes in the model. On the other hand, in a smeared approach, the concrete and reinforcement bar are discretized into elements with the same geometrical boundaries, and the effects of reinforcement bar are averaged within the pertaining elements.

2.2.2.1. Smeared modeling approach for reinforcement bar

The smeared modeling approach for reinforcement bar embedded in concrete posses ses several advantages over the discrete modeling approach, such as easily applicability and quick convergence. Moreover, the reliability of the smeared modeling approach has been confirmed in the previous studies by comparing with the experimental studies. Therefore, in this study, the smeared modeling approach is employed as well to model the reinforcement bar embedded in the concrete, as displayed in **Figure 2.6**.

The total stress of an RC element can be determined as follows:

$$\sigma_{rc} = (1 - \rho)\sigma_c + \rho\sigma_s \tag{2.10}$$

$$\rho = \frac{A_s}{A_c} \tag{2.11}$$

where σ_{rc}, σ_c, and σ_s represent the stresses for RC element, concrete, and reinforcement bar, respectively; ρ is the reinforcement ratio; A_s is reinforcement bar area; and A_c is concrete area.

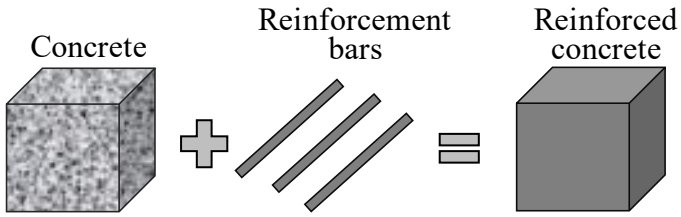

Figure 2.6 Smeared modeling approach

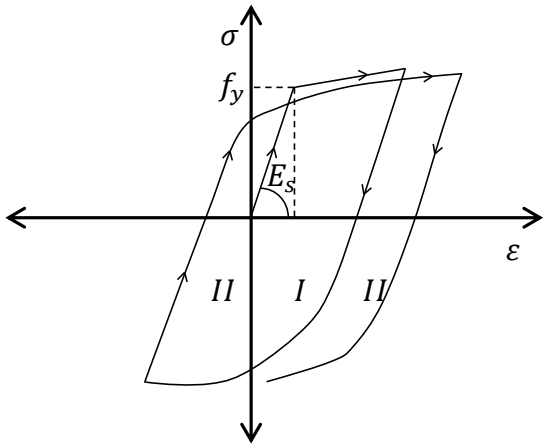

Figure 2.7 Tensile behavior of reinforcement bar under cyclic loading

2.2.2.2. Cyclic behavior of reinforcement bar

To represent the behavior of the reinforcement bar in tension under cyclic loading, the Giuffré-Menegotto-Pinto model is employed as follows [28]:

$$\frac{\sigma}{f_y^*} = H\frac{\varepsilon}{\varepsilon_y^*} + \frac{(1-H)\frac{\varepsilon}{\varepsilon_y^*}}{\left(1+\left(\frac{\varepsilon}{\varepsilon_y^*}\right)^R\right)^{1/R}} \tag{2.12}$$

where f_y^* and ε_y^* are the normalized stress and strain, respectively; H is the hardening parameter; and R is the parameter that affects the shape of the transition curve. The parameter R is expressed as a function of the plastic excursion (ξ_{max}) as follows:

$$R = R_0 - \frac{a_1\xi_{max}}{a_2 - \xi_{max}} \tag{2.13}$$

where R_0 is the value of R for the first loading; a_1 and a_2 are the parameters for the transition of R with cyclic loading, which are experimentally determined as 18.5 and 0.00015, respectively. The yield strength decreases with the increase in the number of loading cycles, as shown in **Figure 2.7**.

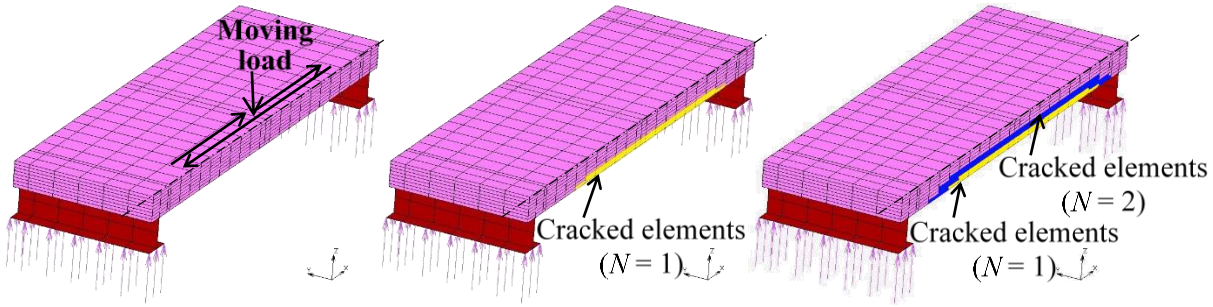

(a) Analytical model **(b)** 1st cycle **(c)** 2nd cycle

Figure 2.8 Analytical procedure

2.2.3 Analytical procedure

Using an FEA software MARC [29], the panel slab is modeled and analyzed. Eight-node 3D solid elements and four-node 3D shell elements are used for the panel slab and steel I-beams, respectively, as shown in **Figure 2.8(a)**. By taking advantage of the symmetrical boundary and loading conditions, only one half of the panel slab is modeled and analyzed to save the computational time. The moving load is applied to the elements in the center of the slab in such a way that the load is first assigned to these elements, and is followed by unloading of these elements and simultaneous loading of adjacent elements making the load movement to be back and forth along the longitudinal direction.

The cracked elements that appeared after the application of the first cycle of moving load are shown in **Figure 2.8(b)**. Consequently, the constitutive laws for the cracked elements are amended considering the bridging stress degradation, and the second loading cycle is applied. The new cracked elements appeared after the second loading cycle, as shown in **Figure 2.8(c)**. The overall panel slab stiffness is reduced with increases in the cycles of the moving wheel loads because of bridging stress degradation and cracked elements propagation. This procedure is repeated until the last loading cycle, and the results are recorded for each loading cycle.

2.3 APPLICABILITY OF FATIGUE ANALYSIS METHOD

In the previous section, section 2.2, the fatigue analysis method based on the bridging stress degradation concept has been explained in detail. In order to confirm the applicability of this method for a panel slab subjected to stepwise loading sequence, a panel slab is selected from the technical note of the National Institute for Land and Infrastructure Management (NILIM), Japan [16]. The reason for choosing this slab is that the panel slab has been designed according to the recent design specifications for highway bridges [30], incorporating improved fatigue durability of slabs and increased loading levels. Moreover, for the comparison purpose, the data of experimental and numerical studies conducted by NILIM, Japan, is available for this panel slab [16].

2.3.1 Details of the panel slab

The panel slab used in this study is an RC plate with (L×W×H) dimensions of (4500×2800×250) mm. In the tension zone, the slab is reinforced with D19@150 mm along the transverse direction and D16@125 mm along the longitudinal direction. Similarly, D19@300 mm along the transverse direction and D16@250 mm along longitudinal direction are provided in the compression zone. The slab dimensions, reinforcement details, and moving wheel load zone are shown in **Figure 2.9**.

The material properties of the concrete and steel reinforcement bars of the panel slab are presented in **Table 2.1**.

2.3.2 Boundary conditions

In the experimental and numerical studies by NILIM [16], the panel slab is equipped with BCs to represent the bridge slab in the continuation of the adjacent spans. The same BCs with these studies by NILIM are employed in this study as well, as shown in **Figure 2.10**. Simple supports along the longitudinal edges and steel I-beams along the transverse edges of the slab are used as BCs of the panel slab. The bottom flanges of the steel I-beams are restrained for vertical displacement.

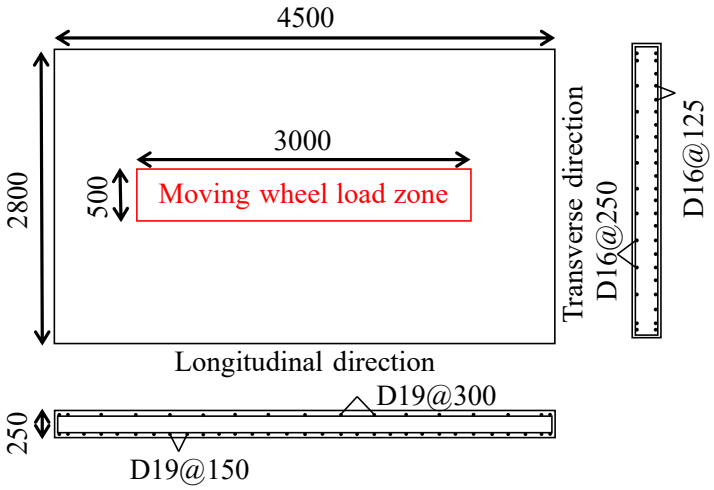

Figure 2.9 Dimensions and reinforcement details of the panel slab (mm)

Table 2.1 Material properties [16]

Material	Property	Value (MPa)
Concrete	Compression strength (f_c')	33.1
	Tensile strength (f_t)	1.9
	Elastic modulus (E_c)	27,900
Steel reinforcement bars	Yield strength (f_y)	345
	Elastic modulus (E_s)	200,000

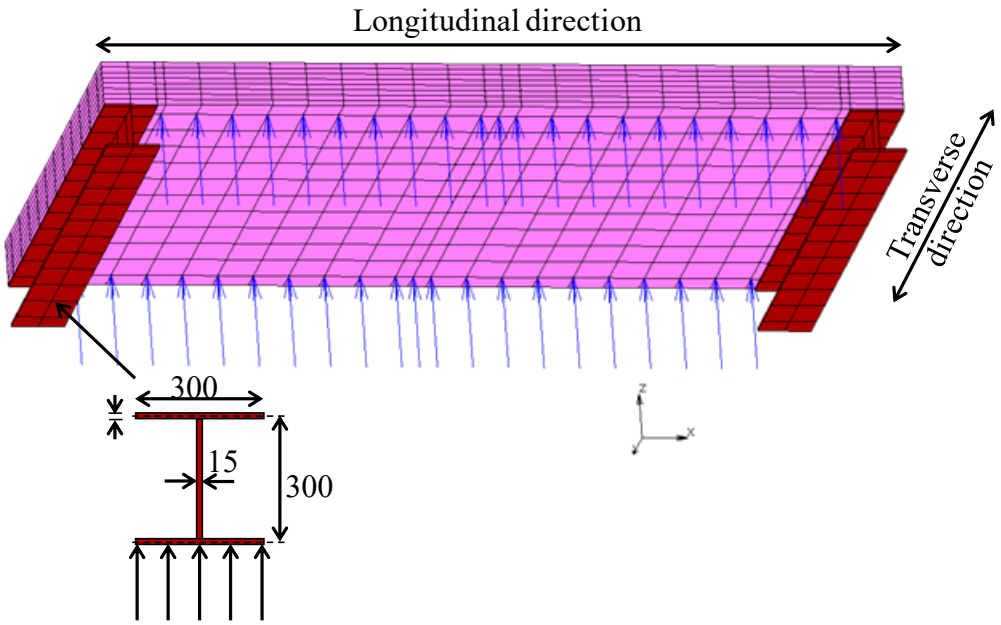

Figure 2.10 Illustrations of the BCs (mm)

2.3.3 Stepwise loading sequence

The panel slab is subjected to a moving wheel load along the longitudinal direction with the dimensions of the loading zone of (3000 × 500) mm. The same stepwise loading sequence with the studies by NILIM has been used [16]. In the stepwise loading sequence, the magnitude of moving wheel load is increased in intervals after a certain number of cycles to promote the deterioration at the early stages to save time. The stepwise loading sequence used in this study, which has an initial value of 157 kN and an increasing step of 19.6 kN load after every 40,000 cycles of moving wheel load, is shown in **Figure 2.11**.

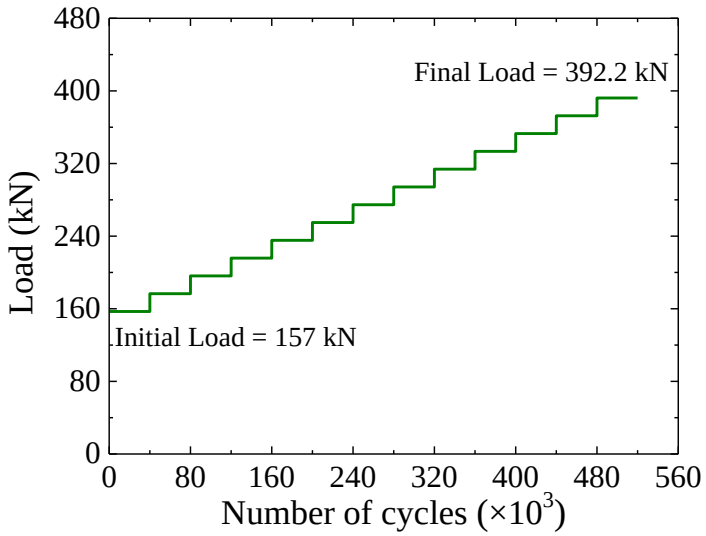

Figure 2.11 Stepwise loading sequence

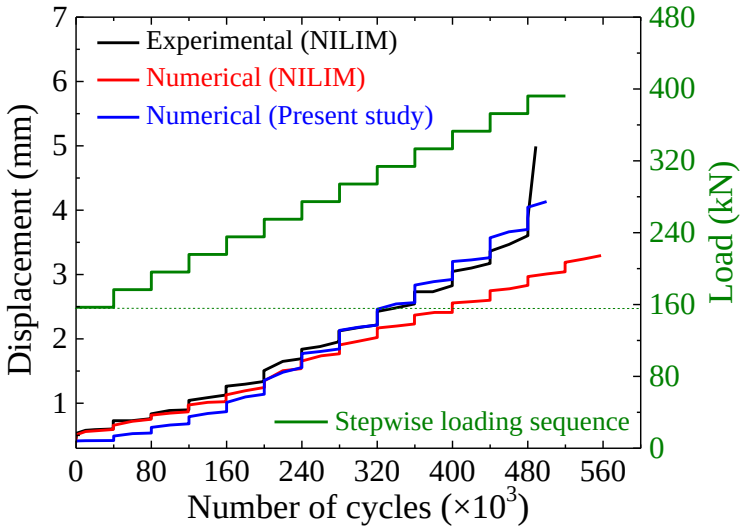

Figure 2.12 Centre displacement evolution

2.4 FATIGUE ANALYSIS RESULTS

Fatigue analysis based on the bridging stress degradation concept is conducted for a panel slab subjected to a stepwise loading sequence.

2.4.1 Center displacement evolution

The displacements at the center of the panel slab obtained during the fatigue analysis at different loading cycles in this study and numerical study by NILIM are compared with displacements observed in the experiment, as shown in **Figure 2.12**.

In the numerical method by NILIM, the damage accumulation theory (miner's rule) has been employed, and the cumulative damage degree of the concrete element after the analysis step is calculated. If the cumulative damage degree reaches 1, the concrete element is considered to be cracked, and the elastic modulus of the cracked concrete element is reduced to 1/10th of the original elastic modulus. The two extreme stages have been considered whether the concrete element is undamaged or damaged completely. In reality, the stiffness of the concrete element gradually reduces due to the fatigue phenomenon. The approach of treating the element between healthy and damaged has resulted in smaller displacements as compared to experimental ones.

In this present numerical model based on the bridging stress degradation concept, the bridging stress degradation equation is introduced after the initiation of cracking. After each analysis step, the reduction of bridging stress in the concrete element is employed majorly depending upon the number of cycles (N) and maximum tensile strain (ε_t). Also, cracks are permitted to begin in three perpendicular directions in each cracked element according to the principal stress cracking criteria. The numerical model predicts smaller center displacements at initial cycles as compared to those of experimental, but it well accurately predicts the similar center displacements to experimental

ones after initial cycles of moving load. The reason for the accurate displacement prediction is that the numerical model is able to capture the dominant degradation mechanism. However, the degradation mechanism may not be so dominant in the initial cycles.

2.4.2 Propagation of cracked elements

This numerical model considers the primary aspect that the propagation of cracked elements and degradation of bridging stress are the core reasons for the fatigue failure. Thus, it is significant to show the propagation of cracked elements. The uncracked elements are indicated by white color, and the cracked elements after the first cycle of moving load are displayed by red color. Similarly, the cracked elements caused by a different number of cycles are indicated with different colors, as shown in **Figure 2.13**.

After the first cycle of moving wheel load, only six elements on the bottom of the panel slab are cracked, as displayed in **Figure 2.13**. With the increase in the number of cycles of moving wheel load, the cracked elements propagate in the longitudinal, transverse and vertical directions. This is because the bridging degradation of the concrete occurs due to the process of crack opening and closing. The load capacity from the concrete bridging stress cannot reach the same level as in the 1st cycle with the already formed cracked state, and the cracked elements propagate in the other directions to reach the load level. At the 200,000th cycle, the cracked elements propagate in the diagonal direction and reach to the corner supports. At the 280,000th cycle, almost all the elements on the bottom surface of the panel slab are cracked, and the cracked elements propagate vertically up to 3/4th of the total thickness of the panel slab at the loading point and corner supports. At the last cycle of moving wheel load (i.e., 500,000th cycle), the corner supports are entirely cracked, and the cracked elements propagate in a diagonal direction on the upper layers from the corner supports. This is because the corner supports experience a negative bending, and the top surface elements of the corner supports are cracked.

Figure 2.14 shows a comparison of the maximum principal strain distribution on the bottom surface of the panel slab after 1st cycle and last cycle. In all contours, the maximum principal strain value is higher than the cracking strain value of the concrete except for the contour shown by dark gray color. The maximum principal strain is found to be increased in a diagonal direction from the loading point towards the supporting corner. The increase in maximum principal strain in the diagonal direction verifies the propagation of cracked elements in the diagonal direction shown in **Figure 2.13**.

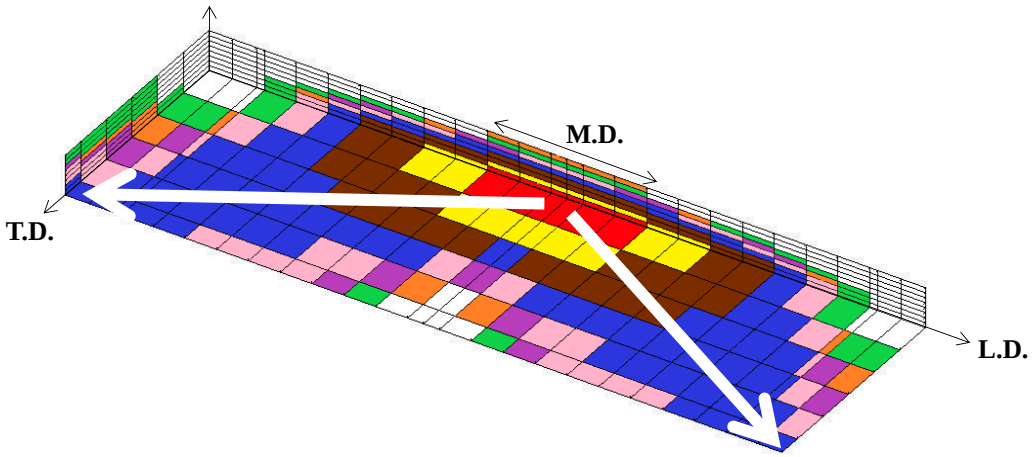

N1 N40,000 N120,000 N200,000 N280,000 N360,000 N440,000 N500,000

M.D.: Moving Direction **L.D.**: Longitudinal Direction **T.D.**: Transverse Direction

Figure 2.13 Propagation of cracked elements

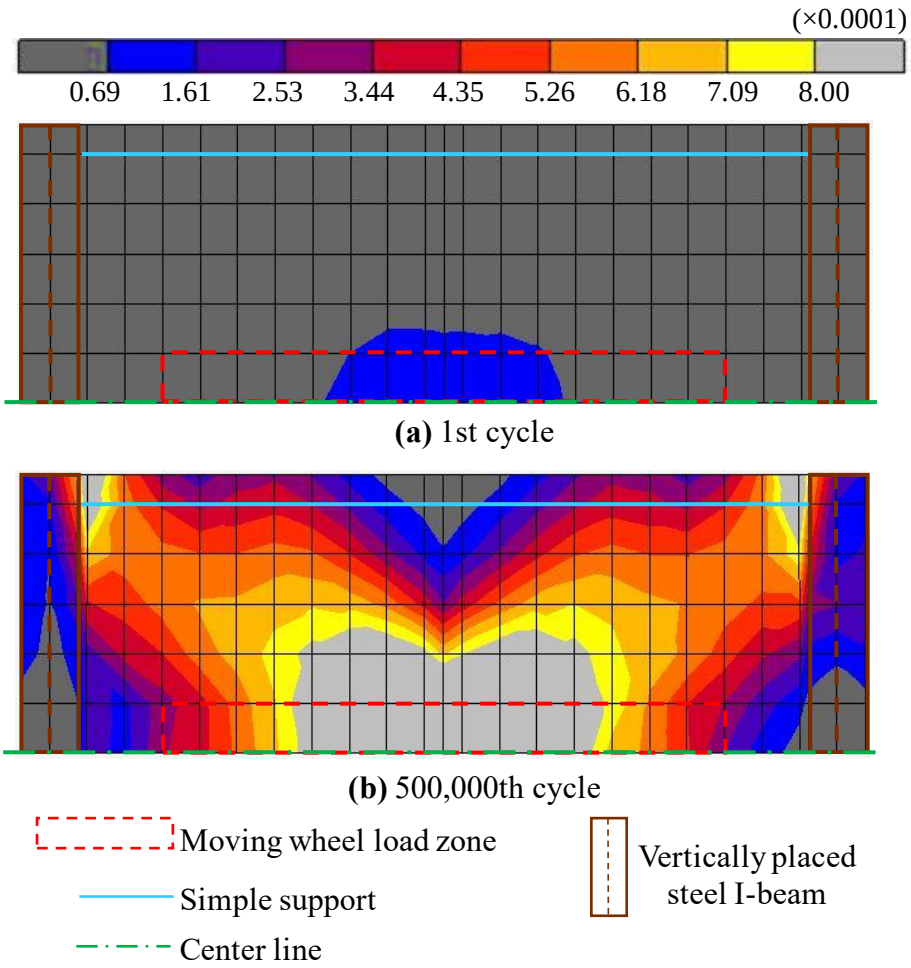

(a) 1st cycle

(b) 500,000th cycle

Figure 2.14 Maximum principal strain distribution on the bottom surface

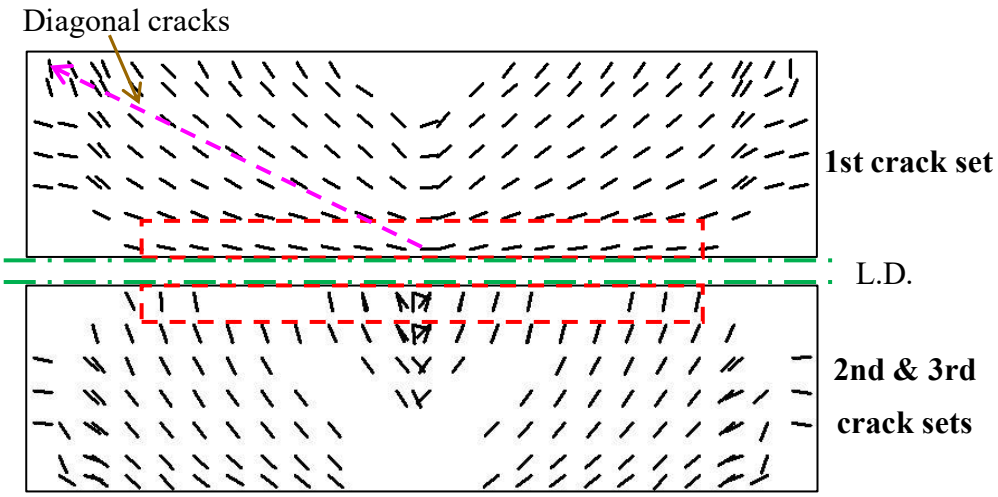

Figure 2.15 Crack pattern

2.4.3 Crack pattern

The crack pattern on the bottom surface of the panel slab under the moving wheel load at the last loading cycle is displayed in **Figure 2.15**. The main crack originates at the center, which is the first location of the moving wheel load; subsequently, it extends to the supporting corners. As the load begins to move, the diagonal cracks are formed between the locations of the moving wheel load in the longitudinal direction and the supporting corner, making the first crack set. At the same time, other cracks are formed perpendicular to the existing cracks as second and third crack sets, surrounding the moving wheel load zone. An increase in the number of cycles has resulted in much more extensive cracking. This numerical study predicts the same diagonal crack pattern in the panel slab, as observed in the experimental research by NILIM [16].

2.5 SUMMARY AND CONCLUSIONS

A fatigue analysis method based on the bridging stress degradation concept has been developed in the past studies to simulate the fatigue behavior of panel slabs [12, 19]. In these studies, the panel slabs are subjected to a constant loading sequence. However, a stepwise loading sequence has been introduced in the improved specification of the road bridge for the fatigue durability of the slabs. The panel slabs employed in this study, chapters 4 and 6, are subjected to a stepwise loading sequence. Thus, the applicability of this fatigue analysis method based on the bridging stress degradation concept for the panel slabs subjected to stepwise loading sequence has to be investigated.

Therefore, in this chapter, the fatigue analysis method based on the bridging stress degradation concept is introduced, and its applicability for the panel slab subjected to stepwise loading sequence is investigated. For this purpose, the fatigue analysis of a panel slab subjected to stepwise loading sequence is conducted. The center displacement evolutions of the panel slab obtained in this study

and numerical study by NILIM are compared with the experimental one.

The developed fatigue analysis method based on the bridging stress degradation concept for the panel slab shows a good agreement with the experimental results.

The fatigue analysis method successfully simulates the fatigue behavior, such as center displacement evolution, propagation of cracked elements, and crack pattern, of the panel slab subjected to stepwise loading sequence.

Chapter 3

METHOD FOR DETERMINATION OF APPROXIMATE BCS FOR A PANEL SLAB

3.1 GENERAL

The bridge slabs are susceptible to fatigue failure, as they directly sustain heavy traffic loads. To investigate the fatigue failure of the bridge slabs, Okada et al. (1978) and Maeda and Matsui (1984, 1987) have developed the test set-ups in their studies [6-8]. In these studies, a panel of a bridge slab has been considered due to limitations in cost, time, and space. In order to represent the bridge slab with continuity to adjacent spans, the BCs comprised of simple supports along the longitudinal edges and steel I-beams along the transverse edges of the panel slab have been used. Following the same concept, different institutes, such as Public Work Research Institute (PWRI), Civil Engineering Research Institute (CERI), and NILIM, have developed their own test set-ups of the panel slabs with BCs. After that, many researchers have also adopted the same concept of the panel slabs with typically used BCs in their experimental and numerical studies [9-11, 18, 19].

However, the panel slabs with typically used BCs failed to reproduce the behaviors of the bridge slabs. For example, in a bridge slab, the bending moment distribution and deformations around the loading locations remain almost unchanged as the load moves along the slab axis [20, 21]. On the other hand, a panel slab with typically used BCs shows remarkable variations of bending moment distribution and deformations as the wheel load moves along the slab axis. Moreover, the typically used BCs lead to cracks originating from the loading point and propagating in a diagonal direction towards the corners of the panel slab. This is unlike the extensive grid crack pattern that is generally observed in the bridge slabs [6, 24]

Therefore, in this chapter, new BCs for the already available panel slabs are proposed, which approximately investigate the realistic behaviors of the bridge slabs. By following the proposed method in this chapter, one can easily determine the approximate BCs for different dimensions of the already available panel slabs as well capable of reproducing the realistic behaviors of the bridge slabs.

3.2 PROBLEM FORMULATION

To facilitate the investigation of fatigue behavior of a bridge slab, a panel slab equipped with BCs comprising of simple supports along the longitudinal edges and steel I-beams along the transverse edges have been generally employed in the previous studies [7-10]. The steel I-beams

in the typically used BCs restrict the panel slab from experiencing the same bending moment distribution and displacements around the loading locations as the wheel load moves along the slab axis. However, in a bridge slab, the bending moment distribution and displacements around the loading locations remain almost unchanged as the wheel load moves along the slab axis. A bridge slab and its corresponding panel slab with the typically used BCs are shown in **Figure 3.1**, where the deformations of both slabs under the same load are shown schematically as well. Even though the displacements at the location of the load application are almost the same for both the bridge slab and its corresponding panel slab, the displacements deviate from each other at locations away from the loading point. This difference is more pronounced near the steel I-beams in the panel slab, as can be seen in **Figures 3.1(c, d)**. This is because the vertically placed steel I-beams along the transverse edges restrict the displacement of the panel slab at the supports, which is contrary to the case of a bridge slab. Furthermore, the vertically placed steel I-beams lead to a difference in the rotation around the steel I-beams in the panel slab, from that of the bridge slab, as shown in **Figure 3.1(c, d)**.

In a bridge slab, the displacement (δ_{real}) and rotation (θ_{real}) at the corresponding locations of the transverse edges of the panel slab are constrained from the adjacent parts of the RC slab rather than any vertical support as shown in **Figure 3.1(c)**. To simulate the deformation in the panel slab, the steel I-beams are horizontally placed along the transverse edges of the panel slab in this study. As a result, the real deformation of the bridge slab can be reproduced in the panel slab by adjusting the bending and rotational stiffness of the horizontally placed I-beams.

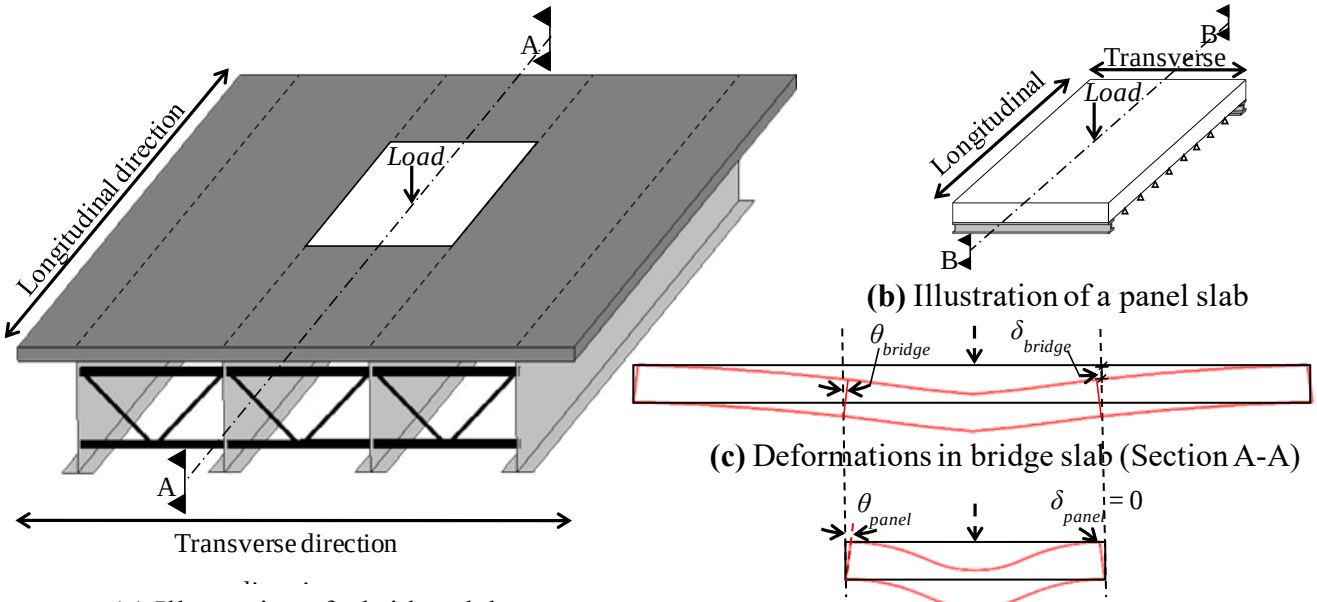

(a) Illustration of a bridge slab

(b) Illustration of a panel slab

(c) Deformations in bridge slab (Section A-A)

(d) Deformations in panel slab (Section B-B)

Figure 3.1 Illustration of a bridge slab and the corresponding panel slab, and a comparison of their deformations

3.3 DETERMINATION OF APPROXIMATE BCS FOR A PANEL SLAB

The flowchart of the method used to determine the approximate BCs for the panel slab is shown in **Figure 3.2**, wherein the panel slab is modeled in an FEA software. To save time and simplify the calculation of the sectional moments in the panel slab, an elastic analysis method is considered in this chapter. Moreover, the panel slab without reinforcement bars is considered in the elastic analysis method. The elastic analysis method is available, and most design codes permit its use for the RC slabs [31]. The height of the flange, length of the web, and web thickness of the steel I-beam are assumed to be constant parameters. However, the flange thickness of the steel I-beam is considered as a variable parameter, since the bending stiffness of the steel I-beam in this horizontal orientation is majorly depended upon the flange thickness. By varying the flange thickness, the bending stiffness of the steel I-beam is changed, which changes the deformation behavior of the panel slab. Thus, with an appropriate flange thickness of the steel I-beam, the deformation behavior of the panel slab similar to that of a bridge slab can be achieved.

A panel slab with loading locations is displayed in **Figure 3.3**. A static load is applied at the center of the loading zone (loading location A), and the elastic analysis is carried out. The bending moments parallel to the x- and y-axes (M_{xx} and M_{yy}, respectively) are calculated in the panel slab equipped with the selected BCs. Similarly, M_{xx} and M_{yy} are computed for the loading locations away from the center of the loading zone (i.e., at loading locations B, C, and D). To determine the cracking zones for the bending moments, the cracking bending moment (M_{crack}) is calculated as follows:

$$M_{crack} = \frac{\sigma_t I_c}{y} \tag{3.1}$$

where I_c is the second moment of area per unit width; σ_t is the tensile strength of the concrete; and y is equal to half of the slab thickness. The cracking zones for M_{xx} and M_{yy} are checked for loading locations A, B, C, and D. If the cracking zones are similar around all the loading locations for M_{xx}, as well as M_{yy}, the assumed dimensions of the steel I-beams would allow the panel slab to experience the same bending moment distribution around all the loading locations. Consequently, the displacement profile in the longitudinal and transverse directions would also be the same for all the loading locations. In such a case, the assumed configuration for the BCs would be assigned to the approximate BCs for the panel slab. If the bending moment distribution around all the loading locations are not similar, the flange thickness of the steel I-beams would be further adjusted. This process is repeated until the approximate BCs are obtained for the panel slab.

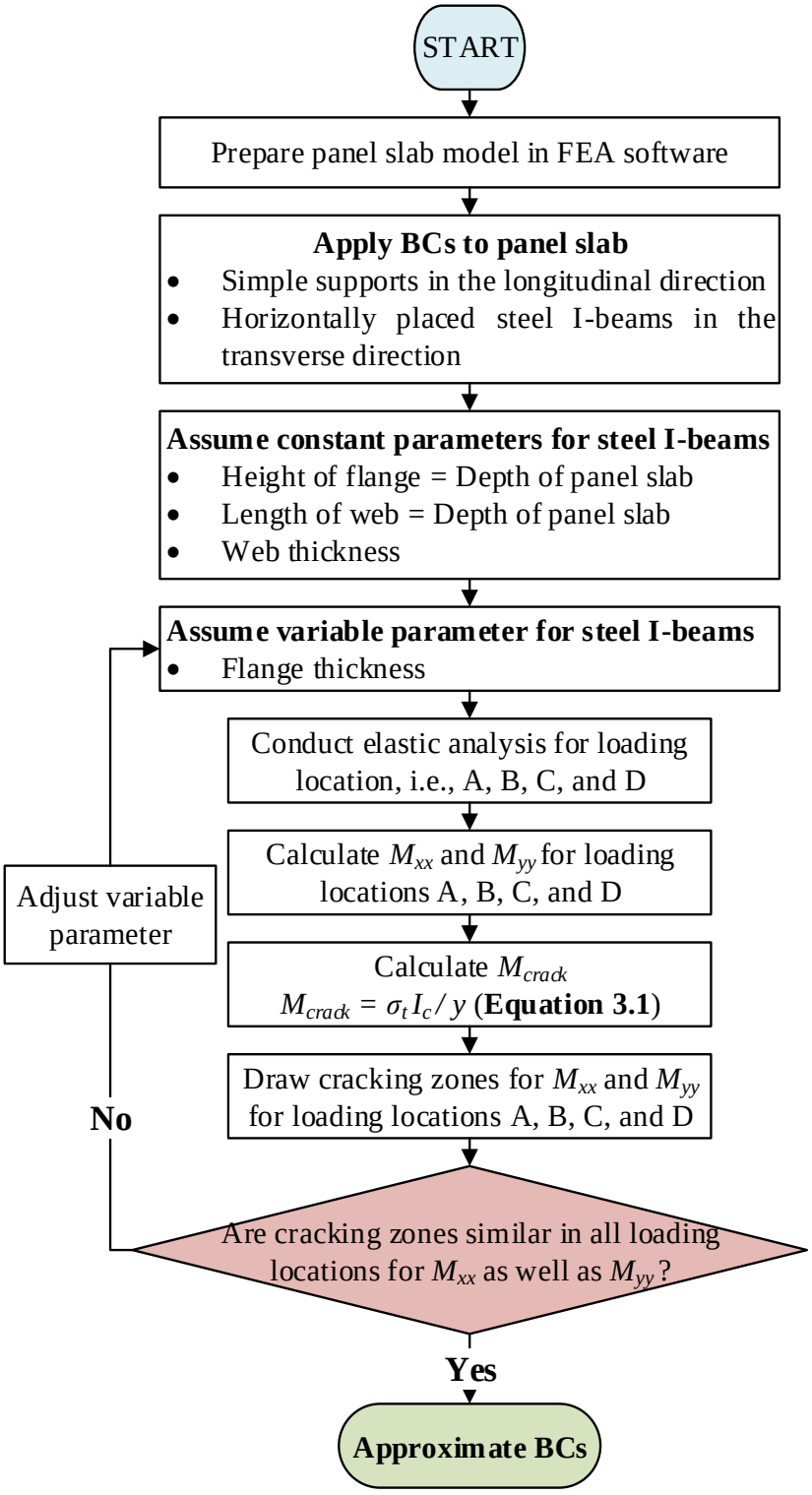

Figure 3.2 Method for the determination of approximate BCs for the panel slab

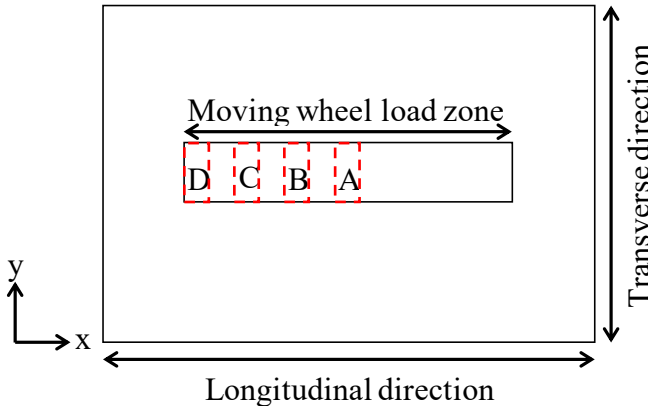

Figure 3.3 Plan view of the panel slab showing the loading locations

Table 3.1 Material properties

Material	Property	Value (MPa)
Concrete	Compression strength (f_c')	33.1
	Tensile strength (f_t)	1.9
	Elastic modulus (E_c)	27,900
Steel rebar	Yield strength (f_y)	345
	Elastic modulus (E_s)	200,000

3.4 STATIC ANALYSIS OF THE PANEL SLAB

Using an FEA software MARC [29], only one half of the panel slab is modeled in view of the symmetry in the loading and boundary conditions. Static analysis of the panel slab is conducted for the different loading locations, i.e., loading locations A, B, C, and D.

3.4.1 Description of the panel slab

For static analysis of the panel slab, the panel slab is selected from the technical note of NILIM, Japan [16]. The reason for choosing this slab is that the panel slab has been designed according to the recent design specifications for highway bridges [30], incorporating improved fatigue durability of slabs and increased loading levels. The selected panel slab has (L×W×H) dimensions of (4500×2800×250) mm.

The same material properties of concrete and steel with the NILIM [16] are used for the panel slab, as presented in **Table 3.1**.

3.4.2 Boundary conditions

A total of five BCs cases are considered, as shown in **Figure 3.4**. In case 1, the same BCs with the experimental study [16] are considered. As discussed in detail in section 3.2, in a bridge slab, the displacement (δ_{real}) and rotation (θ_{real}) at the corresponding locations of the transverse edges of

the panel slab are constrained from the adjacent parts of the slab rather than any vertical support. Therefore, in case 2 to 5, the steel I-beams are horizontally placed as supports along the transverse edges of the slab to simulate the deformation in the panel slab. Moreover, the flange thickness of those horizontally placed steel I-beams is progressively varied. The reason for varying the flange thickness is to obtain the appropriate bending stiffness of the steel I-beams, which allows the panel slab to experience the same bending moment distribution and displacements around the loading locations as the load moves along the slab axis.

It is worth mentioning here that the primary objective of this study is to numerically propose the BCs for a panel slab for simulating the behaviors of a bridge slab. For the experimental study of the panel slab with the proposed approximate BCs, the experimental setup would be designed in such a way to ensure the proposed BCs.

3.4.3 Loading conditions

A static load of 157 kN, which is the initial load of the stepwise loading sequence, is applied at the center of the panel slab (loading location A). Elastic analysis of the panel slab is conducted for the static load at location. Similarly, the elastic analysis is conducted for the loading locations B, C, and D as well for the same load of 157 kN. The loading locations in the panel slab are displayed in **Figure 3.5**.

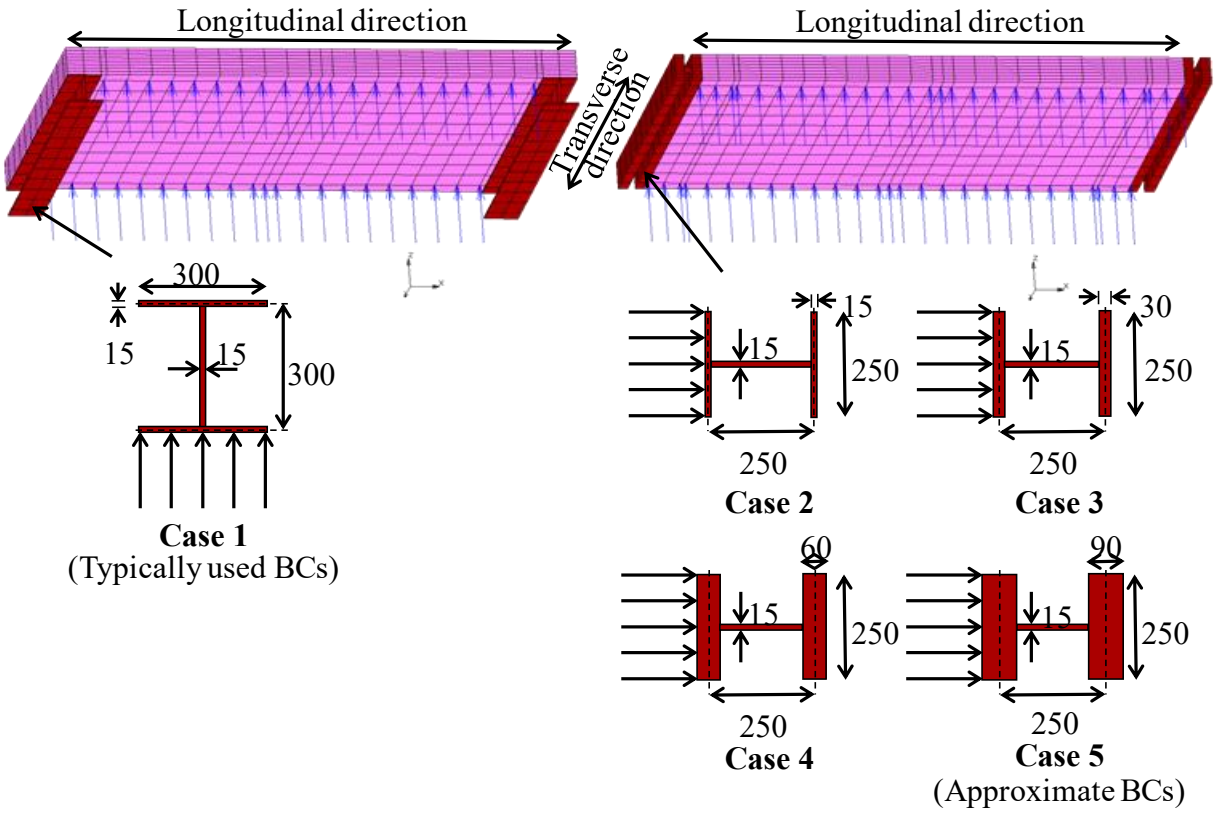

Figure 3.4 Illustration of the BCs (mm)

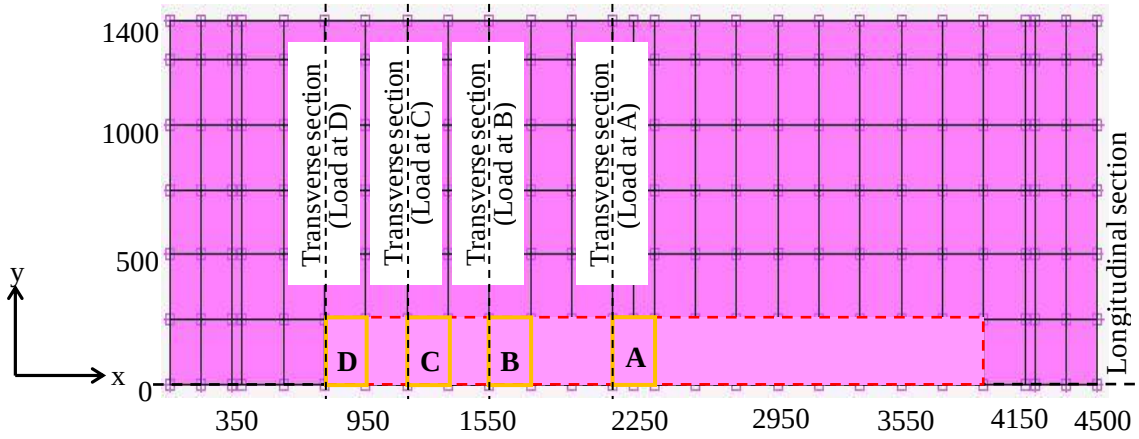

Figure 3.5 Loading locations in the panel slab

3.5 STATIC ANALYSIS RESULTS

Static analysis of a panel slab is conducted for different loading locations. A total of five BCs cases are considered in this study. The bending moments parallel to x- and y-axes (M_{xx} and M_{yy}, respectively) are calculated in the slab for the loading locations. To determine the cracking zones for the bending moments, the cracking bending moment (M_{crack}) is calculated using **Equation 3.1**.

Furthermore, the displacements in the longitudinal and transverse directions are obtained for the loading locations A, B, C, and D.

3.5.1 Bending moment cracking zones

A comparison of the bending moment cracking zones for M_{xx} and M_{yy} for the five cases of BCs is shown in **Figure 3.6**, corresponding to a static load of 157 kN applied at the loading locations A, B, C, and D successively.

For case 1, the cracking zones for M_{xx} due to the load at locations A, B, C, and D are similar to one another, as shown in **Figure 3.6(a)**. However, the cracking zones for M_{yy} are reduced significantly with an increase in the distance of the loading point from the center. This effect is more pronounced for the loading locations C and D. This is because the vertically placed steel I-beams result in a higher bending stiffness parallel to the y-axis. These strong steel I-beams restrict the panel slabs from possessing the same bending moment distribution and deformations around the loading locations as the wheel load moves along the slab axis. This phenomenon is contrary to that observed in a real bridge RC slab.

For cases 2, 3, and 4, the cracking zones for M_{xx} as well as the cracking zones for M_{yy} are quite different from each other, as shown in **Figures 3.6(b–d)**. However, the difference in bending moments cracking zones is reduced with an increase in the flange thickness of the steel I-beams. This is because the horizontally placed steel I-beams with appropriate stiffness in the transverse

direction allow the panel slab to experience the same deformations around the loading locations as the load moves along the slab axis.

For case 5, the cracking zones for M_{yy} due to the load at locations A, B, C, and D are approximately the same as one another. In addition, a similar trend is observed for the cracking zones for M_{xx} for all the loading locations (**Figure 3.6(e)**).

3.5.2 Displacement distribution

The displacements in the longitudinal and transverse sections for the loading locations A, B, C, and D are compared for the five cases of BCs and shown in **Figure 3.7**.

In **Figure 3.7(a)**, the displacement for the load at location A is quite high as compared to the displacements for the load at locations B, C, and D for case 1. This is because the steel I-beams play a significant role in reducing the displacements as the load moves along the slab axis. However, a bridge slab experiences the same displacements around the loading locations as the load moves along the slab axis.

The displacement for the load at location D is quite high compared to that at the other loading locations for case 2. It demonstrates that the horizontally placed steel I beams have low bending stiffness. For case 3, the bending stiffness of the steel I-beams is increased by increasing the flange thickness of the steel I-beams, which results in reducing the variation in the displacements around the loading locations, as shown in **Figure 3.7(c)**. The flange thickness of the steel I-beams is further increased for case 4, and consequently, the variation in the displacements around the loading locations is reduced even more significantly. Thus, the flange thickness of steel I-beams is increased more to minimize the displacement variation. For case 5, the bending stiffness of the steel I-beams becomes such that it allows the panel slab to experience the same displacements around all the loading locations (A, B, C, and D), as shown in **Figure 3.7(e)**.

A comparison of the displacement values for loading locations A, B, C, and D is made among all the five BCs cases, as presented in **Table 3.2**. The difference in the maximum displacement between loading locations A and D is 40.2% for case 1, which shows that the vertically placed I-beams reduce the displacement significantly as the load moves along the slab axis. The corresponding difference in the maximum displacement is –22.1% for case 2, implying that the bending stiffness of the steel I-beams is very low when placed horizontally. As the flange thickness of the steel I-beams is increased for cases 3, 4, and 5, the bending stiffness is improved in these cases, resulting in the decrease of the displacement difference, as can be seen from **Table 3.2**. Finally, the difference in the maximum displacement between the loading locations A and D is decreased to a reasonably small value of –3.1% for case 5, which is determined as the approximate BCs. This observation implies that the panel slab with approximate BCs experiences almost the

same displacements around the loading locations as the load moves along the slab axis. As discussed earlier in detail in section 3.2, in a bridge slab, the displacements are not restricted by any vertical support at the corresponding locations of the transverse edges of the panel slab (see **Figure 3.1**). As a result, displacements around the loading locations would remain almost similar as the load moves along the slab axis of the bridge slab. Thus, it can be safely said that the panel slab with approximate BCs can replicate the displacement behavior of a bridge slab.

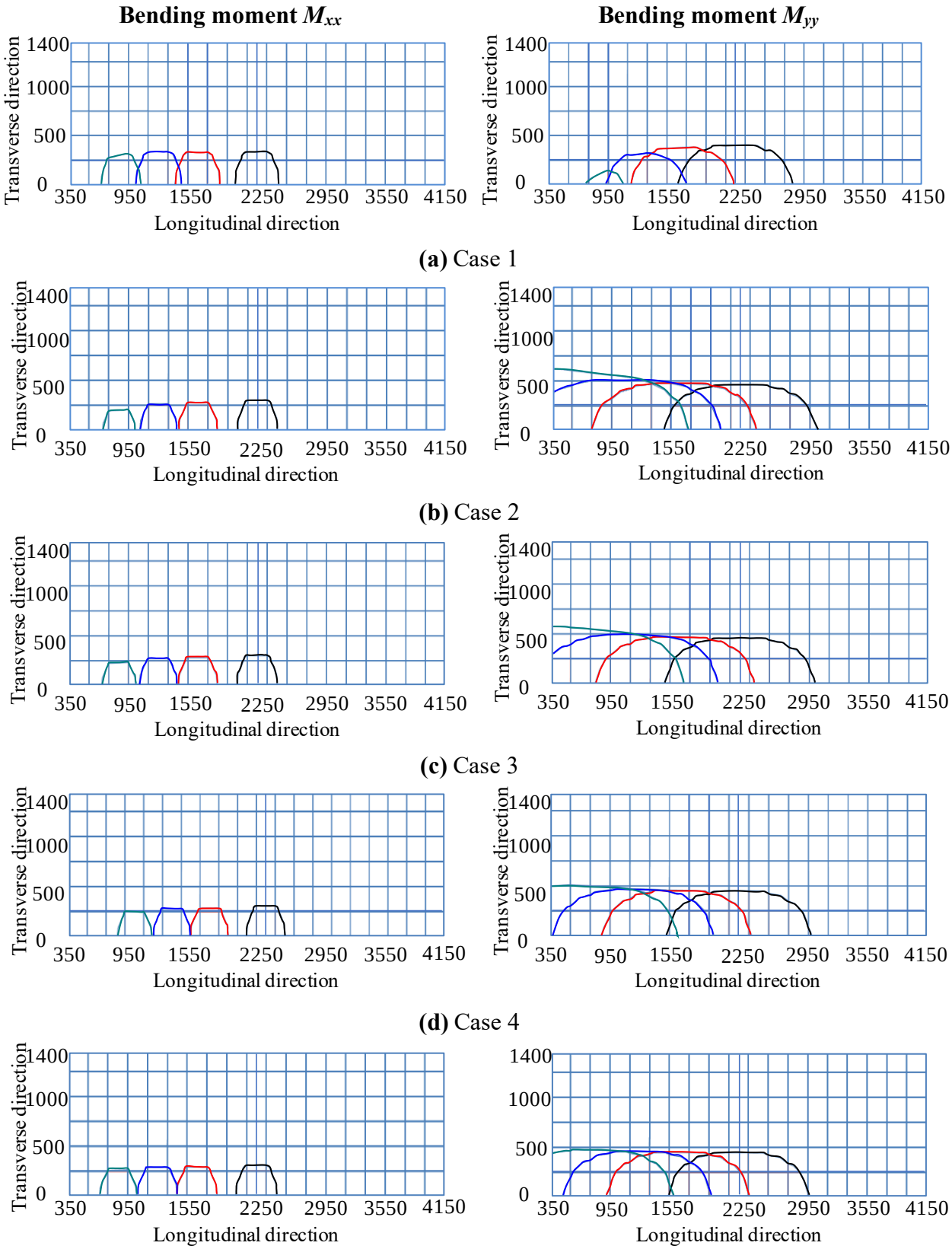

Figure 3.6 Bending moment cracking zones

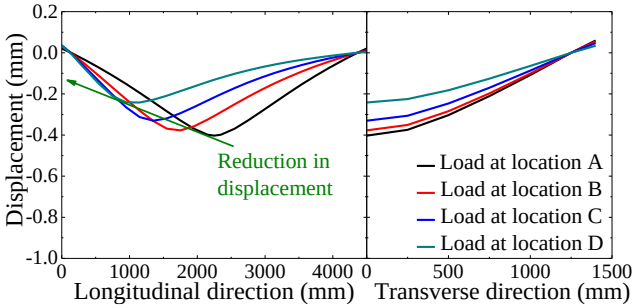

(a) Case 1

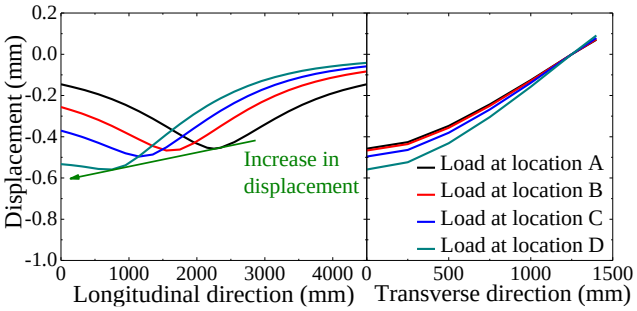

(b) Case 2

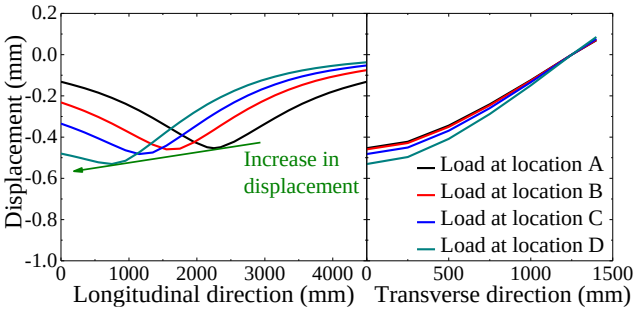

(c) Case 3

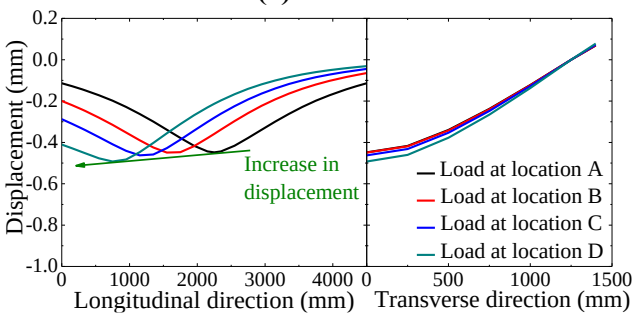

(d) Case 4

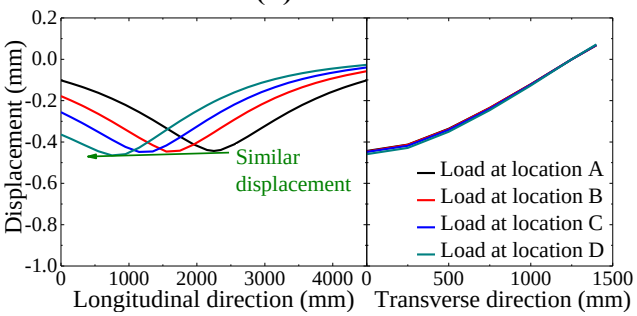

(e) Case 5

Figure 3.7 Displacement distributions in the longitudinal and transverse sections

Table 3.2 Comparison of maximum displacement

BCs cases	Maximum displacement (mm)				Displacement difference (%)
	Load at A	Load at B	Load at C	Load at D	(A–D)/A
Case 1	0.403	0.378	0.331	0.241	40.2
Case 2	0.458	0.467	0.496	0.559	–22.1
Case3	0.454	0.459	0.482	0.531	–16.0
Case 4	0.448	0.449	0.463	0.492	–9.8
Case 5	0.444	0.446	0.448	0.458	–3.1

3.6 SUMMARY AND CONCLUSIONS

To investigate the fatigue behavior of bridge slabs, many research institutes and groups have developed their test set-ups of panel slabs in lieu of the whole bridge slabs due to cost, time, and space restraints. In these studies, the BCs comprised of simple supports along the longitudinal edges and steel I-beams along the transverse edges of the panel slab have been typically used to represent the bridge slab with continuity between adjacent spans. However, the panel slabs with typically used BCs failed to capture the behaviors of the bridge slabs. Therefore, this study mainly aims to develop a numerical method for the determination of the approximate BCs for the already available panel slabs to capture the realistic behaviors of the bridge slabs.

Furthermore, by following the flowchart presented in this chapter, one can easily determine the approximate BCs for different dimensions of the panel slabs as well capable of reproducing the realistic behaviors of the bridge slabs.

To validate the method for the determination of approximate BCs, an FEA of a panel slab with approximate BCs is conducted. For the comparison purpose, the FEA of a panel slab with BCs typically employed in the past studies is also carried out.

The FEA results show that the panel slab with typically used BCs shows remarkable variations of bending moment distribution and deformations as the wheel load moves along the slab axis, in contrast to a bridge slab. On the other hand, the approximate BCs reproduce the same bending moment distribution and displacements around the loading locations as the wheel load moves along the slab axis in the panel slab, which are similar to those of the bridge slab.

Chapter 4

FATIGUE ANALYSIS OF A PANEL SLAB WITH APPROXIMATE BCS

4.1 GENERAL

As discussed in chapter 3, in the past studies, panel slabs with typically used BCs have been considered to investigate the fatigue behavior of bridge slabs due to cost, time, and space restraints [7-10]. However, the panel slabs with typically used BCs failed to capture the behaviors of the bridge slabs. For instance, contrary to the bridge slab, a panel slab with typically used BCs shows remarkable variations of bending moment distribution and deformations as the wheel load moves along the slab axis. Furthermore, when the panel slabs with typically used BCs are exposed to the fatigue loading, the diagonal cracks are formed that initiate from the loading location and extend towards the corners of the slabs. This diagonal crack pattern is very different from the grid crack pattern that is commonly witnessed in bridge slabs [6, 24]. Therefore, in chapter 3, a method for the determination of the approximate BCs for the panel slabs is numerically developed to capture the realistic behaviors of the bridge slabs. The FEA results confirm that the approximate BCs reproduce the same bending moment distribution and displacements around the loading locations as the wheel load moves along the slab axis in the panel slab, similar to a bridge slab.

In this chapter, to reproduce the fatigue behavior of the bridge slabs, a fatigue analysis of the panel slab with approximate BCs is conducted. Furthermore, a fatigue analysis of the panel slab with typically used BCs is also conducted for the sake of comparison. In the fatigue analysis, the FEM-based numerical model considering the bridging stress degradation, as discussed in detail in chapter 2, is used.

4.2 DETAILS OF THE PANEL SLAB

In chapters 2 and 3, the panel slab is selected from the technical note of NILIM, Japan [16]. The same panel slab is considered for the fatigue analysis of a panel slab with approximate BCs. The selected panel slab has (L×W×H) dimensions of (4500×2800×250) mm. In the tension zone, the slab is reinforced with D19@150 mm along the transverse direction and D16@125 mm along the longitudinal direction. Similarly, D19@300 mm along the transverse direction and D16@250 mm along longitudinal direction are provided in the compression zone (see **Figure 2.9**).

Material properties of the concrete and steel reinforcement of the panel slab are presented in **Table 2.1**.

4.3 BOUNDARY CONDITIONS

In chapter 3, approximate BCs for a panel slab are determined. The same approximate BCs determined in chapter 3 are utilized for the panel slab for the fatigue analysis. Moreover, for the sake of comparison, fatigue analysis of the panel slab with typically used BCs is also conducted.

4.3.1 Typically used BCs

In the case of the simulations with the typically used BCs, the panel slab is supported by simple supports along the longitudinal edges, and the steel I-beams are vertically placed along the transverse edges of the slab. The bottom flanges of the steel I-beams are restrained for vertical displacement. The same dimensions of the steel I-beams as those adopted in the experimental study [16] are used, and are presented in **Figure 4.1**.

4.3.2 Approximate BCs

In the case of the simulations with the approximate BCs, the simple supports along the longitudinal edges of the panel slab are the same as those in the typically used BCs case; however, the steel I-beams are horizontally placed as supports along the transverse edges to achieve a deformation behavior similar to that of a bridge slab. The outer flange of the steel I-beams is restrained in the longitudinal direction of the panel slab. The dimensions of steel I-beams used for the approximate BCs are shown in **Figure 4.1**.

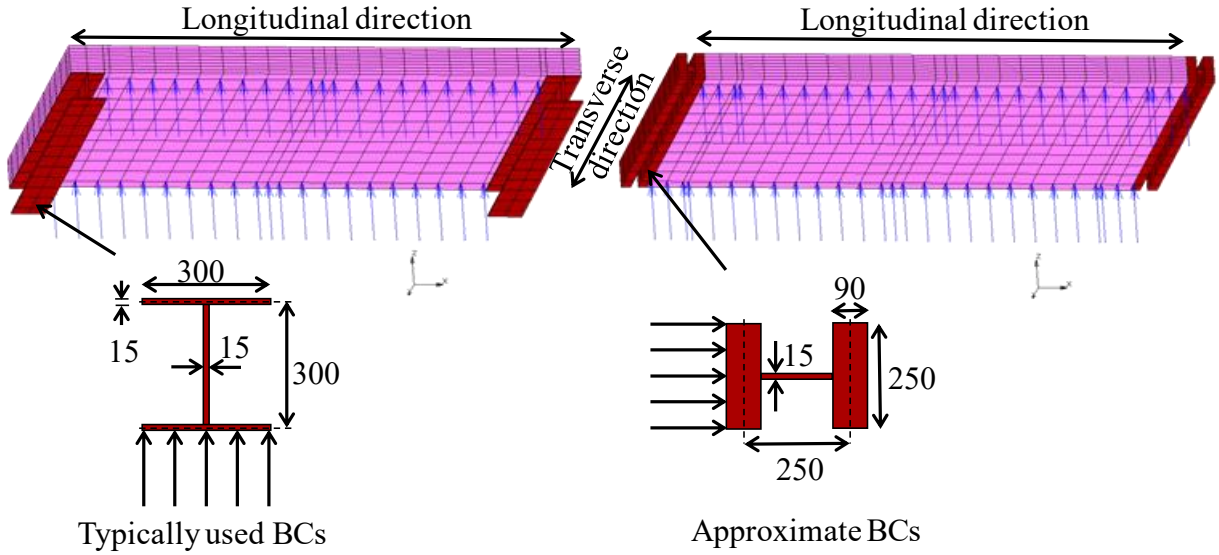

Figure 4.1 Illustration of BCs (mm)

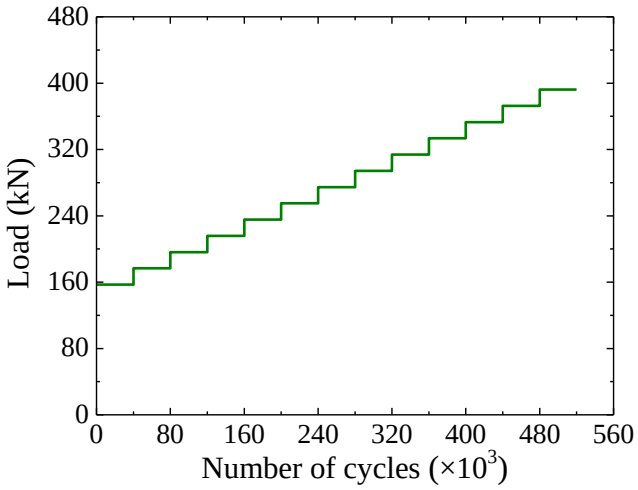

Figure 4.2 Stepwise loading sequence

4.4 LOADING SEQUENCE

The panel slab is subjected to moving wheel load along the longitudinal direction with the dimensions of the loading zone of (3000 × 500) mm. The same stepwise loading sequence with the experimental study [16] has been used. In the stepwise loading sequence, the magnitude of moving wheel load is increased in intervals after a certain number of cycles to promote the deterioration at the early stages to save time. The stepwise loading sequence used in this study, which has an initial value of 157 kN and an increasing step of 19.6 kN load after every 40,000 cycles of moving wheel load, is shown in **Figure 4.2**.

4.5 FATIGUE ANALYSIS RESULTS

Fatigue analysis method is an FEM-based numerical model considering the bridging stress degradation. The fatigue analysis method is explained in detail in chapter 2. Using the fatigue analysis method, fatigue analysis is conducted for the panel slab with the approximate BCs as well for the panel slab with typically used BCs.

4.5.1 Propagation of cracked elements

In the fatigue analysis method, the constitutive law for the cracked elements is modified after each cycle according to the bridging stress degradation concept. The cracked elements propagate and degrade after moving wheel load cycles. Therefore, it is imperative to describe the propagation of cracked elements. The propagation of cracked elements of the panel slab with the typically used BCs and approximate BCs at different numbers of cycles are shown in **Figure 4.3**. The uncracked elements are shown by white color, and the cracked elements caused by the different number of cycles of moving wheel load are displayed with different colors.

For the typically used BCs case, only a few elements on the bottom of the panel slab are cracked after the first cycle of moving wheel load, as displayed in **Figure 4.3(a)**. With the increase

in the number of cycles of moving wheel load, the cracked elements propagate in the longitudinal, transverse and vertical directions. This is because the bridging degradation of the concrete occurs due to the process of crack opening and closing. The load capacity from the concrete bridging stress cannot reach the same level as in the 1st cycle with the already formed cracked state, and the cracked elements propagate in the other directions to reach the load level. At the 200,000th cycle, the cracked elements propagate in the diagonal direction and reach to the corner supports. At the 280,000th cycle, almost all the elements on the bottom surface of the panel slab are cracked, and the cracked elements propagate vertically up to 3/4th of the total thickness of the panel slab at the loading point and corner supports. At the last cycle of moving wheel load (i.e., 500,000th cycle), the corner supports are entirely cracked, and the cracked elements propagate in a diagonal direction on the upper layers from the corner supports. This is because the corner supports experience a negative bending, and the top surface elements of the corner supports are cracked. These cracked elements at the top surface of the corner supports then propagate in the diagonal direction from the corner supports towards the loading point, whereas a bridge slab does not experience this kind of crack propagation on the top surface.

On the other hand, for the approximate BCs case, significant elements on the bottom of the panel slab are cracked after the application of the first loading cycle as shown in **Figure 4.3(b)**, as the horizontally placed I-beams allow the panel slab to experience the same cracking behavior as the wheel load moves along the slab axis. The cracked elements propagate in the longitudinal and transverse directions, as well as the vertical direction, with an increase in the number of cycles of moving load. At the 200,000th cycle, the cracked elements propagate in the longitudinal and transverse directions, in contrast to the typically used BCs case. At the 280,000th cycle, the cracked elements reach the corner supports, start to propagate in the vertical direction, and reach up to 3/4th of the total thickness of the panel slab at the loading point. At the last cycle of moving load (500,000th cycle), the corner cracked elements are reached up to 3/4th of the total thickness of the panel slab. The corner supports are not fully cracked, and no cracked elements propagate in the diagonal direction from the corner supports to the loading location on the top surface of the slab.

The volumes of the cracked elements for the typically used BCs case and the approximate BCs case are compared and are plotted in **Figure 4.4**. The cracked elements volume for the typically used BCs case is smaller than that for the approximate BCs case for the first 200,000th cycles. Subsequently, for the typically used BCs case, the cracked elements propagate in the diagonal direction, reach the corner supports, and propagate in the vertical and diagonal directions. This phenomenon results in a larger cracked elements volume after the 200,000th cycle for the typically used BCs case compared to the approximate BCs case. The average degradation ratios for the typically used BCs and the approximate BCs cases are 2487 mm^3/cycles and 2017 mm^3/cycles,

respectively. The formation of the cracked elements in the diagonal direction triggers the degradation phenomenon in the panel slab with the typically used BCs, which leads to the panel slab degradation earlier than with approximate BCs.

The panel slab with the typically used BCs experiences smaller cracked elements zone at the bottom surface of the slab after the first loading cycle as compared to the approximate BCs case. However, the cracked elements propagate in the diagonal direction and reach the corner supports in fewer cycles, compared to the approximate BCs case. This is because the vertically placed steel I-beams in the typically used BCs case restrict the panel slab from deflecting in the longitudinal direction around these steel I-beams. As a result, the cracked elements propagate in the diagonal direction instead of the longitudinal and transverse directions, which is generally not observed in a bridge slab. The corner cracked elements then propagate in the vertical and diagonal directions, resulting in a larger cracked elements zone in the typically used BCs case. The larger cracked elements zone is undergone the bridging stress degradation mechanism (**Equation (2.8)**), causing the deterioration of the panel slab to a greater extent. This additional deterioration due to the propagation of the cracked elements in the diagonal direction leads to a shorter fatigue life of the panel slab with the typically used BCs compared to that of a bridge slab.

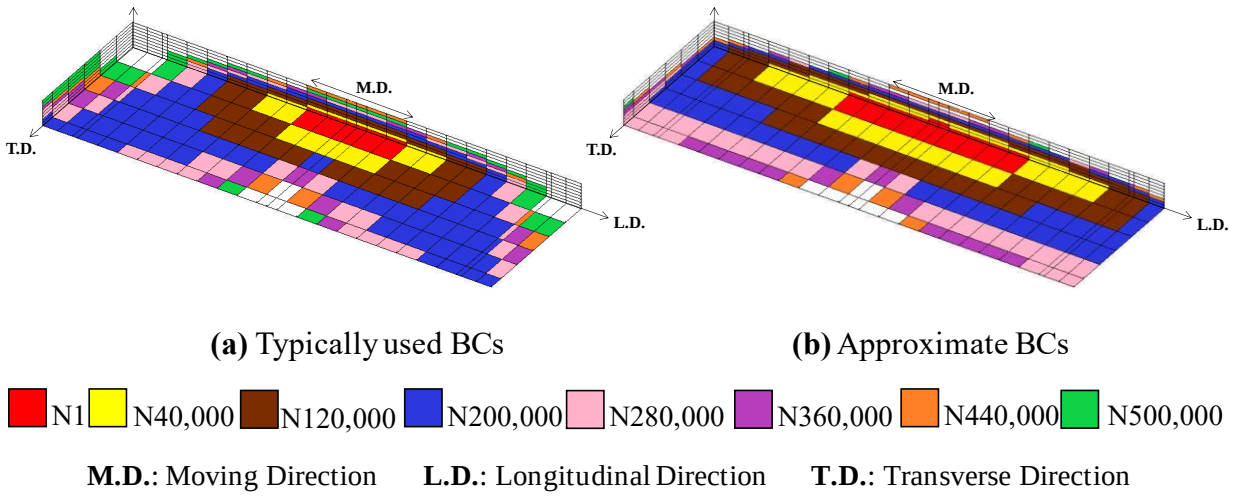

(a) Typically used BCs **(b)** Approximate BCs

M.D.: Moving Direction **L.D.**: Longitudinal Direction **T.D.**: Transverse Direction

Figure 4.3 Propagation of the cracked elements

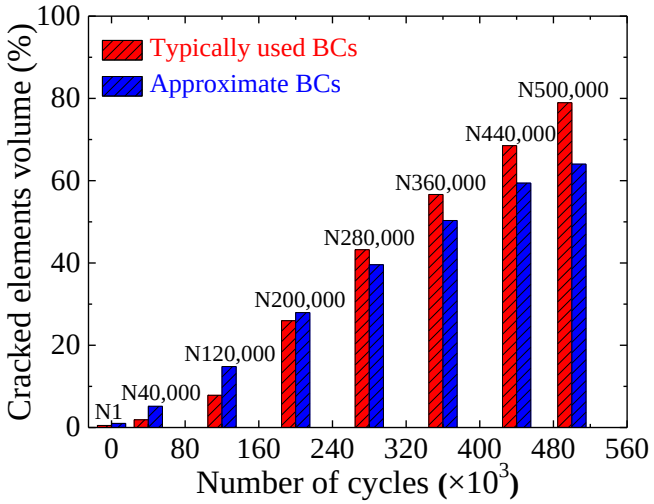

Figure 4.4 Percentage of the volume of cracked elements

4.5.2 Maximum principal strain distribution

Figure 4.5 shows a comparison of the maximum principal strain distribution on the bottom surface of the panel slab at different loading cycles for both the BCs cases. In all contours, the maximum principal strain value is higher than the cracking strain value of the concrete except for the contour shown by dark gray color. After the first loading cycle, the maximum principal strain distribution is spread to a greater extent in the longitudinal direction in the approximate BCs case, compared to the typically used BCs case. At the 200,000th cycle, for the typically used BCs case, the maximum principal strain distribution is in the diagonal direction starting from the loading point and reaching towards the slab corners, different from the maximum principal strain distribution along the longitudinal and transverse directions in the approximate BCs case. This distribution confirms the crack propagation in the diagonal direction in the typically used BCs case. At the 280,000th cycle, the maximum principal strain distribution is mainly along the diagonal direction with significantly increased strain value around the loading point and at the slab corners in the typically used BCs case; however, the distribution is along the longitudinal and transverse directions for the approximate BCs case. At the last cycle of moving wheel load (i.e., 500,000th cycle), the value of maximum principal strain is highest around the loading point, and it spreads in the diagonal direction in the typically used BCs case while the spread is in the longitudinal and transverse directions in the approximate BCs case.

After the first loading cycle, the panel slab with the approximate BCs experiences the cracking strain at a larger portion of the bottom surface in the longitudinal direction, compared to the typically used BCs case. With an increase in the cycles of moving wheel load, the maximum principal strain spreads in the longitudinal direction as well in the transverse direction of the panel slab for the approximate BCs case. This is because of the fact that the horizontally placed steel I-beams in the approximate BCs allow the maximum principal strain to spread along the longitudinal

and transverse directions of the panel slab similar to that of a bridge slab. However, the vertically placed steel I-beams in the typically used BCs have high bending stiffness, and these steel I-beams lead to the maximum principal strain distribution in the diagonal direction of the panel slab. Despite a very high maximum principal strain in the diagonal direction, there are uncracked zones in the longitudinal direction at the bottom surface of the panel slab with the typically used BCs even at the final cycle of moving wheel load, which is not observed in a bridge slab.

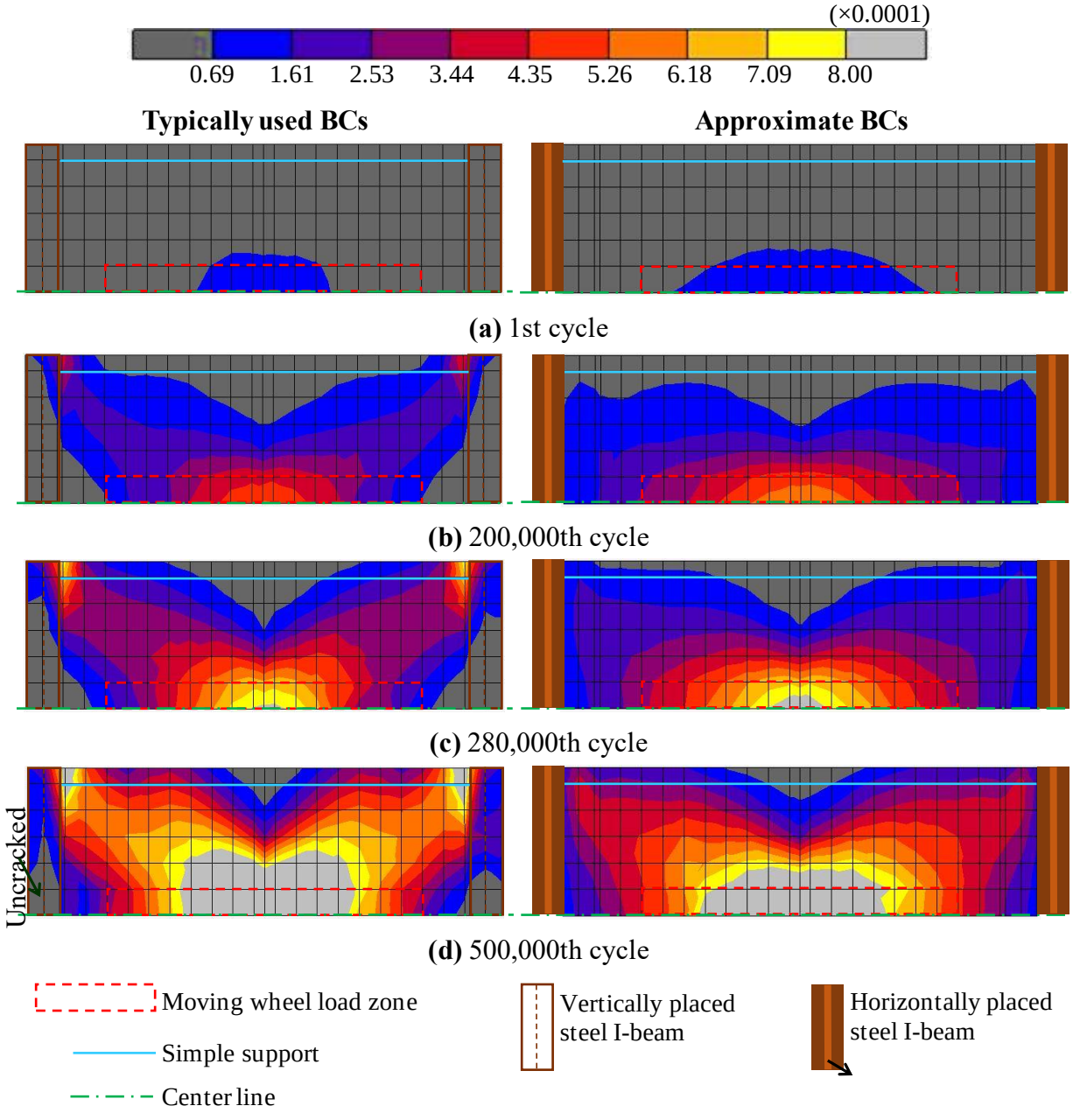

Figure 4.5 Maximum principal strain distribution on the bottom surface

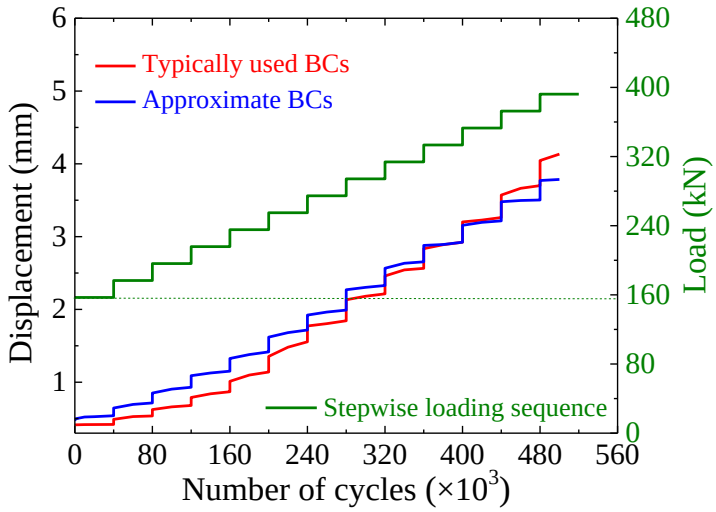

Figure 4.6 Center displacement evolution

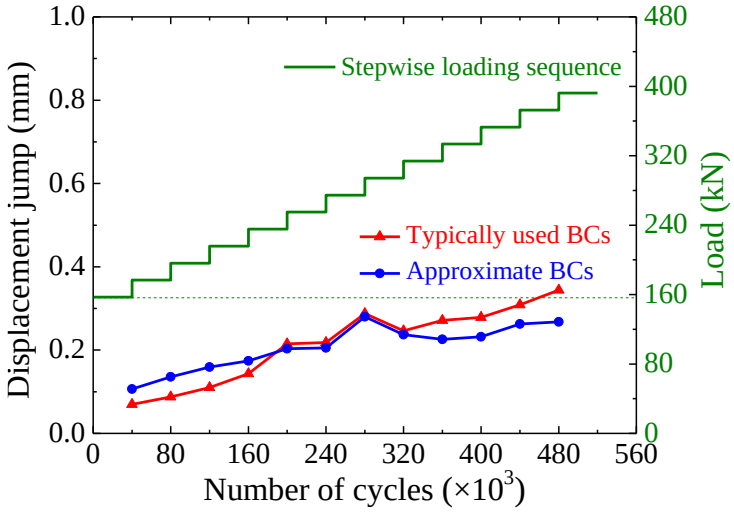

Figure 4.7 Displacement jump

4.5.3 Center displacement evolution

Figure 4.6 shows a comparison of center displacement evolution of the panel slab for typically used and approximate BCs cases. For the typically used BCs case, the center displacement is comparatively lesser than that of approximate BCs at the initial loading cycles. However, the displacement is determined to be relatively higher at the final loading cycles.

For a detailed comparison, a comparison of the displacement jump obtained during the fatigue analysis at different loading cycles is made for the typically used BCs and the approximate BCs cases, as shown in **Figure 4.7**. The displacement jump indicates a sudden increase in the displacement due to an increase in the intensity of the moving wheel load in a stepwise loading sequence. For the typically used BCs case, a significant high displacement jump is observed at the 200,000th cycle due to the formation of diagonal cracks, contrary to the approximate BCs case. However, there is another significantly large displacement jump at the 280,000th cycle for both the

BCs cases. This is because almost all the elements on the bottom surface of the panel slab are cracked, and the cracked elements propagate up to 3/4th of the total thickness of the panel slab at the loading point leading to a decrease in the compression zone. For the typically used BCs case, the displacement jump is larger after the 320,000th cycle as compared to the approximate BCs case due to the propagation of the corner cracked elements in the vertical direction, in addition to their propagation in the diagonal direction. The propagation of the corner cracked elements in the vertical and diagonal directions leads to a larger displacement in the typically used BCs case in contrast to a bridge slab.

The panel slab with the typically used BCs exhibits smaller displacement evolution at the initial cycles of the moving wheel load compared to the approximate BCs case. The reason for this is that the vertically placed steel I-beams in the typically used BCs case provide high resistance against bending and deflection as the wheel load moves along the slab axis. However, diagonal cracks are formed, and the corner cracks propagate in the vertical direction, resulting in larger displacement in the typically used BCs case, which is dissimilar to a bridge slab.

4.5.4 Crack patterns

The crack patterns on the bottom surface of the panel slab under moving wheel load at the last loading cycle for both the BCs cases are compared and displayed in **Figure 4.8**. For the typically used BCs case, the main crack originates at the center, which is the first location of the moving wheel load; subsequently, it extends to the supporting corners. As the load begins to move, the diagonal cracks are formed between the locations of the moving wheel load in the longitudinal direction and the supporting corner, making the first crack set. At the same time, other cracks are formed perpendicular to the existing cracks as second and third crack sets, surrounding the moving wheel load zone. An increase in the number of cycles results in much more extensive cracking. However, the horizontal cracks are formed in the approximate BCs case, different from the formation of the diagonal cracks in the typically used BCs case. Moreover, the cracks propagate until the end of the moving wheel load zone in the longitudinal direction for the typically used BCs case. This is in contrast to the cracks propagation that happened throughout the length of the panel slab, surrounding the moving wheel load zone in the longitudinal direction for the approximate BCs case.

The crack angles at three different sections (I, II, and III) are determined for both the BCs cases and shown in **Figure 4.9**. The crack is categorized into two types depending upon the angle of the crack in the 1st crack set obtained from the numerical model. If the angle of the crack with the x-axis is lesser than 22.5°, it is considered as a horizontal crack. Otherwise, it is regarded as a diagonal crack (angle greater than 22.5°). The horizontal cracks form the grid crack pattern, and the diagonal cracks lead to the formation of the diagonal crack pattern.

The grid crack patterns for both the BCs cases are compared in **Figure 4.10**. For the typically used BCs case, the grid crack pattern is reproduced only within the moving wheel load zone in the longitudinal and transverse directions, in contrast to a bridge slab. However, the panel slab with approximate BCs reproduces a grid crack pattern in the transverse direction that is almost twice as the grid crack pattern reproduced by the panel slab with typically used BCs. Moreover, the approximate BCs allow the propagation of the grid crack pattern in the panel slab along the longitudinal direction to a greater extent compared to the typically used BCs case.

It is essential to mention here that degradation and crack patterns of bridge slabs are primarily associated with the accumulated loads of daily traffics, i.e., moving wheel loads. Therefore, in this study, the moving wheel load is considered as the main cause of degradation and crack pattern. However, the other factors, such as drying shrinkage, restriction of steel girder, less concrete cover due to poor construction and reinforcement bar arrangements, can also play a part in producing the crack pattern of a bridge slab. These factors should also be considered together with the moving wheel load in the future study. The panel slab with the approximate BCs considering the moving wheel load and other important factors would yield to a more realistic simulation of the bridge slab.

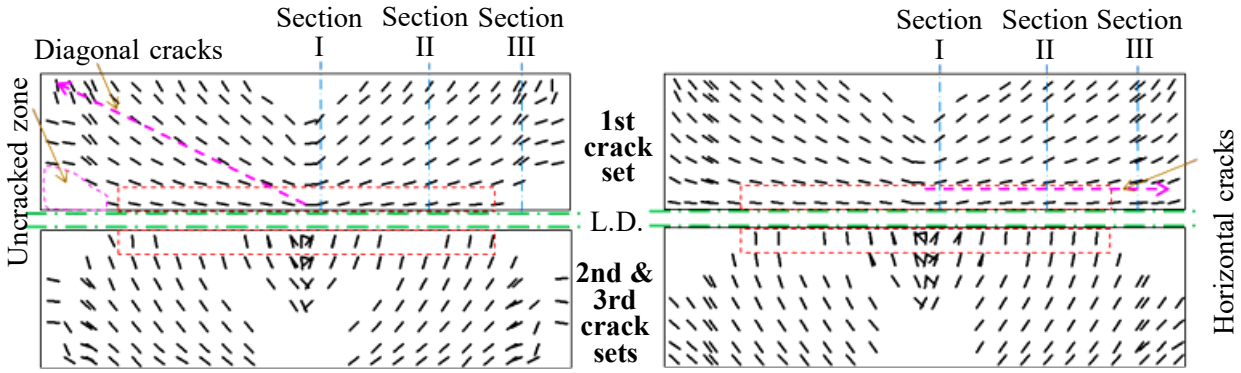

(a) Typically used BCs **(b)** Approximate BCs

Figure 4.8 Crack pattern

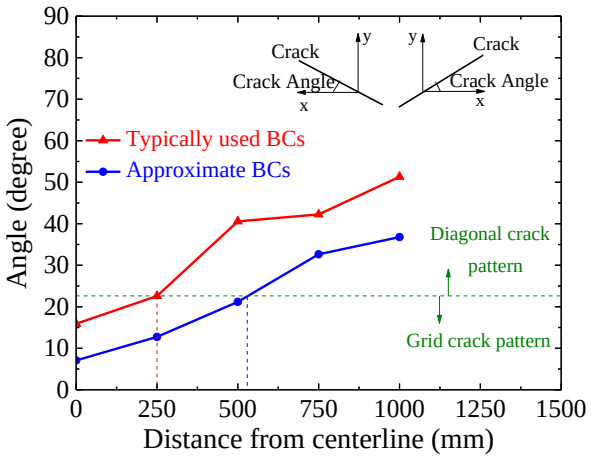

(a) Section I

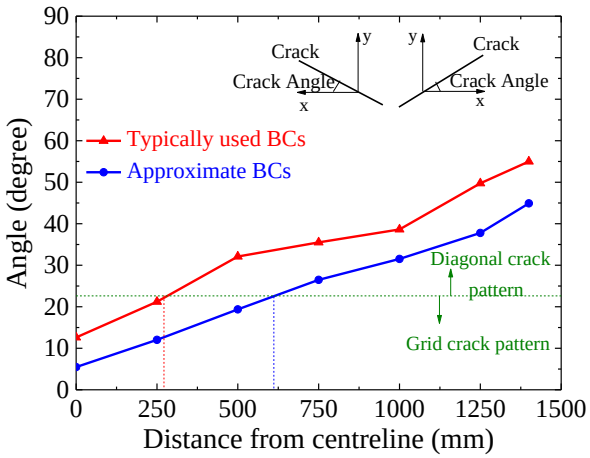

(b) Section II

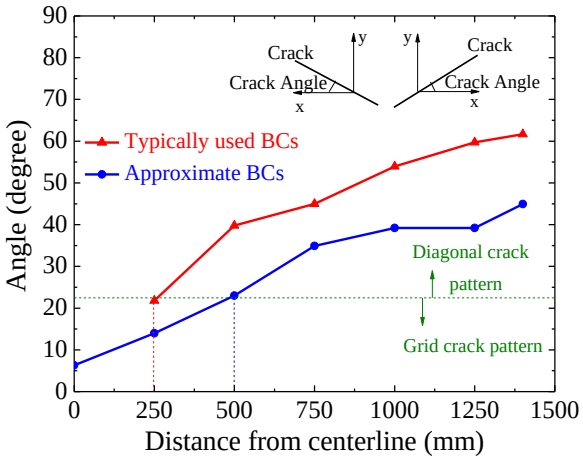

(c) Section III

Figure 4.9 Crack angle along the transverse direction

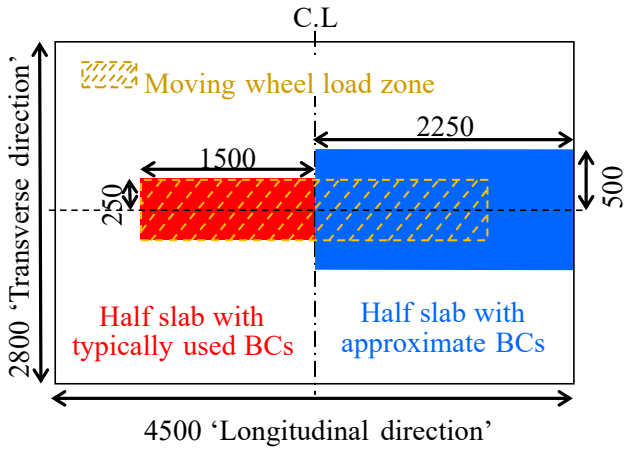

Figure 4.10 Grid crack pattern zone (mm)

4.6 SUMMARY AND CONCLUSIONS

In this chapter, fatigue analysis of a panel slab with the approximate BCs is conducted in addition to the panel slab with the BCs typically used in the past studies. An FEM-based numerical

model considering the bridging stress degradation is used in the fatigue analysis.

The fatigue analysis results show that the approximate BCs do not result in a negative bending at the corners of the panel slab, and the cracked elements do not propagate on the top surface from the corners to the loading point, which is similar to a bridge slab. However, in the panel slab with the typically used BCs, the negative bending at the corners and the propagation of the cracked elements on the top surface from the corners to the loading point produce an additional deterioration in the panel slab, which leads to a shorter fatigue life estimation of a bridge slab.

Furthermore, the panel slab with the approximate BCs reproduces the extensive grid crack pattern well in accordance with that of a bridge slab. However, in contrast to a bridge slab, the panel slab with typically used BCs reproduces the grid crack pattern only within the moving wheel load zone.

Chapter 5

METHOD FOR DETERMINING THE EQUIVALENT BCS FOR A PANEL SLAB

5.1 GENERAL

As discussed in detail in chapter 3, to investigate the fatigue behavior of bridge slabs, many research institutes and groups have developed their test set-ups of panel slabs in lieu of the whole bridge slabs due to cost, time, and space restraints [6-11]. In these studies, the BCs comprised of simple supports along the longitudinal edges and steel I-beams along the transverse edges of the panel slab have been typically used to represent the bridge slab with continuity between adjacent spans. However, the panel slabs with typically used BCs failed to capture the behaviors of the bridge slabs. Therefore, in chapter 3, new BCs for the already available panel slabs are proposed, which approximately investigate the behaviors of the bridge slabs. As the bending moment distribution and deformations remain almost unchanged as the load moves along the slab axis in a bridge slab, the bending moment distribution and deformations are investigated for the panel slab with different BCs. The steel I-beams are horizontally placed, and their bending and rotational stiffness are adjusted so that these beams allow the panel slab to experience the same bending moment distribution and deformations as the load moves along the slab axis, which are similar behaviors of a bridge slab. However, this is a hit and trial method of determining the BCs for a panel slab and BCs are determined approximately for a panel slab.

Therefore, in this chapter, for more accurate and realistic fatigue behavior analysis of a bridge slab, an equivalent BCs determination and sophisticated method is developed numerically for a panel slab. For this purpose, an FEA of a bridge slab is conducted, and based on the calculated stiffness of the bridge slab, equivalent BCs for the corresponding panel slab are determined.

In order to validate the determined equivalent BCs, a static analysis of the panel slab with equivalent BCs is conducted. Furthermore, a static analysis of the panel slab with typically used BCs is also conducted for the sake of comparison.

5.2 PROBLEM FORMULATION

To investigate the fatigue behavior of a bridge slab, a panel of the bridge slab has been usually considered in place of the whole bridge slab due to limitations in budget, time, and space in past studies. In these studies, the panel slab is supported with simple supports along its longitudinal edges and steel I-beams along its transverse edges so as to achieve the bending moments and

cracking behavior comparable to those of the bridge slab [6-10]. However, the panel slab with BCs typically used in the past studies failed to simulate the bending moments and cracking behavior of the bridge slab. **Figure 3.1** shows a bridge slab and its corresponding panel slab with typically used BCs in addition to a schematic comparison of the deformations of the slabs subjected to the same static load. The vertical displacements in the bridge slab are different from those of the panel slab, especially at the areas away from the loading locations. This difference is more evident at the locations closer to the steel I-beams in the corresponding panel slab, which is shown in **Figures 3.1(c, d)**. This is due to the fact that the panel slab directly rests on the steel I-beams, which restrains the vertical displacements of the panel slab at the transverse edges, in contrast to the bridge slab. Moreover, the steel I-beams placed in the vertical direction result in a different rotation around the steel I-beams in the panel slab, as compared to that of the bridge slab displayed in **Figures 3.1(c, d)** [22].

In a bridge slab, the displacement (δ_{bridge}) and rotation (θ_{bridge}) at the corresponding positions of the transverse edges of the panel slab are restrained by the neighboring RC slab portions (see **Figure 3.1(c)**). Moreover, in the bridge slab, the bending moment distributions and deformations around the loads remain almost unchanged upon movement of the load along the slab axis [20-23]. Furthermore, an extensive grid crack pattern is commonly witnessed in the bridge slab due to fatigue loading [6, 24]. On the other hand, the steel I-beams are vertically placed along the transverse edges of the panel slab, which restrict the deformations especially at the areas near the transverse edges (see **Figure 3.1(d)**). These steel I-beams in the vertical orientation restrain the panel slab from experiencing the same bending moment distributions and deformations around the loads upon the movement of the load along the slab axis [23]. Furthermore, these vertical steel I-beams result in forming the diagonal crack pattern in the panel slab. Consequently, the diagonal cracks lead to an additional degradation of the panel slab, which results in a shorter life prediction of a bridge slab [23].

The real deformation and cracking behaviors of the bridge slab can be simulated in the panel slab by providing the bending and rotational stiffness at the transverse edges of the panel slab, which are equivalent to the stiffness of the bridge slab at the corresponding locations. As, in the bridge slab, the stiffness at the corresponding positions of the transverse edges of the panel slab are due to the neighboring RC slab portions, it is most appropriate to attach the steel I-beams horizontally along the transverse edges of the panel slab, which possess the same stiffness of the bridge slab. This horizontal orientation of the steel I-beams would not result in restricting the bending moment distributions and deformations around the loads upon movement of the load along the slab axis. As a result, the panel slab would yield to reproduce the real deformation and cracking behaviors of the bridge slab.

In this study, the FEA of a bridge slab is carried out in order to calculate the rotational and

bending stiffness of the bridge slab at the corresponding positions. Based on the calculated stiffness, the steel I-beams for the panel slab are determined.

5.3 FINITE ELEMENT ANALYSIS OF A BRIDGE SLAB

Using an FEA software MARC [29], a bridge slab is modeled and analyzed. The bridge data is taken from the technical note from the Japan Bridge Association (JBA), Japan [32]. In the selected bridge, an RC slab with 34000×9700×220 mm (L×W×T) dimensions is supported by the four longitudinal steel I-girders, which is shown in **Figure 5.1**.

Eight-node 3D solid elements and four-node 3D shell elements are used for the bridge slab and steel members, i.e., I-girder and bracing system, respectively. The same material properties of concrete and steel with the JBA [32] are used, as displayed in **Table 5.1**. To save time, and for the sake of simplification, an elastic analysis method of the bridge slab without reinforcement bars is considered. Because the purpose here is to calculate the sectional forces in the bridge slab under static loads, the elastic analysis method serves this purpose efficiently [31].

The elastic analysis is separately conducted for the static load of 157 kN at the center of the bridge slab and away from the center of the slab, i.e., location A and location D, which is shown in **Figure 5.1**. As the bending and rotational stiffness cannot be directly obtained from the analysis of the bridge slab in the FEA software MARC, the stiffness along the transverse edge of the panel slab are calculated using the analysis results. The bending stiffness can be calculated as follows:

(1) Obtain the nodal stress component in the y-direction (σ_{yy}) and displacement in the z-direction (δ_{zz}) along the transverse edge of the panel of bridge slab.
(2) From the obtained values of σ_{yy}, calculate the moment (M_{yy}) along the transverse edge of the panel slab.
(3) From the obtained values of δ_{zz} along the transverse edge of the panel slab, construct a best-fit equation as:

$$\delta_{zz} = f(y) \tag{5.1}$$

where y is the distance along the transverse edge.

(4) Take the second derivative of the equation 5.1 with respect to y, which is equal to $1/R_s$ according to the Bernoulli-Euler equation that can be expressed as follows:

$$\frac{d^2\delta_{zz}}{dy^2} = \frac{1}{R_s} \tag{5.2}$$

where R_s is the radius of curvature along the transverse edge of the panel slab.

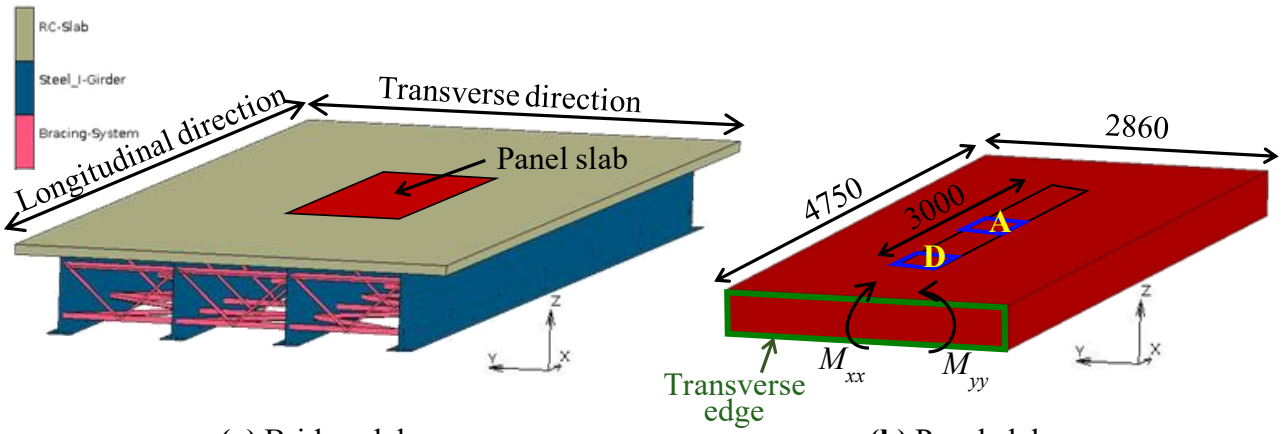

(a) Bridge slab **(b)** Panel slab

Figure 5.1 Illustration of the bridge slab and its corresponding panel slab (mm)

Table 5.1 Material properties [32]

Material	Property	Value (MPa)
Concrete	Compressive strength (f_c')	30
	Tensile strength (f_t)	2.22
	Elastic modulus (E_c)	28,000
Steel	Yield strength (f_y)	345
	Elastic modulus (E_s)	200,000

(5) Calculate the bending stiffness (EI) along the transverse edge of the panel slab as:

$$EI = M_{yy}R_s \tag{5.3}$$

where M_{yy} is considered to be playing a major role in producing R_s.

By following the above-mentioned procedure of calculation of bending stiffness, the bending stiffness along the transverse edge of the panel slab is determined for the loading locations A and D, as shown in **Figure 5.2** and **Figure 5.3**, respectively.

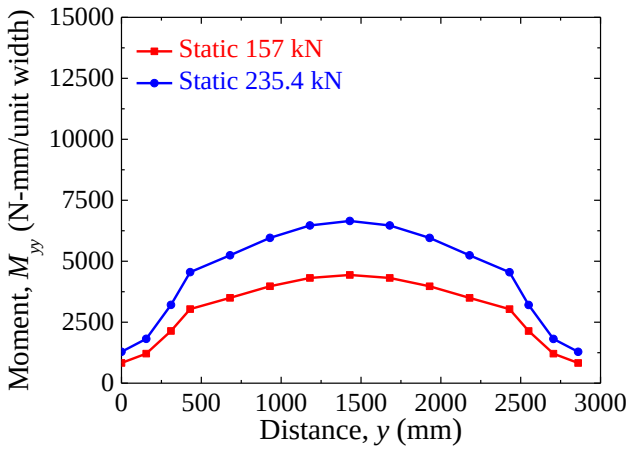

(a) Moment M_{yy} along the transverse edge

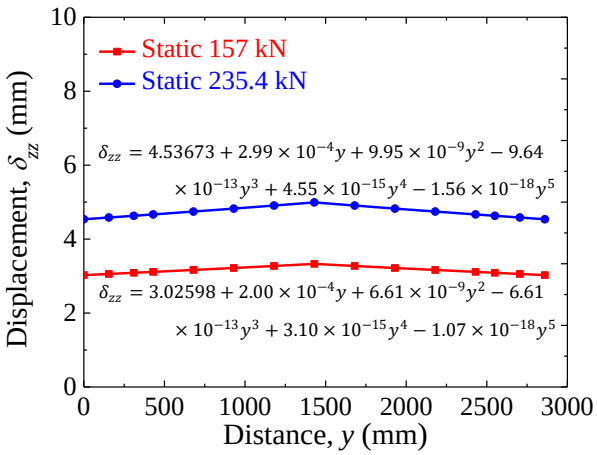

(b) Displacement δ_{zz} along the transverse edge

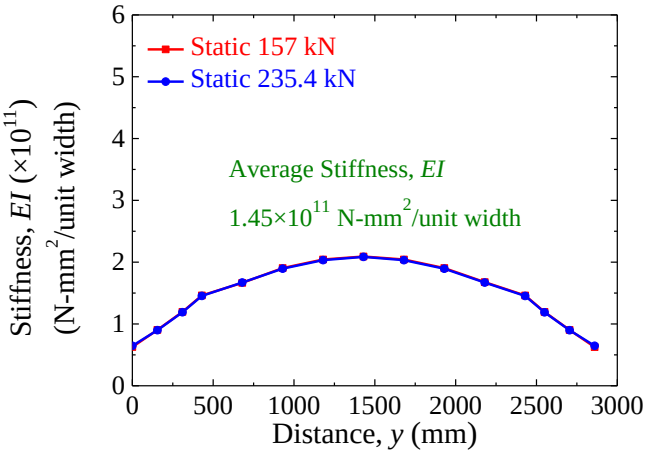

(c) Bending stiffness EI along the transverse edge

Figure 5.2 Bending stiffness EI along the transverse edge of the panel slab (load at location A)

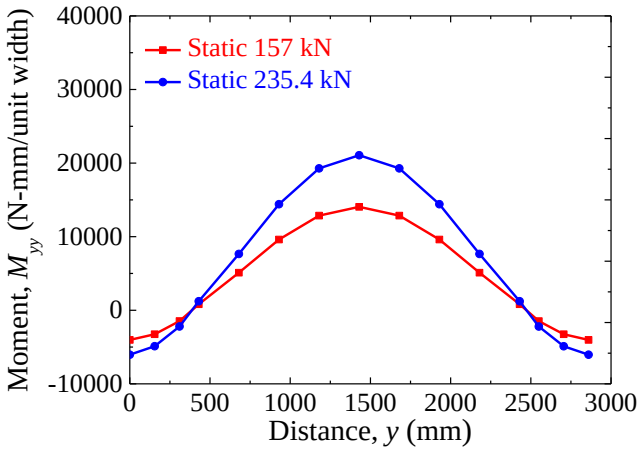

(a) Moment M_{yy} along the transverse edge

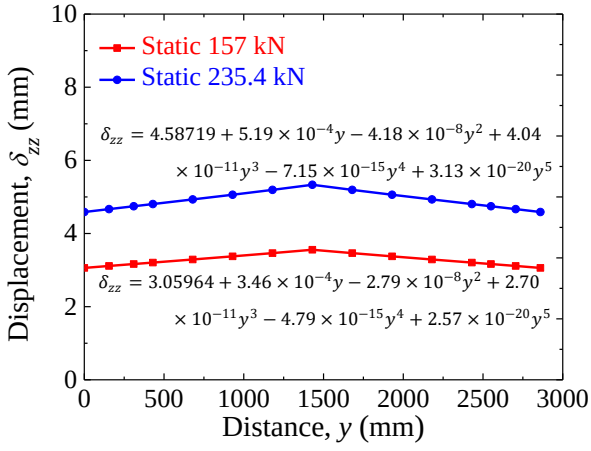

(b) Displacement δ_{zz} along the transverse edge

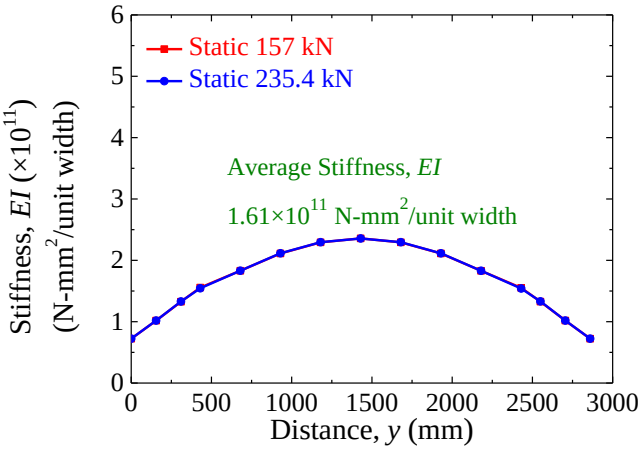

(c) Bending stiffness EI along the transverse edge

Figure 5.3 Bending stiffness EI along the transverse edge of the panel slab (load at location D)

The average bending stiffness value for unit width for the loading locations A and D is calculated to be 1.525×10^{11} N-mm^2.

The rotational stiffness can be calculated as follows:

(1) Obtain the nodal stress component in the x-direction (σ_{xx}) and displacement in the x-direction (δ_{xx}) along the transverse edge of the panel slab.

(2) From the obtained values of σ_{xx}, calculate the moment (M_{xx}) along the transverse edge of the panel slab.

(3) From the obtained values of δ_{xx}, calculate the rotation (θ_{xx}) along the transverse edge of the panel slab.

(4) Calculate the rotational stiffness (k) along the transverse edge of the panel slab as follows:

$$k = \frac{M_{xx}}{\theta_{xx}} \tag{5.4}$$

By following the procedure as mentioned above of calculation of rotational stiffness, the rotational stiffness along the transverse edge of the panel slab is determined for the loading locations A and D, as shown in **Figure 5.4** and **Figure 5.5**, respectively.

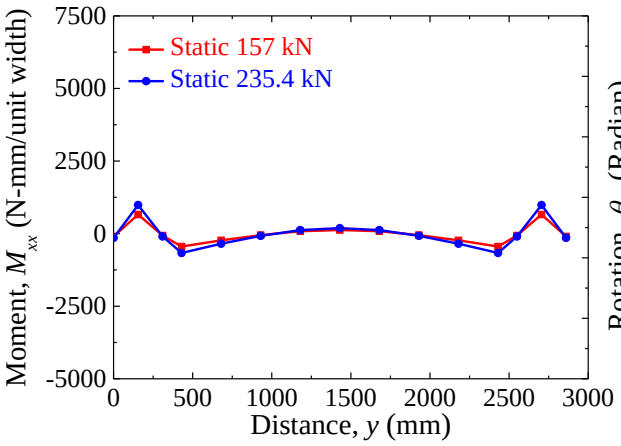

(a) Moment M_{xx} along the transverse edge

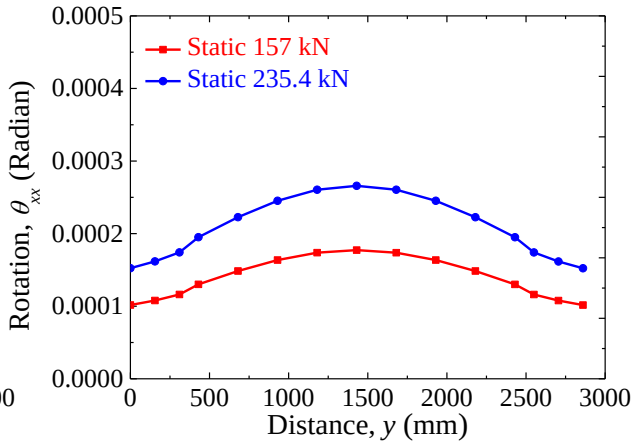

(b) Rotation θ_{xx} along the transverse edge

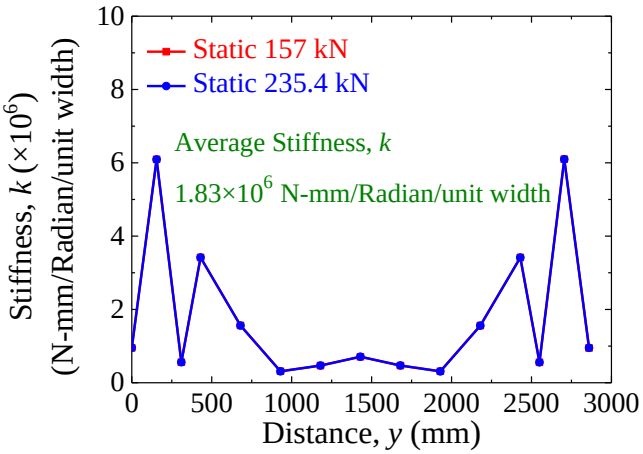

(c) Rotational stiffness k along the transverse edge

Figure 5.4 Rotational stiffness k along the transverse edge of the panel slab (load at location A)

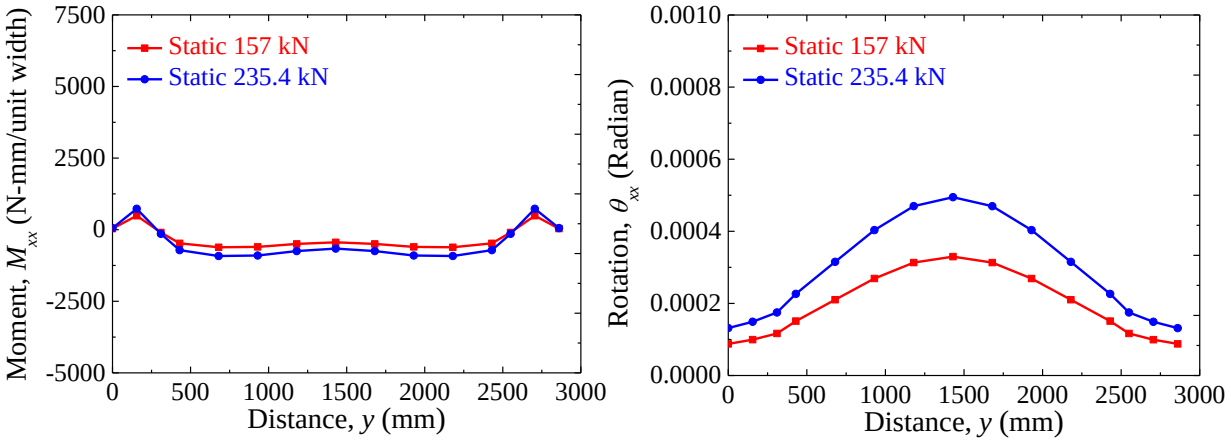

(a) Moment M_{xx} along the transverse edge **(b)** Rotation θ_{xx} along the transverse edge

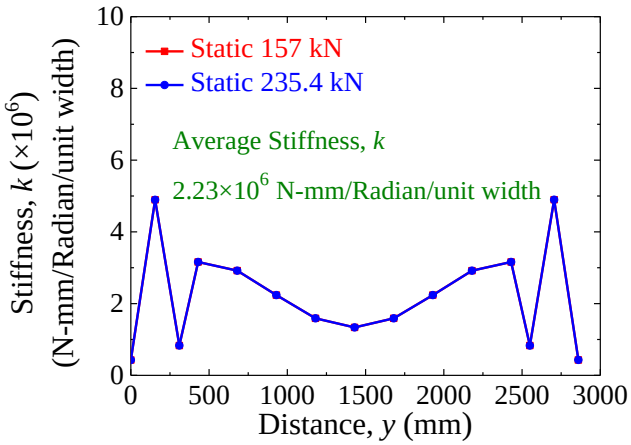

(c) Rotational stiffness k along the transverse edge

Figure 5.5 Rotational stiffness k along the transverse edge of the panel slab (load at location D)

The average rotational stiffness value for unit width for the loading locations A and D is calculated to be 2.029×10^{06} N-mm/Rad.

5.4 DETERMINATION OF EQUIVALENT BCS FOR A PANEL SLAB

The elastic analysis of the bridge slab is conducted, and the average bending and rotational stiffness are calculated along the transverse edge of the panel slab. Based on the calculated bending and rotational stiffness, the steel I-beam to be employed at the transverse edge of the panel slab is determined. **Figure 5.6(a)** shows the cross-section of the horizontally placed steel I-beam where B is the total width of the beam; H_f is the flange height; W_f is the flange width; T_w is the web thickness; and L_w is the web length. These cross-sectional parameters can be determined as follows:

(1) Select B and H_f to be equal to the slab thickness (T).

(2) Calculate the second moment of the area parallel to the y-axis (I_y) per unit width as $I_y = T_w^3/12$ and regard E_sI_y, where E_s is the elastic modulus of steel, as the rotational stiffness of the steel

I-section as shown in **Figure 5.6(b)** because T_w plays a major role in resisting the rotation of the I-section around the y-axis.

(3) Assume L_w to be equal to the radius of curvature (R) for the rotation (θ) of 1 Radian (see **Figure 5.6(b)**).

(4) Obtain the L_w-T_w relationship using the Bernoulli-Euler equation, $R = E_s I_y / M$, where M is the rotational moment for the unit rotation.

(5) Determine W_f, L_w, and T_w by considering the bending stiffness ($E_s I_x$) of the steel I-beam to be equal to the previously calculated bending stiffness at the transverse edge of the panel of the bridge slab.

It is important to mention that bending stiffness and rotational stiffness in this kind of arrangement of steel I-beam are majorly dependent on W_f and T_w, respectively.

By following the procedure mentioned above, the cross-sectional parameters of the steel I-beam to be employed at the transverse edge of the panel slab are determined and shown in **Figure 5.7(b)**.

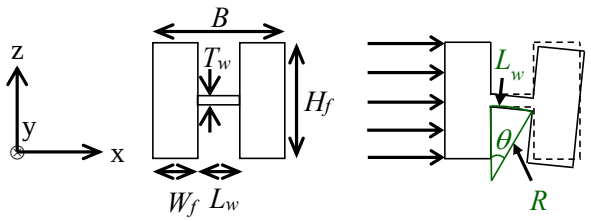

(a) Cross-section **(b)** Rotation

Figure 5.6 Cross-section and rotation of the steel I-beam

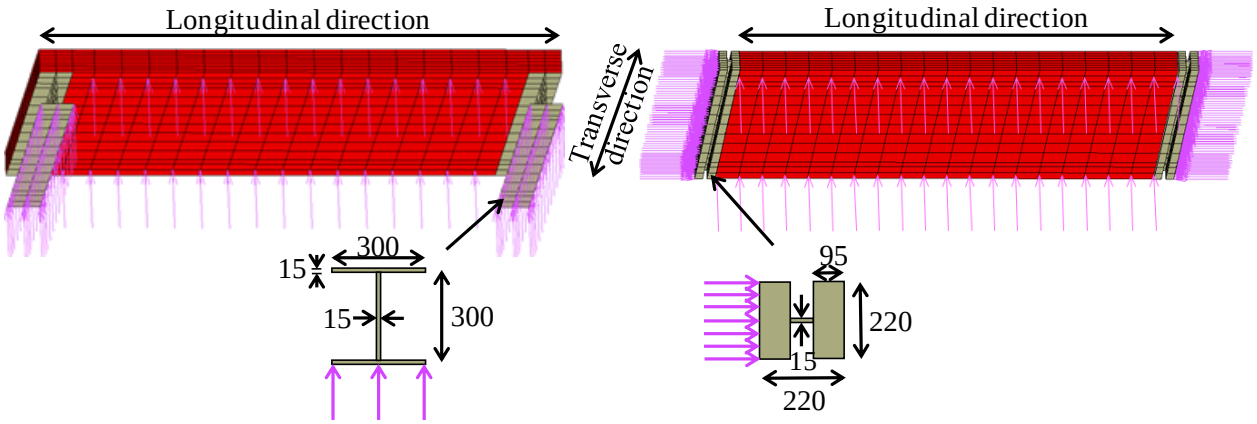

(a) Typically used BCs **(b)** Equivalent BCs

Figure 5.7 Illustration of the boundary conditions (mm)

5.5 STATIC ANALYSIS OF THE PANEL SLAB

In the previous section, a static analysis of a bridge slab is conducted, and equivalent BCs for its corresponding panel slab are determined based on the calculated stiffness of the bridge slab. In order to validate the determined equivalent BCs, a static analysis of the panel slab with equivalent BCs is conducted. Furthermore, a static analysis of the panel slab with typically used BCs is also conducted for the sake of comparison.

5.5.1 Description of the panel slab

The dimensions (L×W×T) of the panel slab are 4750×2860×220 mm. The same thickness of the bridge slab is selected for the panel slab. The length and width of the panel slab are chosen to be similar to the panel slab studied by NILIM, Japan [16]. The reason for selecting the similar dimensions with the panel slab of NILIM is that the same typically used BCs adopted by NILIM can be used in this study for the comparison purpose.

The same material properties of concrete and steel with the JBA [32] are used for the panel slab as well. Since, in the previous section, static analysis of the bridge slab without reinforcement bars was conducted, the panel slab without reinforcement bars was considered for static analysis in this section as well for the sake of comparison.

5.5.2 Boundary conditions

The static analyses of the panel slab were carried out for the following BCs cases.

5.5.2.1 Typically used BCs

For the simulation with BCs typically utilized in past studies, the panel slab is supported using simple supports along the longitudinal edges. The steel I-beams are vertically oriented along the transverse edges of the slab, and these beams are restrained at their bottom flanges against vertical displacement. Because the dimensions of the panel slab in this study are near to the dimensions of the panel slab studied by NILIM [16], the same typically used BCs with NILIM are adopted in this study and are displayed in **Figure 5.7(a)**

5.5.2.2 Equivalent BCs

In the previous sections, the FEA of a bridge slab is conducted, and based on the calculated stiffness of the bridge slab, the steel I-beams to be employed along the transverse edges of the panel slab are determined. The determined steel I-beams are horizontally positioned as supports along the transverse edges of the panel slab to elicit deformation behavior that is similar to the bridge slab. The same dimensions of the steel I-beams as determined, in section 5.4, are used for the equivalent BCs, as shown in **Figure 5.7(b)**. These beams are restrained at their outer flanges in the

longitudinal direction of the panel slab. Moreover, the panel slab is supported with simple supports along the longitudinal edges of the panel slab, similar to the typically used BCs.

5.5.3 Loading conditions

A static load of 157 kN, an initial load of the stepwise loading sequence, is applied at the center of the slab, i.e., location A, and an elastic analysis is conducted. Similarly, elastic analyses are conducted for the loading locations away from the center of the slab, i.e., B, C, and D, as shown in **Figure 5.8**.

5.6 STATIC ANALYSIS RESULTS

The static analysis is carried out for the panel slab with the determined equivalent BCs in this study in addition to the panel slab with typically used BCs, as displayed in **Figure 5.7**. Furthermore, the static analysis is also carried out for the bridge slab for the comparison purpose.

The bending moments parallel to the x-axis and y-axis, M_{xx} and M_{yy}, are calculated for the bridge slab and the panel slab. To facilitate the observation, comparison, and to roughly check the cracking regions, the cracking moment (M_{crack}) is calculated as:

$$M_{crack} = \frac{\sigma_t I_c}{y} \tag{5.5}$$

where σ_t is the concrete strength in tension; I_c is the second moment of area; and y is the half-thickness of the panel slab.

Moreover, the displacements in the longitudinal and transverse directions are attained for the static load at the center and away from the center of the slabs. The loading locations are shown in **Figure 5.8**.

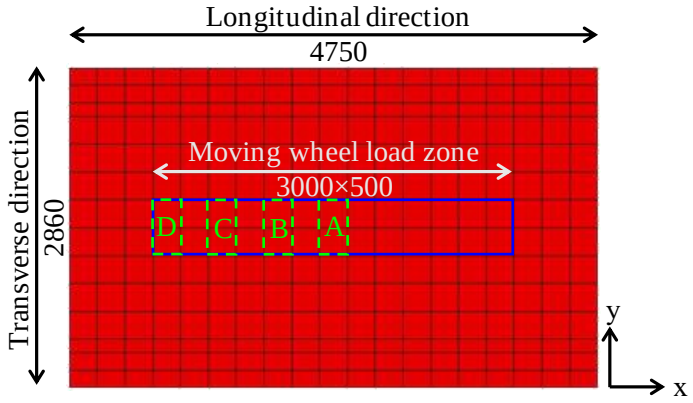

Figure 5.8 Panel slab showing loading locations (mm)

5.6.1 Bending moment cracking zones

Figure 5.9 shows the bending moment cracking zones for the bridge slab and the panel slab with BCs, including the equivalent BCs and the typically used BCs.

For the bridge slab, the cracking zones for M_{xx} due to load at locations A, B, C, and D are identical to each other (see **Figure 5.9(a)**). Similarly, the cracking zones for M_{yy} for all the loading locations are also similar to each other. These results confirm that the bridge slab exhibits the same bending moment distributions around the loading locations as the load moves along the slab axis.

For the panel slab with typically used BCs, the cracking zones for M_{xx} due to load at locations A, B, C, and D are very similar to each other (**Figure 5.9(b)**). On the other hand, the cracking zones for M_{yy} are significantly condensed with increasing distance from loading point in the center, especially for the loading locations C and D. The reason is that the steel I-beams in vertical positioning possess higher bending stiffness parallel to the y-axis. These steel I-beams with high bending stiffness restrain the panel slabs from experiencing the same bending moment distributions around the loading locations upon the movement of the load along the slab axis, which is contrary to the bridge slab.

For the panel slab with equivalent BCs, the cracking zones are observed to be similar in all loading locations for M_{xx} as well as $M_{yy,}$ as shown in **Figure 5.9(c)**, which is identical to the bridge slab. This implies that the determined steel I-beams of the equivalent BCs for the panel slab correctly represent the longitudinal continuity of the bridge slab.

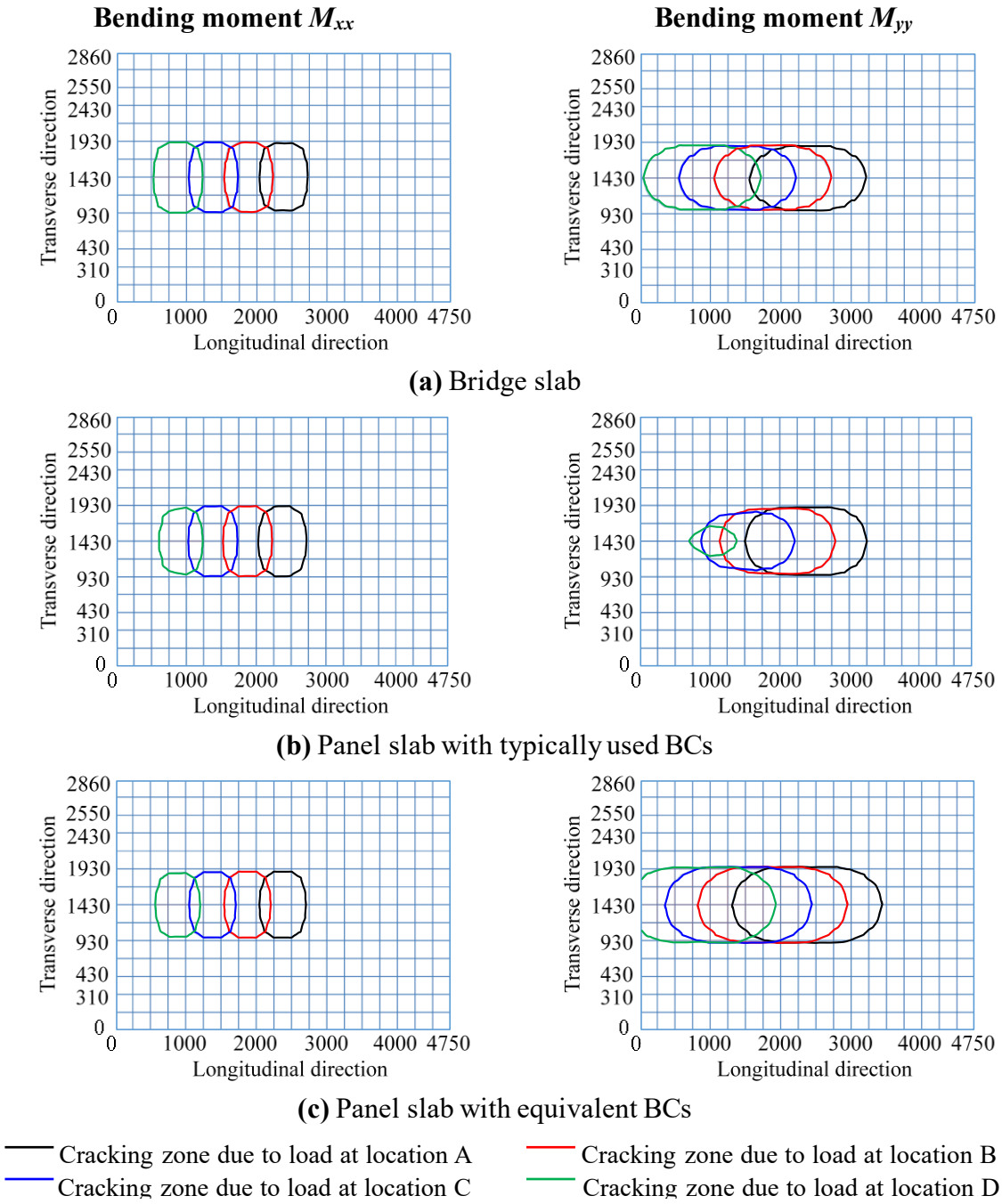

Figure 5.9 Bending moment cracking zones

5.6.2 Displacement distribution

The displacements in the longitudinal and transverse directions are compared for the bridge slab and the panel slab with BCs, as displayed in **Figure 5.10**.

For the bridge slab case, the displacements around all the loading locations are found to be similar to each other as the load moves along the slab axis, which is shown in **Figure 5.10(a)**.

In **Figure 5.10(b)**, for the panel slab with typically used BCs, the displacements for loading locations B, C, and D are significantly reduced as compared to the displacement for loading

location A. This displacement difference is more pronounced for the loading location near the steel I-beams, i.e., location D. The reason is that the panel slab is directly resting on the vertically placed steel I-beams and these steel I-beams restrain the displacements of the panel slabs, which is contrary to the bridge slab.

For the panel slab with equivalent BCs, the displacements for all loading locations are found to be similar to each other, as shown in **Figure 5.10(c)**, which is identical behavior to the bridge slab. Thus, the panel slab with equivalent BCs can replicate the displacement behavior of the bridge slab. However, the displacement values for the bridge slab case are much higher than the displacement values for the panel slab with equivalent BCs, which is obviously due to the longer longitudinal span of the bridge slab.

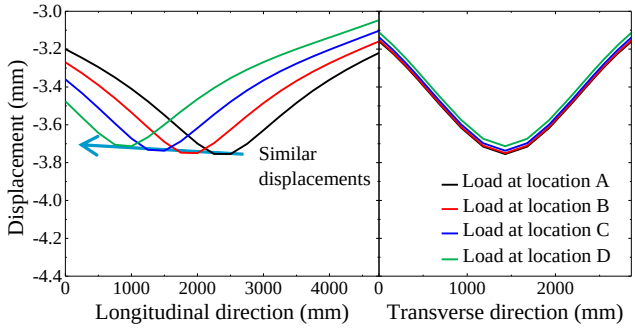

(a) Bridge slab

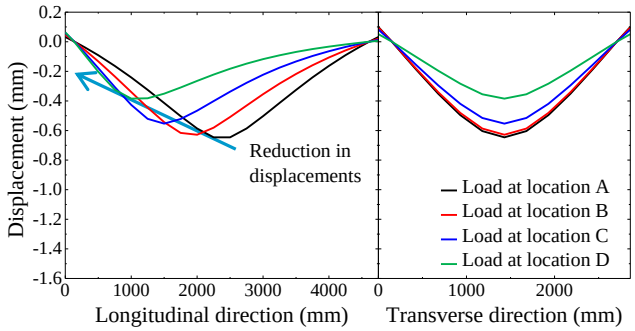

(b) Panel slab with typically used BCs

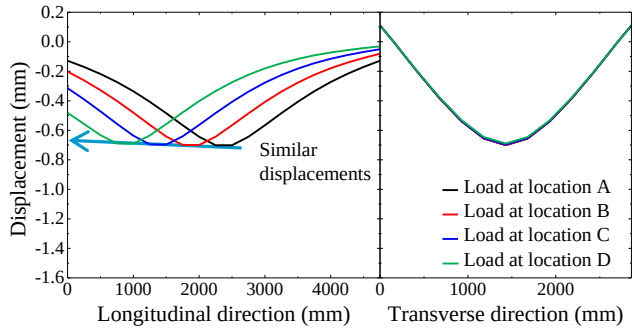

(c) Panel slab with equivalent BCs

Figure 5.10 Displacement distribution

Table 5.2 Comparison of relative displacements

Loading location	Relative displacement (mm)			Displacement difference (%)	
	Bridge slab	Typically used BCs	Equivalent BCs	Typically used BCs	Equivalent BCs
	X	Y	Z	(X-Y)/X	(X-Z)/X
Load at A	0.576	0.678	0.571	17.71	0.87
Load at B	0.572	0.661	0.571	15.56	0.17
Load at C	0.554	0.585	0.566	5.60	2.17
Load at D	0.544	0.416	0.56	23.53	2.94

For the sake of quantitative comparison of displacements, relative displacements of the bridge slab and panel slabs with BCs are obtained for all the loading locations, as displayed in **Table 5.2**. Contrary to the panel slab with typically used BCs, the panel slab with equivalent BCs possesses almost the similar relative displacements with the bridge slab for all the loading locations. Furthermore, the differences in relative displacements for the panel slabs with BCs are also calculated with respect to the relative displacements of the bridge slab, as shown in **Table 5.2**. The maximum difference in the relative displacement is 23.53% for typically used BCs case, which shows that the panel slab with typically used BCs behaves quite differently from the bridge slab. On the other hand, for the equivalent BCs case, the maximum difference in the relative displacement is 2.94%, which is quite a reasonably small value. This observation implies that, contrary to the panel slab with typically used BCs, the panel slab with equivalent BCs experiences the same displacement behavior of the bridge slab.

5.7 SUMMARY AND CONCLUSIONS

In this chapter, an equivalent BCs determination method is developed numerically for a panel slab to analyze the behaviors of a bridge slab realistically. For this purpose, an FEA of a bridge slab is conducted, and the bending and rotational stiffness are determined along the transverse edge of the corresponding panel of the bridge slab. Based on the determined stiffness, the equivalent steel I-beams to be employed at the transverse edge of the panel slab are determined.

To validate the method, an FEA is carried out for the panel slab with the determined equivalent BCs, as well as the panel slab with typically used BCs. Furthermore, the FEA is also carried out for the bridge slab for the comparison purpose.

The results of the panel slab with equivalent BCs are found to have more similar bending moment distributions and displacement behaviors to the corresponding results of the bridge slab.

On the other hand, the panel slab with typically used BCs shows remarkable variations in results of bending moment distribution and deformations as compared to the corresponding results of the bridge slab.

Conclusively, the panel slab with equivalent BCs behaves in the same manner as a bridge slab, and consequently, results in a more realistic analysis of the bridge slab.

Chapter 6

FATIGUE ANALYSIS OF A PANEL SLAB WITH EQUIVALENT BCS

6.1 GENERAL

In chapter 5, an equivalent BCs determination method is developed numerically for a panel slab to realistically analyze the deformation and fatigue behaviors of a bridge slab. Furthermore, in order to validate the determined equivalent BCs, a static analysis of the panel slab with equivalent BCs is conducted in addition to the static analysis of a bridge slab. The static analysis results of the panel slab with equivalent BCs are found to have more similar bending moment distributions and displacement behaviors to the corresponding results of the bridge slab.

In this chapter 6, for the simulation of fatigue behavior, fatigue analysis of a panel slab with equivalent BCs is carried out along with the panel slab with the BCs typically used in previous studies. The FEM-based numerical model that considered bridging stress degradation is employed in these fatigue analyses. Contrary to the typically used BCs, the equivalent BCs allow the propagation of cracked elements in the longitudinal and transverse directions in a similar manner as the bridge slabs. Consequently, the panel slab with equivalent BCs is able to simulate the extensive grid crack pattern, which is identical to the typical crack pattern observed in bridge slabs.

6.2 DETAILS OF THE PANEL SLAB

Fatigue analysis is carried out for the same panel slab as considered for static analysis of the panel slab in the previous chapter. The considered panel slab is an RC plate with 4750×2860×220 mm (L×W×H) dimensions. In the tension zone, the slab is reinforced using D19@125 mm and D19@120 mm in the transverse and longitudinal directions, respectively. In the compression zone, D19@250 mm and D19@120 mm are provided in the transverse and longitudinal directions, respectively. The same reinforcement bar size and reinforcement arrangement of the bridge slab [32] are used for the considered panel slab. **Figure 6.1** shows the detailed information for panel slab geometry, reinforcement arrangements, and a moving wheel load zone.

The same material properties of concrete and reinforcement bars with the JBA [32] are used for the panel slab.

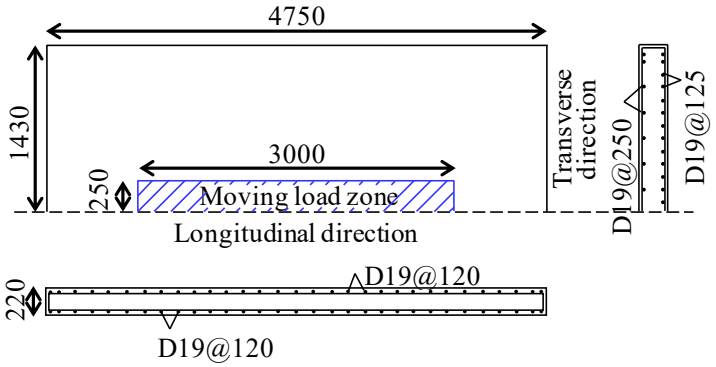

Figure 6.1 Details of the panel slab (mm)

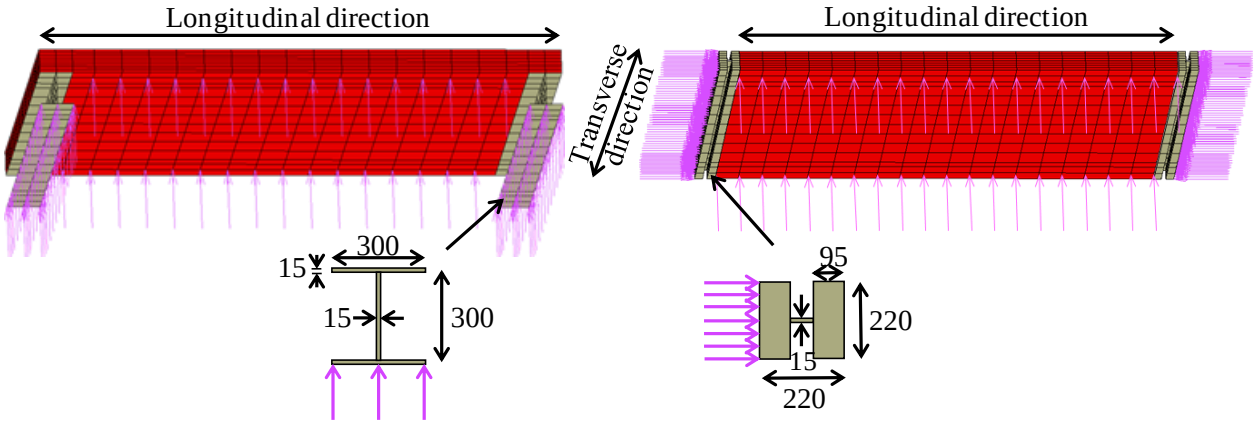

(a) Typically used BCs **(b)** Equivalent BCs

Figure 6.2 Illustration of the boundary conditions (mm)

6.3 BOUNDARY CONDITIONS

Fatigue analysis of the panel slab is conducted for the equivalent BCs determined in this study (see Chapter 5). In addition to this analysis, a fatigue analysis is also carried out for the panel slab equipped with BCs typically used by NILIM [16]. The details of the equivalent and typically used BCs are illustrated in **Figure 6.2**.

6.4 LOADING SEQUENCE

The panel slab is subjected to a moving wheel load in the longitudinal direction with 3000 × 500 mm loading zone dimensions, as shown in **Figure 6.1**. The same moving wheel load zone and stepwise loading sequence used in the NILIM study [16] are employed in this study. In the stepwise loading sequence, after a specific number of loading cycles, the intensity of the wheel load is amplified in increments to promote deterioration to save time. In this study, the employed stepwise loading sequence has an initial wheel load of 157 kN, which intensifies to 392 kN in increments of 19.6 kN after each 40,000 loading cycles, as shown in **Figure 6.3**.

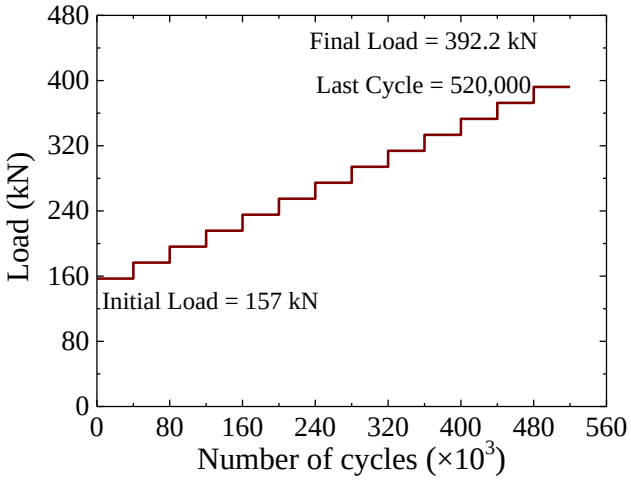

Figure 6.3 Stepwise loading sequence

6.5 FATIGUE ANALYSIS RESULTS

For realistic fatigue behavior analysis of a bridge slab, a fatigue analysis of a panel slab with the determined equivalent BCs is carried out along with the panel slab with the BCs typically used in previous studies. Due to a symmetry in boundary and loading conditions, only one half of the panel slab is considered in the fatigue analysis to save the computational time.

6.5.1 Evolution of cracked elements

The cracked elements have appeared in the bottom layers of the panel slab just after the application of the first loading cycle of moving wheel load. Due to the increases in the number of cycles and intensities of the cyclic moving wheel load, the cracked elements are propagated in various directions. Therefore, it is essential to consider the effects of loading cycles and their intensities over the propagation of cracked elements. The evolutions of cracked elements in the panel slab for the typically used as well as the equivalent BCs cases at the various numbers of loading cycles, are displayed in **Figure 6.4**. Uncracked elements are displayed in white, while different colors show the cracked elements initiated at different loading cycles.

In the case of typically used BCs, the cracked elements that appeared at the bottom of the panel slab after the first loading cycle are highlighted in red in **Figure 6.4(a)**. The cracked elements propagate in the longitudinal, transverse, and vertical directions due to the further increases in the number of loading cycles. The reason is that the bridging stress degradation of the concrete happens because of the process of crack opening and closing. The loading capacity from the bridging stress of concrete cannot be reached the same level as of the 1st loading cycle with the already formed cracked state, and the cracked elements propagate in other directions to maintain the load level. The cracked elements are propagated diagonally due to the vertically positioned steel I-beams, which restrict the panel slab from cracking and deflecting in the longitudinal direction around these steel I-beams. The diagonal cracked elements reach the corners of the panel slab during the

200,000th loading cycle. Subsequently, the corners cracked elements spread in the vertical direction in addition to the propagation of cracked elements in the diagonal and vertical directions. At the 400,000th cycle, the top surface elements at the loading location are cracked due to the heavy moving wheel load. Furthermore, the corners of the panel slab become entirely cracked at the 400,000th cycle due to negative bending at the corners. At the 520,000th cycle (i.e., the final loading cycle), the panel slab is failed in punching shear due to a complete cracking of the slab section at the loading location. Moreover, the cracked elements are propagated in a diagonal fashion on the upper layers of the slab from the corners due to negative bending at the corners that result in cracked top surface elements. These top surface cracked elements at the corners are then propagated in the diagonal direction toward the loading point. Bridge slabs do not exhibit similar crack propagation phenomena on the top surface as the panel slab with typically used BCs.

On the other hand, in the case of equivalent BCs, multiple cracked elements are appeared on the bottom layers of the panel slab (see **Figure 6.4(b))**, as the first loading cycle was applied. As the number of loading cycles increases, the cracked elements propagate in the longitudinal, transverse, and vertical directions. Contrary to the typically used BCs, the cracked elements spread in the longitudinal and transverse directions at the 200,000th cycle. At the 300,000th cycle, the cracked elements reach the corners of the panel slab and begin to propagate in the vertical direction. Cracked elements are appeared at the loading place on the top layer at the 440,000th cycle due to the heavy load of the stepwise loading sequence. At the 520,000th cycle (i.e., the final loading cycle), the corner cracked elements are penetrated up to 3/4th of the thickness of the panel slab. In contrast to the typically used BCs, the corners of the panel slab are not entirely cracked, and the cracked elements do not progress in a diagonal fashion from the corners to the loading point on the top layer of the panel slab.

A comparison of the volume of cracked elements in typically used and equivalent BCs cases is made in **Figure 6.5**. For the typically used BCs case, the panel slab is found to experience a smaller volume of cracked elements than the equivalent BCs case during the first 200,000 cycles. However, the typically used BCs case exhibits an opposite behavior from the 200,000th cycle to the 520,000th cycle, which is caused by the propagation of the cracked elements in the diagonal direction, reaching the corners of the panel slab and propagating in the vertical as well as in the diagonal direction. The average degradation ratios for the typically used and equivalent BCs cases are 2162 mm^3/cycles and 1803 mm^3/cycles, respectively. This reveals that the diagonal propagation of cracked elements, which are not observed in real bridge slabs, triggers the degradation phenomenon in the case of typically used BCs. As a result, the panel slab with typically used BCs is degraded more as compared to the panel slab with equivalent BCs.

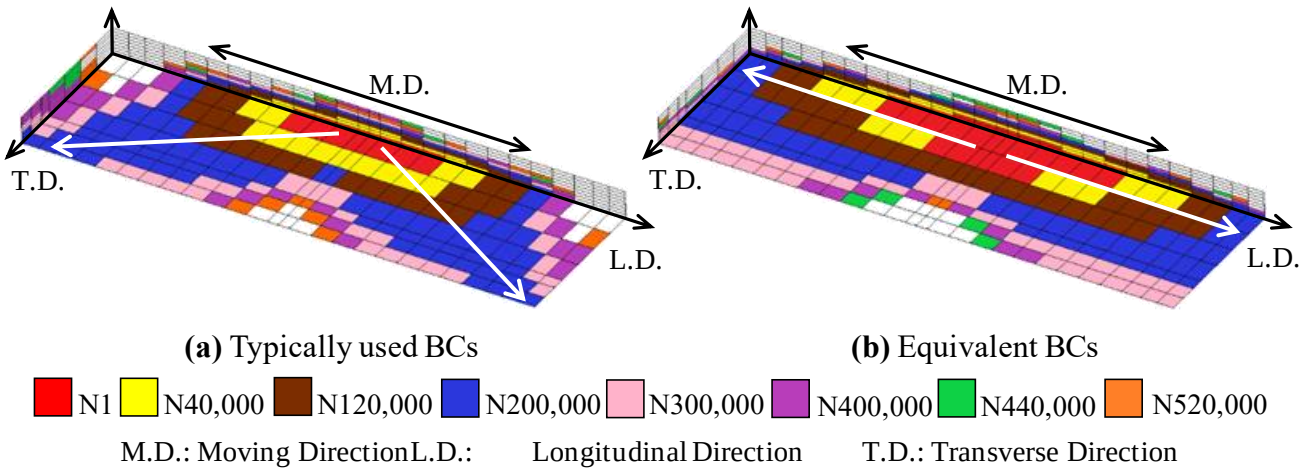

Figure 6.4 Evolution of the cracked elements

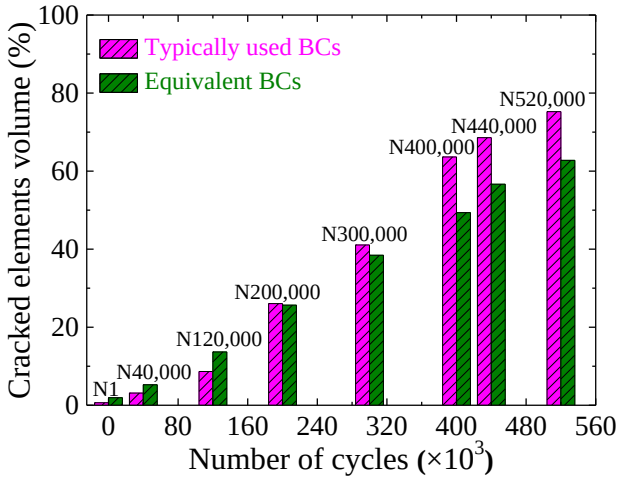

Figure 6.5 Percentage of cracked elements volume

After the first moving load cycle, the panel slab with typically used BCs encounters a lesser cracked element zone than the panel slab with equivalent BCs. However, the cracked elements propagate diagonally and reach the corners of the panel slab in less number of loading cycles in comparison with the equivalent BCs case. This is due to the fact that the steel I-beams are vertically positioned in the typically used BCs, which restrains the panel slab from cracking and deflecting in the longitudinal direction around these steel I-beams. Consequently, the cracked elements proceed diagonally rather than continuing in the longitudinal and transverse directions, which is not commonly witnessed in bridge slabs. After that, the cracked elements at the corners propagate vertically and diagonally, which results in a larger cracked element zone in the case of typically used BCs. The bridging stress degradation of this larger cracked element zone results in greater degradation of the panel slab. This enhanced degradation, caused by the diagonal cracked propagation, results in a shorter fatigue life of the panel slab with typically used BCs in comparison to fatigue life of bridge slabs.

6.5.2 Maximum principal strain distribution

A comparison is made and presented in **Figure 6.6** for the maximum principal strain distribution on the bottom surface of the panel slab under various loading cycles for both BCs cases. White color represents the maximum principal strain value less than the value of cracking strain of the concrete while in all other colors of contours, the maximum principal strain value is higher than the value of concrete cracking strain. After the first cycle of moving wheel load, the maximum principal strain distribution shows a larger longitudinal spread in the case of equivalent BCs than typically used BCs. At the 200,000th cycle, the maximum principal strain is distributed evenly in the longitudinal as well as transverse direction for equivalent BCs, while it is distributed diagonally towards the slab corners after initiating from the loading point in the case of typically used BCs. The principal strain distribution validates that the crack propagates in the diagonal direction for the typically used BCs case. At the 520,000th cycle (i.e., the final loading cycle), the maximum principal strain possesses the highest value around the loading location and spread diagonally toward the corners in the case of typically used BCs. On the other hand, for the equivalent BCs case, the maximum principal strain spreads in the longitudinal and transverse directions at the 520,000th cycle. This principal strain distribution confirms that the crack propagates in the longitudinal and transverse directions for the equivalent BCs case.

For the equivalent BCs case, in comparison with the typically used BCs case, the panel slab experiences the cracking strain on a bigger part of the bottom surface in the longitudinal direction after the first cycle of moving wheel load. Subsequently, the maximum principal strain propagates in the longitudinal and transverse directions with increases in the number of loading cycles. This is because of the close relevance of the panel slab with equivalent BCs to that of bridge slab, as the horizontally placed steel I-beams allow the maximum principal strain distribution in the longitudinal and transverse direction of the panel slab in a similar fashion as bridge slabs. Conversely, the vertically placed steel I-beams in the case of typically used BCs possess high bending stiffness, which ultimately proceeds the maximum principal stress distribution in the diagonal direction of the panel slab. Moreover, the maximum principal strain concentration is found to be quite high in the diagonal direction, leaving uncracked regions in the longitudinal direction at the bottom of the panel slab with typically used BCs, even after the last loading cycle, which is not generally seen in bridge slabs.

6.5.3 Evolution of mid-span displacement

Figure 6.7 shows a comparison of mid-span displacement evolution of the panel slab for typically used and equivalent BCs cases. For the typically used BCs case, the mid-span displacement is comparatively less than that of equivalent BCs at the initial loading cycles. However, the displacement is determined to be relatively higher at the final loading cycles.

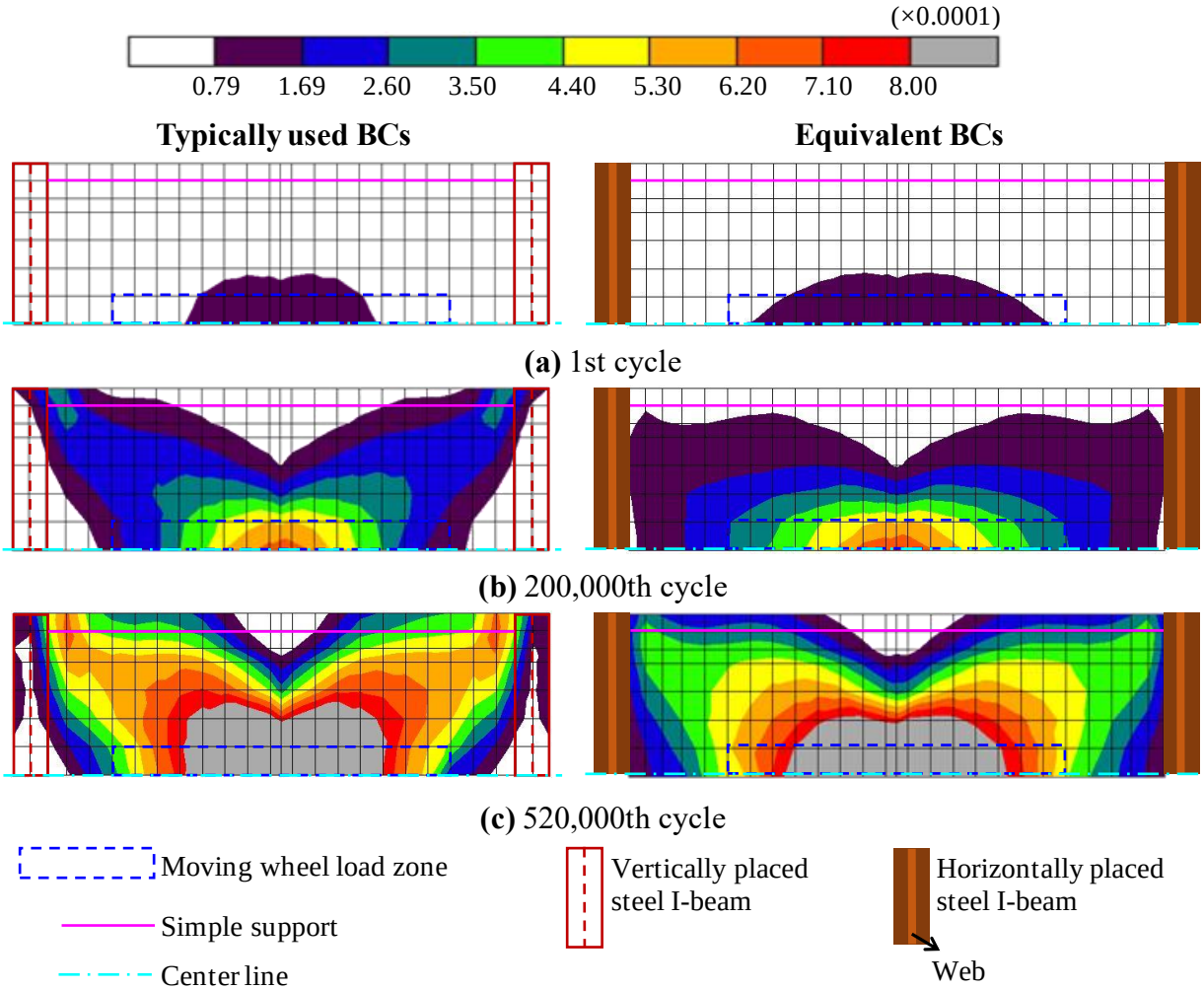

Figure 6.6 Maximum principal strain distribution

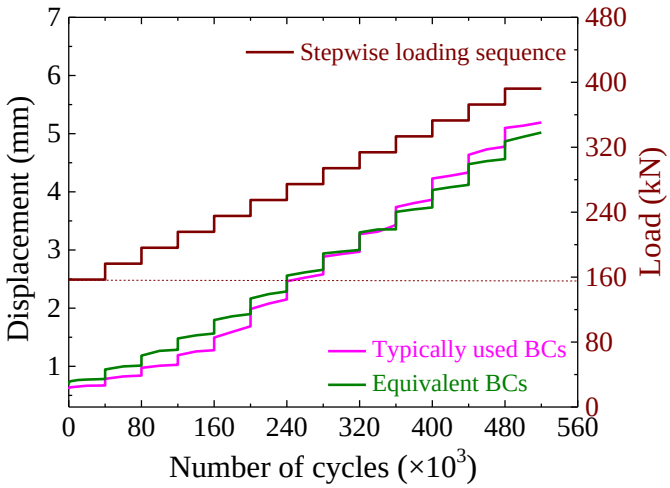

Figure 6.7 Evolution of mid-span displacement

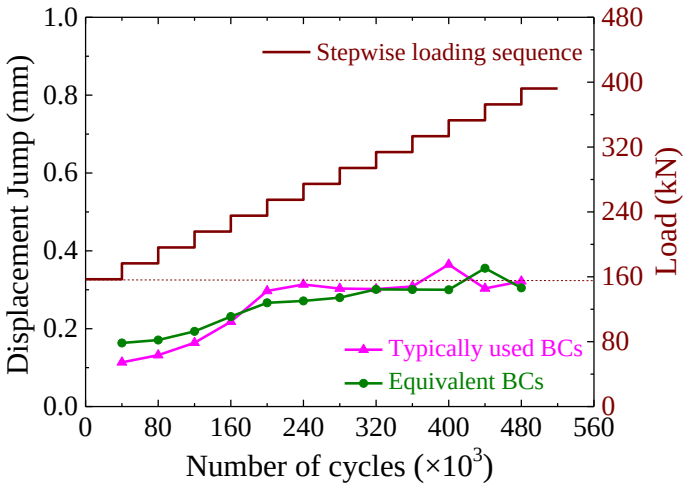

Figure 6.8 Displacement jump

For a detailed comparison of mid-span displacement, the displacement jumps attained during the fatigue analysis at various cycles for both cases of BCs are shown in **Figure 6.8**. A displacement jump denotes a sharp rise in the displacement that occurred during an increment in the loading intensity in a stepwise loading sequence. Two sharp peaks are found in the case of typically used BCs. The first steep rise in the displacement jump is seen for the typically used BCs case at the 200,000th cycle, which is because of the development of the diagonal cracks. The second significant displacement jump is found at the 400,000th cycle when the top surface elements at the loading locations are cracked due to heavy loading. In the case of equivalent BCs, the top surface elements at the loading location are cracked at 440,000th cycle, where a significant displacement jump has occurred in the equivalent BCs case.

The panel slab, in the case of typically used BCs, displays a smaller displacement evolution in initial loading cycles than that of equivalent BCs case. This is because of the high resistance against bending and the displacement upon movement of the load along the slab axis due to the vertically positioned steel I-beams. However, the formation of diagonal cracks towards the corners and propagation of corner cracks vertically lead to a substantial displacement evolution that is dissimilar to bridge slabs.

6.5.4 Crack patterns

Figure 6.9 illustrates the crack patterns on the bottom surface of the panel slab at the final loading cycle for both the BCs cases. In the case of typically used BCs, the main crack originates at the center of the location of the moving load and extends toward the supporting corners. As the cycles increase, diagonal cracks are formed between the positions of the moving load and supporting corners resulting in a first crack set. Meanwhile, other cracks are formulated perpendicular to the existing cracks as second and third crack sets surrounding the moving wheel load zone. Further increases in the loading cycles result in extensive cracking.

However, in the case of equivalent BCs, horizontal cracks are formed in different orientations than the diagonal cracks in the typically used BCs case. Moreover, the cracks propagate until the end of the moving wheel load zone in the longitudinal direction for the typically used BCs case. For the equivalent BCs case, the crack propagation is occurred throughout the length of the panel slab that surrounds the moving wheel load zone in the longitudinal direction.

The crack angles are obtained at three sections, sections I, II, and III, for both the BCs cases, as presented in **Figure 6.10**. The cracks are classified into two types, horizontal and diagonal cracks, based on the crack angle in the first crack set. In general, the horizontal and diagonal cracks are considered to possess angles of 0 and 45 degrees, respectively, with the x-axis. However, the cracks in the panel slab have a wide range of angles, even within 0 and 45 degrees. Therefore, in order to classify the cracks with a wide range of angles into two types, the middle value of 22.5 degrees is considered in this study. The crack is considered to be a horizontal crack if its angle with the x-axis was less than 22.5 degrees. Otherwise, it is regarded as a diagonal crack, when its angle was greater than 22.5 degrees. The horizontal cracks produce the grid crack pattern, while the diagonal cracks lead to the formation of the diagonal crack pattern.

A comparison of both types of crack patterns for both BCs cases is plotted in **Figure 6.11**. The typically used BCs reproduce the grid crack pattern in the panel slab only within the loading zone in the transverse direction as well as the longitudinal direction, which contrasts with the behavior of the bridge slab. However, in the panel slab with equivalent BCs, the formation of the grid crack pattern in the transverse direction is observed to be almost twice the grid crack pattern that is formed by the panel slab with typically used BCs. Moreover, the panel slab with equivalent BCs reproduces the grid crack pattern in the longitudinal direction to a broader range compared to the panel slab with typically used BCs case.

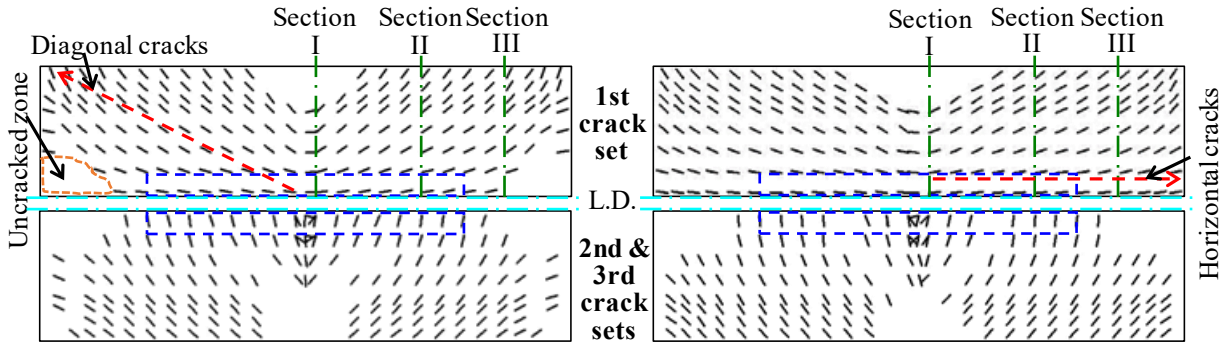

(a) Typically used BCs **(b)** Equivalent BCs

Figure 6.9 Crack patterns

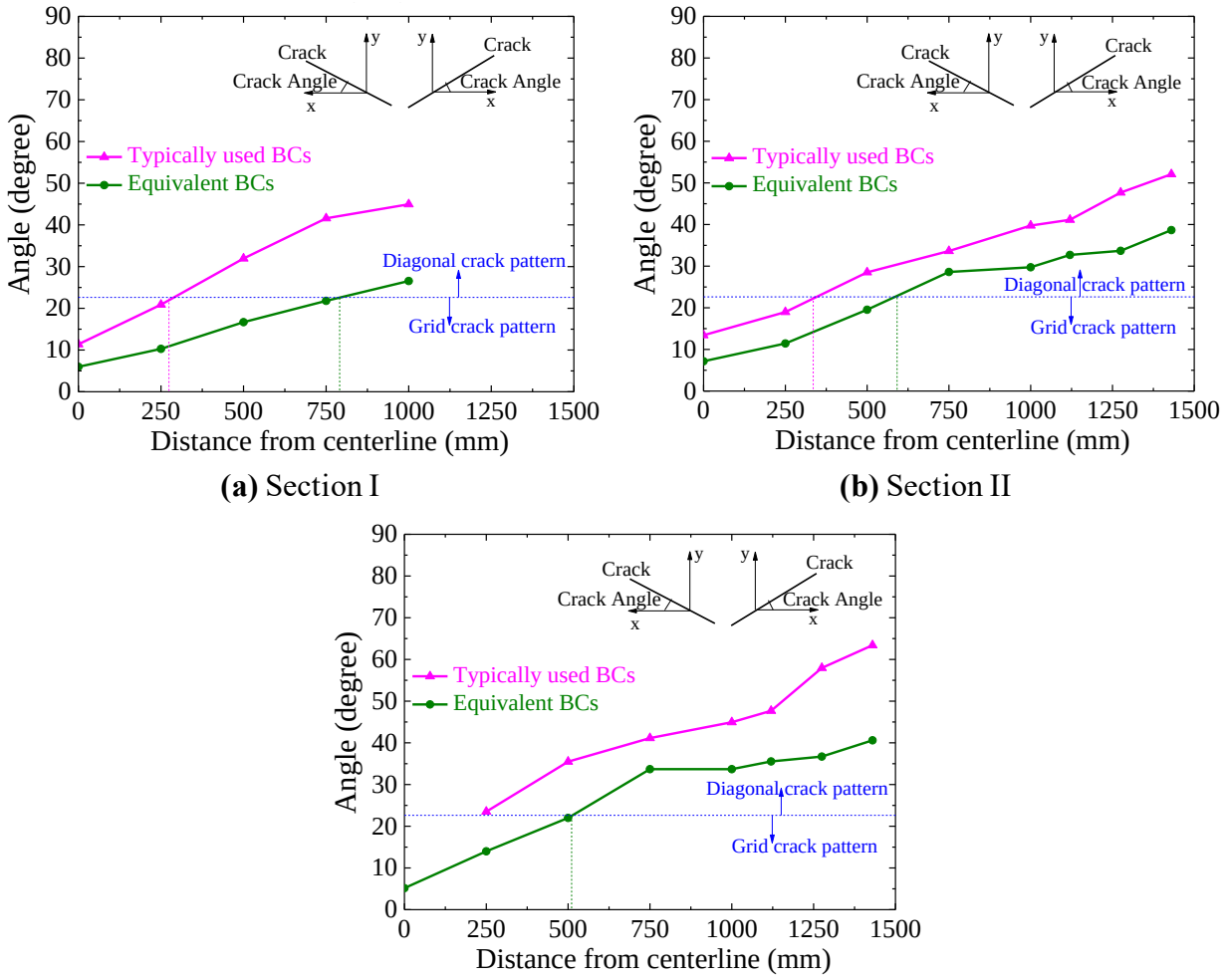

(a) Section I **(b)** Section II

(c) Section III

Figure 6.10 Crack angles along the transverse direction

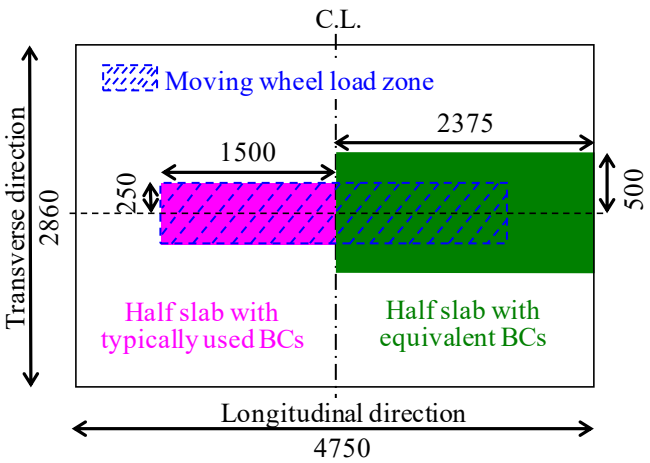

Figure 6.11 Grid crack pattern zone (mm)

It is essential to mention that fatigue-inducing repetitive traffic loads, i.e., cyclic moving wheel loads, are considered to be the primary cause for degradation and crack patterns of bridge slabs. Therefore, this study also focuses on the cyclic moving wheel loads as the main reason for deterioration and crack patterns. However, environmental actions, such as freezing and thawing,

and thermal and drying shrinkage, can also lead to degradation and formation of crack patterns in bridge slabs. These environmental actions should also be considered in combination with the cyclic moving loads in future studies. The panel slab with equivalent BCs subjected to the cyclic moving loads and environmental actions would yield to a more realistic simulation of the bridge slabs.

6.6 SUMMARY AND CONCLUSIONS

In this chapter, to simulate the fatigue behavior, fatigue analysis of a panel slab with equivalent BCs is conducted. Furthermore, for comparison purpose, fatigue analysis of the panel slab with the BCs typically used in past studies is also carried out. The FEM-based numerical model that considered the bridging stress degradation, as discussed in detail in chapter 2, is utilized in these fatigue analyses.

The fatigue analysis results reveal that the equivalent BCs allow the propagation of cracked elements in the longitudinal and transverse directions of the panel slab, in a similar manner as a bridge slab. Moreover, in contrast to the typically used BCs, the equivalent BCs do not lead the cracked elements to propagate on the top surface from the corners to the loading point, which is similar to a bridge slab. On the other hand, the typically used BCs stimulate the propagation of cracked elements in the diagonal direction of the panel slab, which is contrary to a bridge slab. This diagonal propagation of the cracked elements leads to an additional degradation of the panel slab, which results in a shorter fatigue life prediction of a bridge slab.

Furthermore, in contrast to bridge slabs, the typically used BCs reproduce the grid crack pattern only within the moving wheel load zone in the panel slab. However, the equivalent BCs reproduce the extensive grid crack pattern in the panel slab, well in accordance with that generally witnessed in a bridge slab.

All these numerical results conclude that the panel slab with equivalent BCs behaves in the same manner as a bridge slab, which results in a more realistic fatigue behavior analysis of the bridge slab.

Chapter 7

CONCLUSIONS AND RECOMMENDATIONS

7.1 CONCLUSIONS

This study mainly aims to elucidate the effects of BCs and propose BCs for panel slabs to realistically analyze the deformation and fatigue behaviors of bridge slabs. Based on this study, specific outcomes and conclusions can be drawn, which are summarized as follows:

1. The applicability of a fatigue analysis method based on the bridging stress degradation concept for a panel slab subjected to stepwise loading sequence is investigated. The fatigue analysis method based on the bridging stress degradation concept for the panel slab shows a good agreement with the experimental results. The numerical results confirm that the numerical model successfully simulates the fatigue behavior, such as center displacement evolution, propagation of cracked elements, and crack pattern, of the panel slab subjected to stepwise loading sequence.

2. This study proposes a method for the determination of approximate BCs for a panel slab to capture the realistic behaviors of the bridge slab. By following the flowchart presented in this study, one can easily determine the approximate BCs for different dimensions of panel slabs capable of reproducing the behaviors of bridge slabs. Furthermore, the FEA of the panel slab with approximate BCs shows that the approximate BCs reproduce the same bending moment distribution and displacements around the loading locations as the wheel load moves along the slab axis in the panel slab, which are similar to those of the bridge slab.

3. Using the fatigue analysis method based on the bridging stress degradation concept, fatigue analysis of a panel slab with approximate BCs is conducted in addition to the panel slab with the BCs typically used in the past studies. The fatigue analysis results show that the approximate BCs do not result in a negative bending at the corners of the panel slab, and the cracked elements do not propagate on the top surface from the corners to the loading point, which is similar to a bridge slab. However, in the panel slab with typically used BCs, the negative bending at the corners and the propagation of the cracked elements on the top surface from the corners to the loading point produce an additional deterioration in the panel slab, which leads to a shorter fatigue life estimation of a bridge slab.

4. In this study, for more accurate and realistic fatigue behavior analysis of a bridge slab, an equivalent BCs determination and sophisticated method is developed numerically for a panel

slab. For this purpose, an FEA of a bridge slab is conducted, and the bending and rotational stiffness are determined along the transverse edge of the corresponding panel of the bridge slab. Based on the determined stiffness, the equivalent steel I-beams to be employed at the transverse edge of the panel slab are determined. The results of the panel slab with equivalent BCs are found to have more similar bending moment distributions and displacement behaviors to the corresponding results of the bridge slab.

5. To simulate the fatigue behavior, fatigue analysis of a panel slab with equivalent BCs is conducted. Furthermore, for comparison purpose, fatigue analysis of the panel slab with the BCs typically used in past studies is also carried out. The fatigue analysis results reveal that the equivalent BCs allow the propagation of cracked elements in the longitudinal and transverse directions of the panel slab, in a similar manner as a bridge slab. Moreover, in contrast to the typically used BCs, the equivalent BCs do not lead the cracked elements to propagate on the top surface from the corners to the loading point, which is similar to a bridge slab. Furthermore, contrary to the typically used BCs, the equivalent BCs reproduce the extensive grid crack pattern in the panel slab, well in accordance with that generally witnessed in a bridge slab. All these numerical results conclude that the panel slab with equivalent BCs behaves in the same manner as a bridge slab, which results in a more realistic fatigue behavior analysis of the bridge slab.

7.2 RECOMMENDATIONS FOR FUTURE STUDIES

Based on the discussion in the previous chapters, the following developments are recommended for future studies:

1. Consideration of environmental-related effects

The deterioration and crack patterns of bridge slabs are primarily associated with the fatigue-inducing repetitive moving loads and environment-related effects, such as corrosion, dry shrinkage, and freezing and thawing. However, in this study, the repetitive moving wheel loads are considered as the main cause of the deterioration and crack patterns of the bridge slabs.

In the future study, environmental-related effects should also be considered together with the repetitive moving wheel loads. The panel slab with the BCs, proposed in this study, considering the repetitive moving wheel loads and environmental-related effects would yield to a more realistic simulation of the bridge slab.

2. Experimental verification of the proposed BCs for the panel slabs

In the past, numerous experimental researches have been conducted for the panel slabs,

equipped with typically used BCs, in order to investigate the fatigue behavior of the bridge slabs. However, the panel slabs with typically used BCs failed to reproduce the deformation and fatigue behaviors of the bridge slabs.

Therefore, in this study, the BCs are newly proposed through numerical studies for the panel slabs, which can simulate the realistic behaviors of the bridge slabs. The numerical studies show that the panel slabs with the proposed BCs behave in the same manner as the bridge slabs. To validate the numerical results, experimental studies can be conducted for the panel slabs with the proposed BCs.

3. Consideration of reinforcement bars in calculation of stiffness of bridge slab

In chapter 5, an equivalent BCs determination method is developed numerically for a panel slab to realistically analyze the deformation and fatigue behaviors of a bridge slab. For this purpose, an FEA of a bridge slab is conducted, and based on the calculated stiffness of the bridge slab, equivalent BCs for the corresponding panel slab are determined. The panel slab with equivalent BCs successfully captures the deformation and fatigue behaviors of a bridge slab. However, in order to save time and for the sake of simplification in developing the determining method of the stiffness of the bridge slab, an elastic analysis of the bridge slab without reinforcement bars has been considered in this study. In the future study, it is recommended to conduct an analysis of a bridge slab with reinforcement bars and determine equivalent BCs for its corresponding panel slab based on the calculated stiffness of the bridge slab, which would yield a more realistic simulation of the bridge slab.

4. Investigation of the fatigue dependency of the BCs

In past studies and this current study as well, the BCs for the panel slabs are designed for the initial elastic state, and the same determined BCs have been used throughout the fatigue analysis of the panel slabs. However, the panel slab is cracked due to fatigue loading, and consequently, the stiffness of the cracked panel slab is reduced. Consequently, in principle, the stiffness of the BCs for the panel slabs should also be reduced during the fatigue analysis. Therefore, it is vital to investigate the fatigue dependency of the BCs, and hence, the BCs should be updated during the fatigue analysis of the panel slab for a more realistic analysis of fatigue behavior of the bridge slab.

5. Parametric studies

This study mainly aims to clarify the effects of BCs, and determine BCs of panel slabs to realistically analyze the deformation and fatigue behaviors of bridge slabs. The numerical results show that the panel slabs with BCs, proposed in this study, successfully capture the deformation and fatigue behaviors of bridge slabs. In the future researches, parametric studies can be conducted

considering other influencing factors such as length of the loading zone, multiple loading zones, loading intensity, and slab dimensions.

REFERENCES

[1] P. C. Perdikaris and S. Beim, "RC bridge decks under pulsating and moving load," *Journal of Structural Engineering*, vol. 114, no. 3, pp. 591-607, 1988. https://doi.org/10.1061/(ASCE)0733-9445(1988)114:3(591).

[2] M. Schläfli and E. Brühwiler, "Fatigue of existing reinforced concrete bridge deck slabs," *Engineering Structures*, vol. 20, no. 11, pp. 991-998, 1998. https://doi.org/10.1016/S0141-0296(97)00194-6.

[3] J. C. Graddy, J. Kim, J. H. Whitt, N. H. Burns, and E. K. Richard, "Punching-shear behavior of bridge decks under fatigue loading," *ACI Structural Journal*, vol. 99, no. 3, pp. 257-266, 2002. https://doi.org/10.14359/11909.

[4] K. Sonoda and T. Horikawa, "Fatigue strength of reinforced concrete slabs under moving loads," in *Proc. of IABSE Colloquium on Fatigue of Steel and Concrete Structures*, Zurich, Switzerland, pp. 455–462, 1982: International Association for Bridge and Structural Engineering.

[5] NILIM, "*Technical note no. 472: Research on fatigue durability evaluation for highway bridge slabs*," Tokyo: National Institute for Land and Infrastructure Management, 2008 (In Japanese)

[6] K. Okada, H. Okamura, and K. Sonoda, "Fatigue failure mechanism of reinforced concrete bridge deck slabs," in *Proc. of Bridge Engineering Conference*, vol. 1, pp. 136-144, 1978.

[7] Y. Maeda and S. Matsui, "Fatigue of reinforced concrete slabs under trucking wheel load," in *Proc. of Japan Concrete Institute*, vol. 6, pp. 221-224, 1984 (In Japanese).

[8] S. Matsui, "Fatigue strength of RC-slabs of highway bridge by wheel running machine and influence of water on fatigue," in *Proc. of Japan Concrete Institute*, vol. 9, no. 2, pp. 627-632, 1987 (In Japanese).

[9] K. Shakushiro, H. Mitamura, T. Watanabe, and N. Kishi, "Experimental study on fatigue durability of RC slabs reinforced with round steel bars," *Journal of Structural Engineering*, vol. 57, no. A, pp. 1297-1304, 2011 (In Japanese). https://doi.org/10.11532/structcivil.57A.1297.

[10] H. Mitamura, K. Syakushiro, T. Matsumoto, and S. Matsui, "Experimantal study on fatigue durability of RC deck slabs with overlay retrofit," *Journal of Structural Engineering*, vol. 58, no. A, pp. 1166-1177, 2012 (In Japanese). https://doi.org/10.11532/structcivil.58A.1166.

[11] T. Satoh, H. Mitamura, Y. Adachi, H. Nishi, H. Ishikawa, and S. Matsui, "*Report no. 4089: Fatigue durability of a reinforced concrete deck slab in a cold snowy region*," Ibaraki:

Public and Works Research Institute, 2007.

[12] P. Suthiwarapirak and T. Matsumoto, "3D fatigue analysis of RC bridge slabs and slab repairs by fiber cementitious materials," in *Proc. of International Conference FRaMCos-5*, Illinois, USA, vol. 2, pp. 677-684, 2004: International Association for Fracture Mechanics of Concrete and Concrete Structures.

[13] A. A. M. Drar, T. Matsumoto, T. Hayashikawa, and X. He, "Development of a numerical model to predict the fatigue behaviors of RC slabs," *Journal of Japan Society of Civil Engineers A2*, vol. 71, no. 2, pp. 805-812, 2015. https://doi.org/10.2208/jscejam.71.I_805.

[14] P. Deng and T. Matsumoto, "Determination of dominant degradation mechanisms of RC bridge deck slabs under cyclic moving loads," *International Journal of Fatigue*, vol. 112, pp. 328-340, 2018. https://doi.org/10.1016/j.ijfatigue.2018.03.033.

[15] P. Deng and T. Matsumoto, "Fracture mechanics–based fatigue life prediction method for RC slabs in punching shear failure mode," *Journal of Structural Engineering*, vol. 146, no. 1, 2020. https://doi.org/10.1061/(asce)st.1943-541x.0002504.

[16] NILIM, "*Technical note no. 844: Research on fatigue durability evaluation for highway bridge concrete slabs*," Tokyo: National Institute for Land and Infrastructure Management, 2015 (In Japanese).

[17] V. C. Li and T. Matsumoto, "Fatigue crack growth analysis of fiber reinforced concrete with effect of interfacial bond degradation," *Cement and Concrete Composites*, vol. 20, no. 5, pp. 339-351, 1998. https://doi.org/10.1016/S0958-9465(98)00010-9.

[18] P. Suthiwarapirak and T. Matsumoto, "Fatigue analysis of RC slabs and repaired RC slabs based on crack bridging degradation concept," *Journal of Structural Engineering*, vol. 132, no. 6, pp. 939-948, 2006. https://doi.org/10.1061/(ASCE)0733-9445(2006)132:6(939).

[19] A. A. M. Drar and T. Matsumoto, "Fatigue analysis of RC slabs reinforced with plain bars based on the bridging stress degradation concept," *Journal of Advanced Concrete Technology*, vol. 14, no. 1, pp. 21-34, 2016. https://doi.org/10.3151/jact.14.21.

[20] G. R. Frederick, "Experimental and analytical investigation of load distribution in concrete slab bridges," in *Proc. of Spring Conference of Society for Experimental Mechanics*, Connecticut, USA: Society of Experimental Mechanics, 1997.

[21] M. Mabsout, K. Tarhini, R. Jabakhanji, and E. Awwad, "Wheel load distribution in simply supported concrete slab bridges," *Journal of Bridge Engineering*, vol. 9, no. 2, pp. 147-155, 2004. https://doi.org/10.1061/(ASCE)1084-0702(2004)9:2(147).

[22] A. Q. Khan, P. Deng, and T. Matsumoto, "Development of a numerical method for capturing the deformation behaviors of real bridge RC slabs," in *Proc. of Japan Society of Civil Engineers Hokkaido Branch*, Sapporo, Japan, vol. 76, A22, 2020.

[23] A. Q. Khan, P. Deng, and T. Matsumoto, "Approximate analytical conditions of a panel

RC slab for reproducing the fatigue behaviors of a real bridge RC slab," *Journal of Advanced Concrete Technology*, vol. 18, no. 1, pp. 1-16, 2020. https://doi.org/10.3151/jact.18.1.

[24] P. C. Pedikaris, S. R. Beim, and S. N. Bousias, "Slab continuity effect on ultimate and fatigue strength of reinforced concrete bridge deck models," *ACI Structural Journal*, vol. 86, no. 1989. https://doi.org/10.14359/2982.

[25] K. Maekawa, A. Pimanmas, and H. Okamura, "*Nonlinear mechanics of reinforced concrete*," London, UK: Spon Press, 2003. https://doi.org/10.1201/9781482288087.

[26] J. Zhang, H. Stang, and V. C. Li, "Crack bridging model for fibre reinforced concrete under fatigue tension," *International Journal of Fatigue*, vol. 23, no. 8, pp. 655-670, 2001. https://doi.org/10.1016/S0142-1123(01)00041-X.

[27] J. Zhang, "*Fatigue fracture of fiber reinforced concrete - an experimental and theoretical study*," Ph.D. thesis, Department of Structural Engineering, Technical University of Denmark, Lyngby, Denmark, 1998.

[28] M. Menegotto and P. E. Pinto, "Method of analysis for cyclically loaded R.C. plane frames including changes in geometry and non-elastic behaviour of elements under combined normal force and bending," in *Proc. of IASBE Symposium on Resistance and Ultimate Deformability of Structures acted on by Well-Defined Repeated Loads*, Lisbon, Portugal: International Association for Bridge and Structural Engineering, 1973. https://doi.org/10.5169/seals-13741.

[29] MARC, "*Advanced nonlinear simulation solution programming software Marc v. 2018* [online]," California, USA: MSC Corporation, 2018. Available at URL https://www.mscsoftware.com/product/marc.

[30] JRA, "*Design specifications for highway bridges*," Tokyo: Japan Road Association, 1996.

[31] M. A. Muspratt, "Elastic analysis of slabs," *Building and Environment*, vol. 13, no. 1, pp. 51-59, 1978. https://doi.org/10.1016/0360-1323(78)90008-2.

[32] JBA, "*Composite bridge design examples and explanations: Road guide November 2017 version*," Tokyo: Japan Bridge Association, 2018 (In Japanese). Available at URL https://www.jasbc.or.jp/publication/p20180314001.php.

APPENDIX

PUBLICATIONS AND AWARDS

a) Publications

- **Journal papers**

1) A. Q. Khan, P. Deng, and T. Matsumoto, "Approximate Analytical Conditions of a Panel RC Slab for Reproducing the Fatigue Behaviors of a Real Bridge RC Slab," *Journal of Advanced Concrete Technology,* vol. 18, no. 1, pp. 1-16, 2020. https://doi.org/10.3151/jact.18.1.

2) A. Q. Khan, P. Deng, and T. Matsumoto, " Equivalent Boundary Conditions of a Panel RC Slab for Realistic Fatigue Behavior Analysis of a Bridge RC Slab," *Engineering Structures*. (almost submitted)

- **Conference papers**

1) A. Q. Khan, P. Deng, and T. Matsumoto, "Development of an Effective Numerical Model for Fatigue Analysis of RC Bridge Slabs," *Proceedings of JSCE 10th Slab Symposium*, pp. 319-324, Tokyo, Japan, November 1-2, 2018.

2) A. Q. Khan, P. Deng, and T. Matsumoto, "Fatigue Analysis of an RC Bridge Slab Subjected to a Stepwise Loading Sequence using the Bridging Stress Degradation Concept," *Proceedings of JSCE Hokkaido Branch*, vol. 75, no. A-28, Tomakomai, Japan, January 26-27, 2019.

3) A. Q. Khan, P. Deng, and T. Matsumoto, "Numerical Investigation of the Effects of Boundary Conditions on Fatigue Behaviors of RC Slab under Moving Wheel," *Proceedings of Bridge Engineering Institute Conference (BEI-2019)*, pp. 704-708, Hawaii, USA, July 22-25, 2019.

4) A. Q. Khan, P. Deng, and T. Matsumoto, "Development of a Numerical Method for Capturing the Deformation Behaviors of Real Bridge RC Slabs," *Proceedings of JSCE Hokkaido Branch*, vol. 76, no. A-22, Sapporo, Japan, January 24-25, 2020.

b) Awards

1) The 60th JSCE Hokkaido Branch Incentive Award

2) Nitobe School Research Grant